Design and Testing of a DDG51 Destroyer Model

by

Muriel Claire Thomas

Ingénieur diplômée de l'Ecole Polytechnique (July 1999)

Submitted to the Ocean Engineering Department
in partial fulfillment of the requirements for the degree of

Master of Science in Naval Architecture and Marine Engineering

at the

MASSACHUSETTS INSTITUTE OF TECHNOLOGY

February 2002

© Massachusetts Institute of Technology 2002. All rights reserved.

Author .....
Ocean Engineering Department
January 18, 2002

Certified by.....
Michael S. Triantafyllou
Professor of Ocean Engineering
Thesis Supervisor

Accepted by .....
Professor Henrik Schmidt
Chairman, Departmental Committee on Graduate Studies,
Department of Ocean Engineering

MASSACHUSETTS INSTITUTE OF TECHNOLOGY
APR 2 6 2002
LIBRARIES

BARKER

MIT Libraries
Document Services

Room 14-0551
77 Massachusetts Avenue
Cambridge, MA 02139
Ph: 617.253.2800
Email: docs@mit.edu
http://libraries.mit.edu/docs

DISCLAIMER OF QUALITY

Due to the condition of the original material, there are unavoidable flaws in this reproduction. We have made every effort possible to provide you with the best copy available. If you are dissatisfied with this product and find it unusable, please contact Document Services as soon as possible.

Thank you.

The images contained in this document are of the best quality available.

Design and Testing of a DDG51 Destroyer Model

by

Muriel Claire Thomas

Submitted to the Ocean Engineering Department
on January 18, 2002, in partial fulfillment of the
requirements for the degree of
Master of Science in Naval Architecture and Marine Engineering

Abstract

Building an accurately scaled model of a real ship still remains a very important step in ship design. Even though the 3-D computer models are more and more precise and reliable, tests on models give such precious information on the ship behavior that they cannot be avoided yet. The most common test performed with scale models are towing and turning tests, where a scale model of the hull is attached to a carriage in a towing tank (linear or circular). In order to do more complex tests, for example maneuverability tests, a more elaborate model of the ship has to be built. The model needs to have the following characteristics: the model needs to be autonomous, in the sense that it has no physical link with the operator (data are sent wirelessly), and the boat needs to be equipped with sensors to record all the model boat parameters. This implies that not only does the boat need to have its own power supply, but it also needs to have the capacity to receive and execute the commands sent by the operator and finally to store the sensors data or to send them back directly to the operator. The rapid development of computer technologies makes it affordable to equip a model boat with a computer such as a PC104 to execute all the tasks required in real-time. The model boat is controlled remotely by a laptop sending wirelessly the commands entered by the operator to the boat on-board computer. The main motors RPM and rudder position are close-loop controlled. To limit data exchange and the risk of breaking the connection, the sensors data are stored on board and not sent real-time to the operator. Three type of sensors are used: an inertial unit giving x, y and z accelerations and roll, pitch and yaw rotation rates, a magnetometer giving the heading of the boat and a differential GPS giving position, heading, velocity and much more.
Several levels can be distinguished in building a remote control boat. The first three can be defined as follows: first controlling the velocity and the rudder position, which allows driving the boat around completely remotely. The second step is to control the heading of the boat which gives more possibilities in the type of tests that can be performed on the boat. The third step would be to control the position of the boat. A further step would include for example surge control.

At the beginning of this work, the first step in remote control was already achieved, the computer system and data logging system were already operational. The goal was to achieve the second step in remote control and do extensive testing on the model boat. The third step of remote control, closely linked to the second step, was initiated.

Thesis Supervisor: Michael S. Triantafyllou
Title: Professor of Ocean Engineering

Acknowledgments

All the work I present here would not have been possible without the help of many people I would like to thank here.

First, I would like to thank my thesis supervisor Michael S. Triantafyllou and principal research engineer Franz S. Hover for offering me to work on this exciting project and for helping me with the many problems I encountered during my research.

Of course, I cannot forget my friends and fellow students of the towing tank: Craig Martin and Joshua Davis, who both graduated before me, David Beal, Anna Michel, Stephen Licht, Victor Polidoro and Karl-Magnus McLetchie for their advice and support. Special thanks go to Martin Stoffel who helped me from Switzerland and Matt Greytak, who worked as a UROP on this project during the fall semester; their help was extremely valuable to me.

I would also like to thank all the people who made the testing of the boat possible: Fran Charles manager of the MIT Sailing Pavilion, Rich Axtell manager of the Hanscom Swimming Pool, Tom Consi from the OE department, Brian Callahan manager of the MIT swimming pool and finally Rick Meyer and BAE Ocean Systems for letting us use their open water test facility in Braintree.

I am also grateful to the people of the *Délégation Générale pour l'Armement*, *Direction des Constructions Navales* and *Ecole Nationale Supérieure de Techniques Avancées* for giving me the great opportunity to come and study here at MIT.

Finally, I would like to dearly thank my fiancé Geoffroy for his loving and helpful support throughout my studies at MIT.

Contents

1 INTRODUCTION **13**
- 1.1 Background and Previous Work . . . 13
  - 1.1.1 DDG51 Model Hull Background . . . 13
  - 1.1.2 Motivations . . . 14
- 1.2 Thesis Objectives . . . 14
- 1.3 Thesis Contribution . . . 15
- 1.4 Thesis Outline . . . 15

2 SENSORS **18**
- 2.1 DMU (Accelerometers and Gyros) . . . 18
  - 2.1.1 Coordinate System . . . 18
  - 2.1.2 Importance of the Position of the DMU . . . 19
  - 2.1.3 DMU Data . . . 20
  - 2.1.4 Building a Test Bench . . . 20
  - 2.1.5 Processing the Data . . . 23
  - 2.1.6 Obtaining the Boat Data from the DMU Data . . . 25
  - 2.1.7 Boat Path . . . 25
- 2.2 Magnetometer . . . 26
  - 2.2.1 Specifications . . . 26
  - 2.2.2 Position of the Magnetometer in the Boat . . . 26
  - 2.2.3 Data Processing . . . 27
- 2.3 DGPS . . . 28
  - 2.3.1 Data Transmitted . . . 28
  - 2.3.2 Data Processing . . . 28
- 2.4 Data Processing Program . . . 30
- 2.5 Summary . . . 33

3 DESIGN OF A HEADING CONTROLLER **34**
- 3.1 Ship Steering Equations . . . 34
  - 3.1.1 Non-Linear Ship Steering Equations . . . 34
  - 3.1.2 Linear Ship Steering Equations . . . 34
- 3.2 The Models of Nomoto . . . 36
  - 3.2.1 Nomoto's Second Order Model . . . 36
  - 3.2.2 Nomoto's First Order Model . . . 38
- 3.3 Hydrodynamic Coefficients . . . 38
  - 3.3.1 Nomoto's Coefficients from SBT . . . 39
  - 3.3.2 Nomoto's Coefficients from Model Experiments . . . 41

3.4 Designing the Heading Controller . . . 42
3.4.1 Choice of the Type of Controller . . . 42
3.4.2 Controller Equations and Parameters . . . 44
3.5 Adapting the Controller . . . 45
3.5.1 Gain Scheduling . . . 45
3.5.2 The Parameters Which Influence the Controller . . . 46
3.5.3 Study of the Influence of the Forward Velocity . . . 47
3.5.4 Finding the Parameters K_0 and T_0 . . . 48
3.6 Discrete Controller . . . 50
3.6.1 Why Discretize the Controller? . . . 50
3.6.2 Equations for the Discrete Controller . . . 51
3.7 Evaluating the Controller Robustness . . . 51
3.7.1 Measures of the Robustness . . . 52
3.7.2 Implementing Rudder Limitations . . . 53
3.7.3 Analysis of the Matlab Program for Testing the Controller . . . 53
3.8 Summary . . . 55

4 IMPLEMENTATION OF THE HEADING CONTROLLER 56
4.1 Boat Operating System . . . 56
4.1.1 System Overview . . . 56
4.1.2 System Components Description . . . 57
4.2 Controller Specificities . . . 68
4.2.1 Working requirements . . . 68
4.2.2 Implementation . . . 68
4.3 Summary . . . 70

5 TRACK KEEPING 71
5.1 Introduction . . . 71
5.2 Kinematics for track keeping . . . 71
5.3 Guidance by Line of Sight . . . 72
5.4 Matlab Program for Track Keeping system . . . 73
5.4.1 Overall Structure . . . 73
5.4.2 Analyzis of the program . . . 73
5.5 Implementing the Position Controller . . . 76
5.6 Summary . . . 76

6 TESTING THE BOAT 77
6.1 Testing Locations . . . 77
6.2 Preparing the Boat for Outdoors Testing . . . 78
6.3 Presentation of the tests . . . 78
6.3.1 Velocity Tests . . . 79
6.3.2 Simple Turning Tests . . . 79
6.3.3 Dieudonné spiral maneuver . . . 79
6.3.4 ZigZag Maneuver . . . 81
6.3.5 Circle Maneuver . . . 83
6.3.6 Evaluating the Tactical Diameter Before Testing . . . 84

7 RESULTS AND ANALYSIS **86**
7.1 Velocity Tests . . . 86
7.2 Turning Tests . . . 87
7.2.1 Tests Description . . . 87
7.2.2 Values of K_0 and T_0 . . . 87
7.2.3 Analysis of a Turn . . . 88
7.3 Results of the Circle Maneuver Tests . . . 95
7.3.1 Description of the Tests . . . 95
7.3.2 Analysis of The Tests . . . 97
7.4 Summary . . . 103

8 CONCLUSION **105**
8.1 Thesis Summary . . . 105
8.2 Conclusions . . . 106
8.3 Recommendation for Future Work . . . 107

A DDG51 Characteristics **109**

B SHIP MODEL PAYLOAD **112**

C DMU TESTING **113**
C.1 Test Bench . . . 113
C.2 Other Tests . . . 116

D SHIP PATH USING DMU DATA **117**
D.1 Method . . . 117
D.2 Matrices Relations . . . 118

E SLENDER BODY THEORY **123**
E.1 Fluid force - Y hydrodynamic coefficients . . . 123
E.1.1 Reference Frame . . . 123
E.1.2 Elementary Fluid force . . . 124
E.1.3 Total Fluid force . . . 125
E.1.4 Y Hydrodynamic Coefficients . . . 126
E.2 Fluid Moment . . . 126
E.2.1 Elementary Fluid moment . . . 126
E.2.2 Total Fluid Force . . . 127
E.2.3 Hydrodynamic Coefficients . . . 127
E.3 Computing SBT hydrodynamic coefficients . . . 128
E.3.1 Elementary added mass . . . 128
E.3.2 "Rectangular Platform" estimation . . . 128
E.4 Other ways to compute the hydrodynamic coefficients . . . 129
E.4.1 Semi-empirical Methods and Regression Analysis . . . 129
E.4.2 Fossen's approximations . . . 130

F SCALING & NON-DIMENSIONALIZATION **131**
F.1 Scaling process . . . 131
F.2 Non-Dimensionalization . . . 133

G YAW RATE GRAPHS
Hanscom Swimming Pool- Feb. 2001 **134**

H FIFO'S AND THREADS **137**
H.1 FIFO'S 137
H.2 Threads 138
H.2.1 Laptop Threads 138
H.2.2 PC104 Threads 138

I YAW RATE GRAPHS
MIT Alumni Swimming Pool, Dec. 2001 **140**

J GLOBAL RESULTS
MIT Alumni Pool - Dec. 2001 Tests **151**

K TESTS IN BAE TESTING FACILITY **225**

List of Figures

2-1 DMU reference frame 18
2-2 Boat equipment layout 19
2-3 Body frame fixed with the boat 20
2-4 Test Bench for the DMU 21
2-5 Reference frame of Magnetometer 26
2-6 Matlab Graphical User Interface for data processing 31

3-1 Reference frames and motion parameters 35
3-2 Rudder Position 35
3-3 Comparison between the first and second order Nomoto models 41
3-4 Ship Model Experience - Hanscom Swimming Pool 42
3-5 Comparison between the first and second order Nomoto models 43
3-6 Heading controller 44
3-7 Gain scheduling controller 46
3-8 Difference between a continuous and a digital controller 50
3-9 Sampling and Holding Process 51
3-10 Gain and Phase Margin Definitions 52

4-1 Boat Global Operating System 57
4-2 Ship model Graphical User Interface (on Laptop) 61
4-3 Ship model GUI from [17] 61
4-4 PC104 software diagram 67
4-5 Laptop software diagram 68

5-1 Coupled position and heading controller 73
5-2 Step of the autopilot Matlab program 74
5-3 Result of the Matlab autopilot program 75

6-1 Path during a Dieudonné Spiral Maneuver (Stable Ship) 80
6-2 Relation between rudder angle and yaw turning rate 80
6-3 Overshoot and zigzag maneuver 82
6-4 Turning Test 83

7-1 Velocity Tests at the MIT pool and Towing Tank 87
7-2 Velocities and Acceleration during a turn 91
7-3 X, Y and Z accelerations measured by the DMU 93
7-4 Stabilized Pitch and Roll angles measured by the DMU 93
7-5 Roll, Pitch and Yaw Rotation rates measured by the DMU 95
7-6 Surge and Sway Velocities using DMU data 95

7-7 Comparison between the magnetometer heading and the yaw rate integration . . 97

C-1 Testing Configuration 1 for DMU Test Bench 113
C-2 Testing Configuration 2 for DMU Test Bench 114
C-3 Expected Measurement from the DMU 114
C-4 Experimental Data from DMU 115

D-1 Method to obtain the ship path using the DMU data 117
D-2 Comparison between the positions given by the GPS and the DMU method . . . 121

E-1 Coordinate Systems for SBT 124
E-2 Ship Approximation 128

G-1 Experiments in Hanscom Pool - 1/2 135
G-2 Experiments in Hanscom Pool - 2/2 136

I-1 Yaw rotation rates curve fitting for different experiments (1/6) 141
I-2 Yaw rotation rates curve fitting for different experiments(2/6) 143
I-3 Yaw rotation rates curve fitting for different experiments(3/6) 145
I-4 Yaw rotation rates curve fitting for different experiments(4/6) 147
I-5 Yaw rotation rates curve fitting for different experiments(5/6) 149
I-6 Yaw rotation rates curve fitting for full turn experiments(6/6) 149

J-1 Turning Tests at 200 RPM and 30 deg. - Alumni Pool 153
J-2 Turning Tests at 200 RPM and 35 deg. - Alumni Pool 155
J-3 Turning Tests at 300 RPM and 10 deg. - Alumni Pool 157
J-4 Turning Tests at 300 RPM and 20 deg. - Alumni Pool 159
J-5 Turning Tests at 300 RPM and 30 deg. - Alumni Pool 161
J-6 Turning Tests at 400 RPM and 10 deg. - Alumni Pool 163
J-7 Turning Tests at 400 RPM and 20 deg. - Alumni Pool 165
J-8 Turning Tests at 400 RPM and 30 deg. - Alumni Pool 167
J-9 Turning Tests at 400 RPM and 35 deg. - Alumni Pool 169
J-10 Turning Tests at 500 RPM and 10 deg. - Alumni Pool 171
J-11 Turning Tests at 500 RPM and 20 deg. - Alumni Pool 173
J-12 Turning Tests at 500 RPM and 30 deg. - Alumni Pool 175
J-13 Turning Tests at 500 RPM and 35 deg. - Alumni Pool 177
J-14 Turning Tests at 600 RPM and 10 deg. - Alumni Pool 179
J-15 Turning Tests at 600 RPM and 20 deg. - Alumni Pool 181
J-16 Turning Tests at 600 RPM and 35 deg. - Alumni Pool 183
J-17 Turning Tests at 500 RPM and 20 deg. - Alumni Pool 185
J-18 Turning Tests at 500 RPM and 30 deg. - Alumni Pool 187
J-19 Turning Tests at 500 RPM and 35 deg. - Alumni Pool 189
J-20 Turning Tests at 600 RPM and 10 deg. - Alumni Pool 191
J-21 Turning Tests at 600 RPM and 20 deg. - Alumni Pool 193
J-22 Turning Tests at 600 RPM and 35 deg. - Alumni Pool 195
J-23 Turning Tests at 500 RPM and 20 deg. - Alumni Pool 197
J-24 Turning Tests at 500 RPM and 30 deg. - Alumni Pool 199
J-25 Turning Tests at 500 RPM and 35 deg. - Alumni Pool 201
J-26 Turning Tests at 600 RPM and 10 deg. - Alumni Pool 203

J-27 Turning Tests at 600 RPM and 20 deg. - Alumni Pool 205
J-28 Turning Tests at 600 RPM and 35 deg. - Alumni Pool 207
J-29 Turning Tests at 700 RPM and 10 deg. - Alumni Pool 209
J-30 Turning Tests at 700 RPM and 20 deg. - Alumni Pool 211
J-31 Turning Tests at 700 RPM and 30 deg. - Alumni Pool 213
J-32 Turning Tests at 700 RPM and 35 deg. - Alumni Pool 215
J-33 Turning Tests at 800 RPM and 10 deg. - Alumni Pool 217
J-34 Turning Tests at 800 RPM and 20 deg. - Alumni Pool 219
J-35 Turning Tests at 800 RPM and 30 deg. - Alumni Pool 221
J-36 Turning Tests at 800 RPM and 35 deg. - Alumni Pool 223

K-1 GPS position data - BAE Quarry (1/2) 227
K-2 GPS position data - BAE Quarry (2/2) 229
K-3 Circle Maneuver tests at 300 RPM and 10 deg. - BAE Quarry 231
K-4 Circle Maneuver tests at 300 RPM and -20 deg. - BAE Quarry 233
K-5 Circle Maneuver tests at 300 RPM and -30 deg. - BAE Quarry 235
K-6 Circle Maneuver tests at 500 RPM and -10 deg. - BAE Quarry 237
K-7 Circle Maneuver tests at 500 RPM and -20 deg. - BAE Quarry 239
K-8 Circle Maneuver tests at 500 RPM and -30 deg. - BAE Quarry 241
K-9 Circle Maneuver tests at 700 RPM and -10 deg. - BAE Quarry 243
K-10 Circle Maneuver tests at 700 RPM and -20 deg. - BAE Quarry 245
K-11 Circle Maneuver tests at 700 RPM and -30 deg. - BAE Quarry 247

List of Tables

1.1 Principal characteristics of the DDG51 17

2.1 Position of the DMU compared to the center of gravity of the boat 20
2.2 DMU data versus connector pin 21
2.3 Accelerometer Calibration Data 24
2.4 Gyro Calibration Data 24
2.5 Recommended Minimum Specific Data from the DGPS 29

3.1 Values of Dimensional and ND Hydrodynamic Parameters of the Scaled Boat . . 40
3.2 Experimental evaluation of the K ans T coefficients 43
3.3 Non-dimensional values of K and T for different models 48
3.4 RPM - Forward Velocity Correspondence 49
3.5 Nomoto's constants from experiments 49
3.6 Rudder rotation rate limitations 54
3.7 Ship Model Controller Robustness Characteristics 54
3.8 Ship Model Controller Close-Loop Poles 55

4.1 Shell scripts for data transmission 65
4.2 Laptop Fifo's list and description 65
4.3 PC104 Fifo's list and description 66

6.1 Turning radius according to [14] 85
6.2 Turning radius according using hydrodynamic coefficients 85

7.1 RPM - Forward Velocity Correspondence 88
7.2 Experimental evaluation of the K ans T coefficients 89
7.3 Circle Maneuver Macros 97
7.4 Tactical and steady turning diameters and steady yaw rates for circle maneuvers 98
7.5 GPS Velocity and Variation in sway velocity for the GPS 100
7.6 List and Heel at rest, Steady Roll angle during a turn 103
7.7 GPS lag and drift angle 104

A.1 Real DDG51 Parameters 109
A.2 Propeller and LM2500 Characteristics 110

B.1 Weight and position fo the equipment 112

C.1 Macro Description 113

H.1 FIFO list and data structure 137

Chapter 1

INTRODUCTION

1.1 Background and Previous Work

1.1.1 DDG51 Model Hull Background

The hull used for this project is a **1:47** scaled model of a US Navy Arleigh Burke Class Destroyer (DDG51). The dimensions of the real boat are given in Appendix A and the comparison between the model and the real boat is shown in Table (1.1). The hull was built around ten years ago at the David Taylor Model Basin. The hull is made of fiberglass and few pieces of wood at the bow, the stern and on the rim; it has a sonar dome shape at the bow. When given to the MIT Towing Tank, it was a bare hull and basically made only for towing tests. However, it was used for quite different experiments as described below.

The first study carried on this hull was a DPIV (Digital Particle Image Velocimetry) study on the hull. Then, the hull was used for the **foilboat** project (cf. [2]), which was quite successful.

A third study led to modify the hull in order to transform it into a remote control boat. Two shafts and five-blade propellers were added, and two rudders were attached at the stern. The hull was also equipped with two half horse power DC brush motors to drive the two shafts and propellers and a small motor to activate the rudder. An on board computer was also added along with sensors (a six-axis inertial unit and a magnetometer). However, only a few tests were done at the towing tank and the model was never fully remotely controlled (cf. [22]).

Great progress was made on the ship model system by Stoffel (cf. [17]). Actually, Stoffel redesigned the whole operating system: the on board computer was changed and operated

under Linux and a relatively robust remote control program was built along with a data logging system. All the programs were written either in C or C++. A Differential GPS was added to the two other sensors. The boat was successfully tested at the MIT Towing Tank and at Hanscom Swimming pool.

1.1.2 Motivations

The naval ships of the next generation are being considered as having a reduced manning, so more and more control systems have to be developed: controlling the surge, sway, yaw motions, ship tracking, heading, fuel consumption optimization and engine propeller dynamics are a few examples. Ship motions and engine dynamics being multivariable systems, a MIMO (Multiple Input Multiple Output) study should be considered.// Even if a SISO (Single Input Single Output) PID controller is a great simplification compared to the real control case, it can serve as a solid ground to develop more complex controllers afterwards.
Then, considering the limitations and capabilities of actual simulation and design techniques, experimentation on ship models is still needed. Maneuvering of naval combatants is almost completely neglected in the design process and usually the maneuvering capabilities are accepted as determined by the full-scale sea trials after the ship has been built. Consequently, an accurately scaled ship model remotely operated and equipped with controllers for the parameters mentioned above could help to evaluate at a relatively low cost the maneuvering capabilities of the real ship. This could lead to some modifications in order to improve the real boat performance before the boat has actually been built.

1.2 Thesis Objectives

The main thesis objective is to design and implement a simple PID SISO heading controller for the model boat and test it successfully along with doing some other testing on the boat to characterize its maneuvering capabilities.
To achieve the thesis main goal, it was necessary to subdivide it into several specific objectives:

- acquire a full understanding of the system designed in [17],
- design a simple model of the boat **yaw-sway** behavior from available data and experiments,

- optimizing the preparation and time necessary for testing the boat,
- designing a sequence of **tests** that would fully reflect the boat maneuvering capabilities,
- interpreting the results in order to refine the **yaw-sway model** and evaluate the maneuvering capabilities of the model boat.

In fact, the initial global goal of the thesis was broader and included building a surge controller in order to replicate the dynamics of the two LM2500 gas turbine of the real ship. This could not be achieved due to a lack of time, however the same method as the one used to design the heading controller can be used to design the surge controller.

1.3 Thesis Contribution

The thesis presents many processes that are part of the heading controller design and implementation and introduces the required concepts and procedures to build and implement the position controller. The thesis also provides several other main contributions:

- Keep the boat in a good working state and improve the boat layout and the **reliability** of the boat system,
- document thoroughly the boat operating system, the way to prepare the boat for testing, the way to operate it during the test and the way to post-process data. **Organized** documentation is really essential for all the work done in this thesis and in [17] to be used efficiently.
- develop simple and efficient Graphical User Interfaces (GUI) for the boat remote control system and data processing,
- and finally provide data on the ship model that can be used for further maneuvering studies.

1.4 Thesis Outline

The thesis organization follows the chronology of the work done. The five major steps of the work accomplished are each described in a chapter:

- **Chapter 2**: the subject of this chapter is the **three sensors** which equip the boat: the inertial unit, the magnetometer and the DGPS. The main goal of the chapter is to describe data processing for each of the sensors along with the overall post-processing Matlab program. Accurate data processing is crucial to be able to interpret the results of the tests described in Chapter 6.

- **Chapter 3**: this chapter is mainly concerned with the design of a **robust heading controller** for the ship model. The biggest concern of the chapter is to find an accurate plant model for the boat. The **first order Nomoto** model is used and the chapter presents several possible ways to obtain the parameters of this model. The method to verify the robustness of the controller is also described.

- **Chapter 4**: the goal of this chapter is to explain the actual **boat operating system** and especially the modifications which have been applied to the system designed by Stoffel. The GUI, the remote control program and the implementation of the heading controller are described in detail.

- **Chapter 5**: this chapter gives indications on how to use the heading controller to build a track controller.

- **Chapter 6**: its topic is the ship model testing, which was the ultimate goal of the project. the choice of the testing locations is analyzed along with the necessary preparation before testing the boat. Finally the tests performed on the boat are thoroughly described.

- **Chapter 7**: all the results and data processing of the tests listed in Chapter 6 are presented along with a conclusion.

Characteristics	Real Ship	Ship Model[1]
Length (LOA[2])	**149.98 m**	**3.25 m**
Length (LBP[3])	142.04 m	3.15 m
Beam	17.98 m	44 cm
Draft	6.1 m	15.2 cm
Displacement	8340 T	86[4] kg
Waterplane area	2029.23 m^2	1 m^2
LCG [5]	0.85 m after midships	0.05 m
Block Coefficient	0.522	idem
Prismatic coefficient	0.615	idem
Top speed	32 knots (14m/s)	4.67 knots (2.4 m/s)
Sustained speed	20 knots (10.3 m/s)	2.9 knots (1.5 m/s)
Prop. diameter	5.18 m	10.8 cm
Number of propellers	2	2
Number of blade on one prop	5 (CP[6])	5 (fixed pitch)

Table 1.1: Principal characteristics of the DDG51

[1]for LBP, LOA, B and D, measurements were taken on the model hull itself
[2]Length Over All
[3]Length Between Perpendicular
[4]Estimated total weight
[5]Longitudinal center of Gravity
[6]Controllable Pitch

Chapter 2

SENSORS

The boat uses the three following sensors:

- **Three axis accelerometers and three axis gyros**: DMU VGX from Crossbow (www.xbow.com). In the rest of the thesis, it will be referenced to as DMU.
- **Magnetometer**: model 113 from Crossbow,
- **Differential GPS** (DGPS): DGPS 53 from Garmin (www.garmin.com).

In the following, data processing is described sensor by sensor.

2.1 DMU (Accelerometers and Gyros)

2.1.1 Coordinate System

The axis of the DMU are positioned as shown in Figure (2-1). For all the experiments,

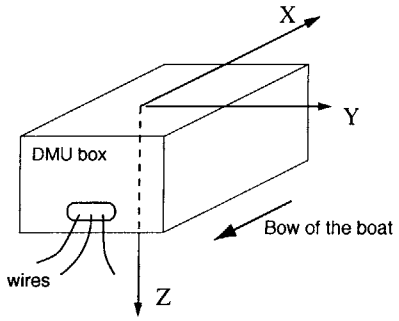

Figure 2-1: DMU reference frame

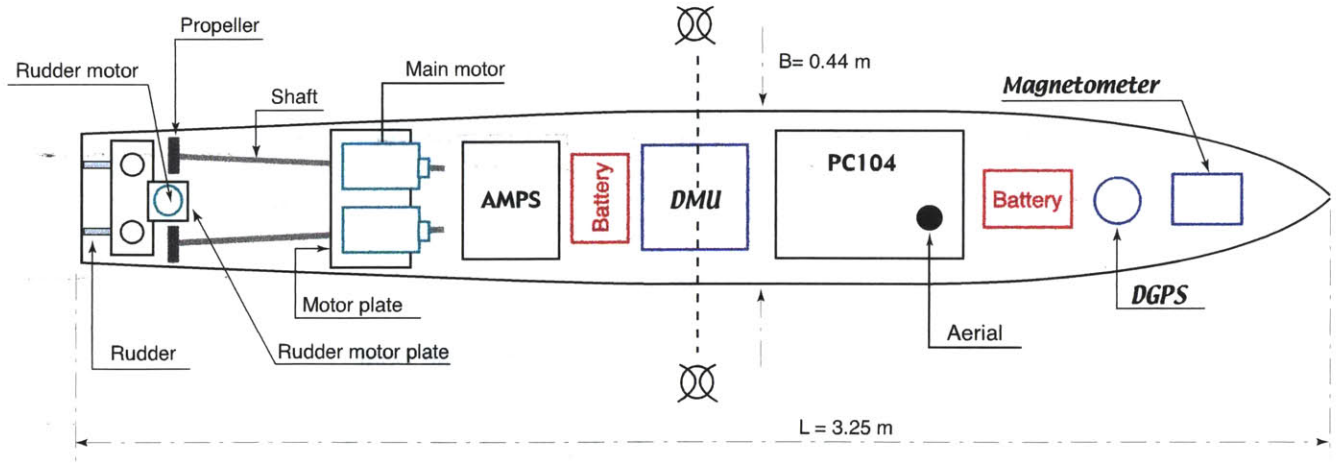

Figure 2-2: Boat equipment layout

due to the layout of the equipment inside the boat (cf. Figure (2-2)), the wires will always be placed facing the bow. .

2.1.2 Importance of the Position of the DMU

Studying the movements of the boat means working with two coordinate systems:

- **the inertial reference frame**, which is Earth based. As the range used for testing the boat is significantly smaller than the Earth dimensions and considering the fact that each test on the boat does not last more than a few minutes, this frame will be considered **fixed**. For the rest of this report, this frame will be referred to as **IF** (**I**nertial **F**rame),

- **the body fixed frame**, which is attached the ship model. This frame is shown on Figure (2-3). The origin of this frame is positioned at midships, X is pointing at the bow, Y is pointing port and Z is pointing down. This is the frame used in references [3] and [8]. One obvious reason for positioning this frame at midships and not at the center of gravity (Cog) is because the center of gravity of the boat depends on the loading of the ship and thus can change over time. For the rest of this report, this frame will be referred to as **BF** (**B**ody **F**rame).

As it will be shown later, knowing the movement of the boat in the BF is crucial to the analysis of the boat behavior. However, the DMU gives the values of the accelerations and the rotation rates in its own reference frame. Consequently, the position of the DMU with respect

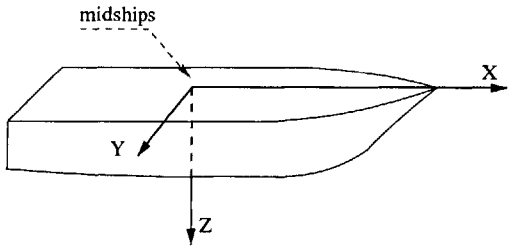

Figure 2-3: Body frame fixed with the boat

Item	Position of the Center of Gravity wrt midships
Total Payload	-0.058 m
Hull + Payload	-0.025 m
DMU center	-0.0475 m

Table 2.1: Position of the DMU compared to the center of gravity of the boat

to the position of the boat should be taken into account.

To determine the position of both the DMU and the Cog with respect to midships, a payload sheet was filled with all the weight and position data available for all the pieces of equipment inside the boat. The complete payload sheet is presented in Appendix B. A brief summary is presented in Table (2.1). In this table, the position of the center of gravity of the boat is only an estimation, but DMU and Cog are very close to each other and also close to midships. The center of the DMU is taken as the center of the sensor black box. Using those results, it was supposed for all data processing that the boat Cog , the DMU frame center and boat midships were merged.

2.1.3 DMU Data

The DMU has three different working modes (cf. [19]). The mode that was used is the so called *angle mode* which allows the gyro to output the **stabilized pitch and roll angles** along with the three angular rates and the three accelerations. The data available in the *angle mode* are given in table Table (2.2).

2.1.4 Building a Test Bench

Building a small testing facility for the DMU was a necessary step in understanding the way the DMU works, and verifying the outputs of this sensor. A photograph of the test bench is

Pin	Signal
5	X-axis acceleration (Analog Voltage)
6	Y-axis acceleration (Analog Voltage)
7	Z-axis acceleration (Analog Voltage)
8	Roll rate analog voltage
9	Pitch rate analog voltage
10	Yaw rate analog voltage
12	Roll analog voltage (stabilized Roll voltage)
13	Pitch analog voltage (stabilized Pitch voltage)

Table 2.2: DMU data versus connector pin

Figure 2-4: Test Bench for the DMU

shown on Figure (2-4) . One of the main motor of the DDG51 ship model was coupled to an axis on which a wooden plate was attached. The DMU was then attached on this plate and could thus be moved.

The motions of the motor were controlled using the remote control program of the DDG51 design by Stoffel (cf [17]). More precisely, the *macro mode* of this remote control program was used. This mode allows for each motion to set the RPM and the duration of the motion. The data from the DMU were recorded using the *data logging* feature of the remote control program. The main asset of such a testing device is that the rotation rates and accelerations are known. Thus, those values can be compared with the DMU logged data.
The test bench allowed to find two mistakes in the previous use of the DMU:

- the wrong working mode was used in [17], which led to having other measurements of the x and y accelerations instead of the stabilized pitch and roll angles on pins 12 and 13 (cf. Table (2.2)).

- the gravity components is opposite to the expected values on the x and y axis but the measured accelerations other than gravity are accurate. On the z axis the gravity component is measured accurately but the accelerations other than gravity are opposite to the real values.

Some of the tests performed with the DMU test bench are presented in Appendix C.

2.1.5 Processing the Data

All the data conversions are detailed in the DMU manual, reference [19]. Here are only mentioned the conversions used in the data processing programs.

The data from the DMU are collected via the Data Acquisition Card (model DAS16jr/12 from Computer Boards) as 12 bits numbers between 0 and 4096. The DAC has 16 analog input channels which can be sampled at a maximum rate of 10kHz. The analog output voltage of the DMU being between +5V and -5V, Equation (2.1) is used to convert the data of the DAC back into volts:

$$V_{out}[V] = \frac{\text{analog data} - 2048}{4096} \cdot 10 \tag{2.1}$$

where V_{out} is the value in volts of the analog output voltage.
Then, each of the voltages has to be converted into the engineering units of the data they represent (m/s^2 for accelerations, deg/s for rotation rates and deg for angles).

Acceleration Data

The analog outputs for acceleration are "raw data" from the DMU, so both **offsets** and **sensitivity** factors are needed to convert the voltage into engineering units. So for the accelerations (pins 5, 6 and 7 of the DMU connector), Equation (2.2) is used for the conversion to m/s^2:

$$\text{accel}[\text{m/s}^2] = (V_{out}[V] - \text{offset}) \cdot \text{sensitivity} \cdot 9.81 \tag{2.2}$$

where the offsets and sensitivities have specific values for each of the three axis. The default values of the offsets and sensitivities are specific to each DMU and given in the specification sheet of the unit. For acceleration data, the specifications of the DMU used in the boat are mentioned in Table (2.3).

Rotation Rate Data

For the rotation rates (roll, pitch and yaw rates on pins 8, 9 and 10), the analog outputs are not the raw values from the sensors, they already have been processed by an internal converter. So the offsets of the axis are not needed and Equation (2.3) is used to convert the volts V_{out} into $°/s$:

$$\text{rate } [°/s] = AR \cdot 1.5 \cdot \frac{V_{out}[V]}{4.096[V]} \tag{2.3}$$

where **AR** is the angular rate range of the sensor which is given in Table (2.4) for each axis of the gyro. The offsets and sensitivities are also given, even if they are not directly used here.

Stabilized Angles

As for the stabilized angles (pitch and roll angles), Equation (2.4) is the formula used to convert the analog data V_{out} into degrees:

$$\text{angle } [°] = 90° \cdot \frac{V_{out}[V]}{4.096[V]} \tag{2.4}$$

Axis	Null Offset (V)	Sensitivity (G/V)	Range (G)
X	2.570	1.007	2.000
Y	2.482	0.990	2.000
Z	2.480	1.009	2.000

Table 2.3: Accelerometer Calibration Data

Axis	Null Offset (V)	Sensitivity (deg/sec/V)	Range (deg/sec)
X	2.522	73.109	150.000
Y	2.513	63.598	150.000
Z	2.517	60.905	150.000

Table 2.4: Gyro Calibration Data

Then, before processing the data, it has to be noted that the **DMU does not internally correct for gravity**. Consequently, the gravity has to be removed from the x, y and z accel-

erations. To do so, the vector $\vec{g}$ has to be projected on the axes of the DMU frame and each of its component then subtracted from the initial x, y and z accelerations.

2.1.6 Obtaining the Boat Data from the DMU Data

In order to obtain the boat parameters from the DMU parameters, three processing steps have to be implemented:

1. modify the DMU data according to Section 2.1.4,

2. remove the gravity from the x and y axis using the stabilized pitch and roll angles. The gravity vector projected on the boat axes and noted $\vec{g_p}$ is:

$$\vec{g_p} = C_\psi \cdot C_\phi \cdot \vec{g}, \qquad \mathbf{C}_\phi = \begin{bmatrix} 1 & 0 & 0 \\ 0 & \cos(\phi) & \sin(\phi) \\ 0 & -\sin(\phi) & \cos(\phi) \end{bmatrix}, \qquad \mathbf{C}_\psi = \begin{bmatrix} \cos(\psi) & 0 & -\sin(\psi) \\ 0 & 1 & 0 \\ \sin(\phi) & 0 & \cos(\phi) \end{bmatrix} \tag{2.5}$$

3. since the position of the DMU frame compared to the body fixed frame has to be taken into account, the DMU data have to be modified through the use of a rotation matrix. The Boat frame is obtained by a rotation of π around the z vertical axis, which is the same for both frame. If $\vec{A}_{DMU}$ and $\vec{A}_{boat}$ are respectively the acceleration vectors in the DMU frame and in the boat frame, and if $\vec{R}_{DMU}$ and $\vec{R}_{boat}$ are the rotation rate vectors:

$$\vec{A}_{boat} = \begin{bmatrix} -1 & 0 & 0 \\ 0 & -1 & 0 \\ 0 & 0 & 1 \end{bmatrix} \cdot \vec{A}_{DMU}, \qquad \vec{R}_{boat} = \begin{bmatrix} -1 & 0 & 0 \\ 0 & -1 & 0 \\ 0 & 0 & 1 \end{bmatrix} \cdot \vec{R}_{DMU} \tag{2.6}$$

The yaw rate and the z accelerations do not need to be changed.

2.1.7 Boat Path

It is possible to use the DMU data to obtain the path followed by the boat. The method is described in detail in Appendix D. It uses integration of the DMU data and the Euler angles. However, this method does not lead to good results, the integration of the DMU data not being precise enough. Some comparisons between the GPS path and the path obtained with DMU data are also given in Appendix D.

2.2 Magnetometer

2.2.1 Specifications

The model 113 from Crossbow is designed to measure magnetic fields up to 1 Gauss. The 113 provides 3 analog output voltages proportional to the magnetic field magnitude measured in three orthogonal directions.
The magnitude of the Earth magnetic field is between 0.6 gauss (at the poles) and 0.3 gauss (at the equator). The *gauss* is the unit used to measure the Earth magnetic field: 1 gauss = 10^{-3} testla. The *gamma*, 1 gamma = 10^{-6} gauss, is the unit used to measure the disturbances of the Earth mean magnetic field.

One particularity of this sensor is that its level of noise is very low so that small magnetic signatures can be measured. However, this proves to be a drawback for our application since the DC brush motors used in the model boat generate magnetic field that can disturb the measurement of the magnetometer. Consequently, the sensor had to be placed the farthest away possible from the motors: at the bow of the boat. If the 113 is not disturbed by the magnetic field created the motors or any other exterior source of magnetic perturbation, it can theoretically provide a **direction accuracy to better than** 0.1°.

2.2.2 Position of the Magnetometer in the Boat

It should be noted that the 3 fluxgate sensors of the magnetometer are positioned such that their axes do not form an direct orthogonal frame. The magnetometer is placed as shown on Figure (2-5).

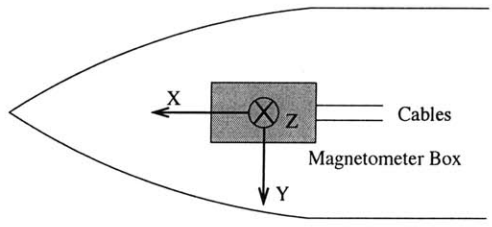

Figure 2-5: Reference frame of Magnetometer

2.2.3 Data Processing

The data from the magnetometer are fairly simple to process since there are **no offsets**. Only a constant factor is needed to convert the analog data into a engineering data in gauss measuring the intensity of the magnetic field : the sensitivity of the magnetometer is **4V/gauss** for all three axes. The formula used to convert analog voltage data to physical data is given in Equation (2.7).

$$\text{magnetic field [gauss]} = \frac{\text{analog data} - 2048}{4096} \cdot \frac{10[V]}{4[V/gauss]} \tag{2.7}$$

Then the value of the y axis is reversed to have the components of the magnetic field in the boat frame.

Heading

The magnetometer is mainly used to give the heading of the ship model by measuring the components of the Earth magnetic field. The heading can also be given by the GPS when GPS signals can be received, however GPS heading measurements are obtained only when the boat is moving, whereas the magnetometer can give heading measurements even when the boat is at a standstill.

A first approximation for data processing is to neglect the **pitch and roll movements** of the boat. The heading of the boat is the angle between the North and the x axis of the ship model frame and is simply obtained using:

$$x_{magn} > 0 \quad \rightarrow \quad \text{Boat heading} \quad = \quad -\arctan\left(\frac{y_{magn}}{x_{magn}}\right) \tag{2.8}$$

$$x_{magn} < 0 \quad \rightarrow \quad \text{Boat heading} \quad = \quad -[\arctan\left(\frac{y_{magn}}{x_{magn}}\right) + 180] \tag{2.9}$$

where heading is computed in **degrees**, which is more representative than radians, and x_{magn} and y_{magn} are the measurements obtained respectively on the x and y axis of the magnetometer. Moreover, heading was chosen to be always given as an angle between 0 and 360 degrees, 0° being North, 90° being East, 180° being South and 270° being West. So the result of Equations (??) and (2.9) has to be adjusted for the angle to be in the [0 , 360] degrees interval.
The heading computation could be refine using the stabilized pitch and roll angles of the DMU,

however, since data processing is needed to obtain them, it may slow the heading display on the graphical user interface.

2.3 DGPS

2.3.1 Data Transmitted

The DGPS uses the **World Geodetic System 1984 (WGS84)** as an earth-centered reference system to localize points. This WGS84 reference system is an earth-centered ellipsoid with the following parameters:

- semi-major axis a = 6,378,137.00 meters
- inverse flattening $\frac{1}{f} = 298.257223563$ (the flattening is defined as $f = \frac{a-b}{b}$ where b is the semi-minor axis).

For more information on the WGS84, the reference [12] can be consulted.

The DGPS has several working modes, each working mode corresponding to a specific output set of data. The set of data used is the **Recommended Minimum Specific GPS/TRANSIT Data** (RMC). The set of data transmitted by this mode are given in Table (2.5) .

2.3.2 Data Processing

Heading

Heading is obtained using data #8 in Table (2.5). The heading thus obtained is the **true heading** (referenced to **geographic North**). For that data to be compared with the heading given by the magnetometer (heading referenced to the **magnetic North**), data #10 (value of the magnetic declination) and #11 (direction of the magnetic declination, West or East) have to be used, using Equation (2.10):

$$\text{true heading} = \text{magnetic heading} +_{(E)} / -_{(W)} \text{magnetic declination} \tag{2.10}$$

The magnetic declination is equal to 15.9 deg. W in Hanscom Air Force Base where the first tests of the ship model were performed, and it is equal to 15 deg. W in the BAE Systems

output sentence:
$GPRMC,<1>,<2>,<3>,<4>,<5>,<6>,<7>,<8>,<9>,<10>,<11>,<12>...
... *hh<CR>< LF >

< 1 >	UTC time of position fix, hhmmss format
< 2 >	Status, A=Valid position, V=NAV receiver warning
< 3 >	Latitude, ddmm.mmmm format (leading zeros will be transmitted)
< 4 >	Latitude hemisphere, N or S
< 5 >	Longitude, ddmm.mmmm format (leading zeros will be transmitted)
< 6 >	Longitude hemisphere, E or W
< 7 >	Speed over ground, 000.0 to 999.9 knots (leading zeros will be transmitted
< 8 >	Course over ground, 000.0 to 359.9 degrees, true (leading zeros will be transmitted)
< 9 >	UTC date of position fix, ddmmyy format
< 10 >	Magnetic variation, 000.0 to 180.0 degrees (leading zeros will be transmitted)
< 11 >	Magnetic variation direction, E or W (westerly variation adds to the course over ground)
< 12 >	Mode indicator (only output if NMEA 2.30 active), A=autonomous, D=differential, E=Estimated, N=data not valid)

Table 2.5: Recommended Minimum Specific Data from the DGPS

testing facilities, where the ship model was tested in January 2002.

Position and Trajectory

The position of the boat in the Earth coordinate system is given by data # 3 to 5 in Table (2.5). The data can be plotted without any processing so that the actual position of the boat will be given in degrees, minutes and seconds. However, given the small scale of the ship model trajectory, the trajectory can be projected onto an horizontal plane and thus can be plotted on a x-y plot in meters. The origin (0,0) of the plot is taken as the initial position of the boat, x pointing to the East and y pointing to the geographic North.

To obtain the x-y coordinates, the projection of the trajectory on a plane tangent to the initial point is used. Around the initial point, the ellipsoid can be approximated by a sphere of radius equal to the radius of the ellipsoid at the initial point, which is computed using Equation (2.11):

$$R = \frac{a}{\sqrt{1 + (\frac{a^2}{b^2} - 1)\sin^2(\theta_{lat,0})}} \tag{2.11}$$

where $\theta_{lat,0}$ is the latitude of the initial point. This previous equation is easy to obtain looking at a vertical slice of the 3D ellipsoid. The equation $\frac{x^2}{a^2} + \frac{y^2}{b^2} = 1$ represents a two dimensional ellipse, where a is the semi-major axis and b the semi-minor axis ($f = \frac{a-b}{a}$), and a (r, θ)

parametric representation of this 2D ellipse can be used to obtain Equation (2.11).
The positions are then computed using the iteration process of Equations (2.12) and (2.13):

$$\Delta x = R \cdot \Delta(\text{latitude}) \tag{2.12}$$

$$\Delta y = R \cdot \cos(\text{latitude}) \cdot \Delta(\text{longitude}) \tag{2.13}$$

where R is computed using Equation (2.11).

Velocity

The velocity can be obtained using two different ways:

- using data #7, which is the speed over ground,
- using the position data obtained at paragraph 2.3.2 and the time between two measurements.

However, in both case, the speed will be the speed **with respect to the ground** and not with respect to the water.
Data #7 is in knots and can be converted into m/s using the following equation (1 knot = 1852 m/h):

$$[m/s] = [knots] \cdot 0.5144$$

To compute the absolute velocity from the position, Equation (2.14) is used:

$$velocity(i) = \sqrt{(x_i - x_{i-1})^2 + (y_i - y_{i-1})^2} \cdot \frac{1}{t_i - t_{i-1}} \tag{2.14}$$

The sign of the velocity can be obtained using the previous information along with the heading, but this was not done because a comparison of the absolute value of the velocity was enough to compare the two methods for computing the velocity.

2.4 Data Processing Program

All the data processing was done with Matlab. Since processing the boat data involved the display of many windows (one window for each type of data: accelerations, rotations rate etc...), a Matlab Graphical User Interface was built to facilitate the task. The GUI window is shown on Figure (2-6).

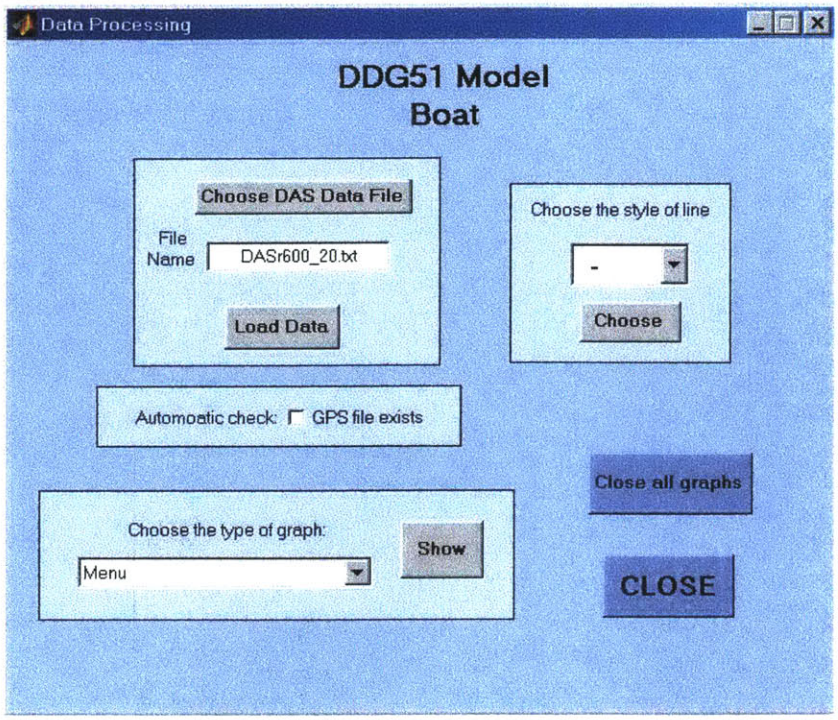

Figure 2-6: Matlab Graphical User Interface for data processing

For each test, at least three logfiles were available: one with DMU and Magnetometer data, another containing commands sent to the MEI card and a third one containing the MEI card data (data sent to the motors). For tests where the GPS signal could be received (outdoors conditions, Hanscom swimming pool), a GPS logfile was also available.
The functionalities of the GUI are the following:

- easy window management: all the data plots do not appear at once, the user actually chooses which windows are displayed,
- possibility of plotting several sets of data on the same figures, each set of data being displayed with a specific type of drawing line.
- automatic check if a GPS logfile exists, the Menu displaying the list of figures available for plotting being updated in consequence. Available choices are:

without GPS:	with GPS:
1. Magnetometer raw/filtered data	same as without GPS plus:
2. DMU raw/filtered accelerations	11. GPS heading
3. DMU raw/filtered rotation rates	12. DMU/GPS/Magnetometer headings
4. DMU filtered yaw rate	13. GPS trajectory
5. DMU Stabilized angles (roll/pitch)	14. GPS+DMU trajectories
6. DMU heading variation	15. GPS velocity
7. Surge and Sway Velocities	
8. DMU path	
9. MEI data	
10. MEI commands	

- a summary graph containing the following plots: accelerations, rotation rates, stabilized angles, heading , surge and sway velocities and finally the ship model path.

2.5 Summary

This chapter was dedicated to the study of the three sensors which equip the boat: the magnetometer, the DGPS and the 6-axis inertial unit. The understanding of their working is a key to being able to analyze the behavior of the boat during any testing. All the equations to convert the analog data which are logged by the ship model software were presented. Particularly, one has to be very careful on the position and orientation of each sensor frame with respect to the ship model frame.

Chapter 3

DESIGN OF A HEADING CONTROLLER

3.1 Ship Steering Equations

3.1.1 Non-Linear Ship Steering Equations

Considering motions in the horizontal plane (i.e. $\theta = \phi = p = q = w = 0$, parameters defined on Figure (3-1)), also supposing the ship symmetric about the x-z plane and neglecting the influence of the vertical position of the center of gravity z_G, the ship equations are:

$$X = m(\frac{\partial u}{\partial t} - rv - x_G r^2) \tag{3.1}$$

$$Y = m(\frac{\partial v}{\partial t} + ru + x_G \frac{\partial r}{\partial t}) \tag{3.2}$$

$$N = I_{zz}\frac{\partial u}{\partial t} + mx_G(\frac{\partial v}{\partial t} + ru) \tag{3.3}$$

3.1.2 Linear Ship Steering Equations

In the previous equations, supposing the forward velocity of the ship is constant and equal to U_0 and neglecting second order terms, the **linear ship steering** equations can be written

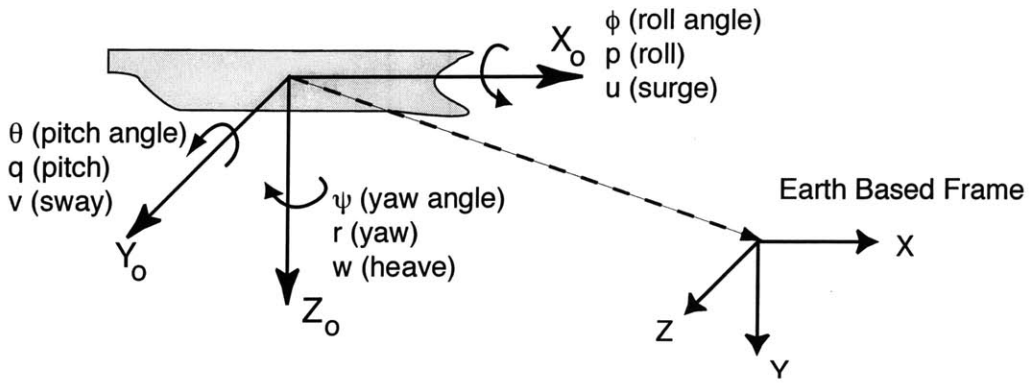

Figure 3-1: Reference frames and motion parameters

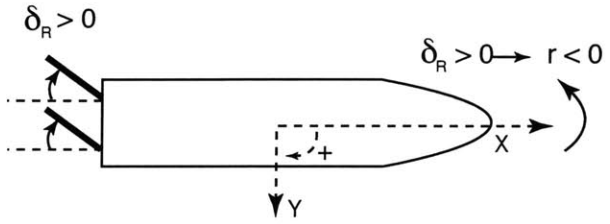

Figure 3-2: Rudder Position

as follows (cf [21]):

$$m(\dot{v} + U_0 r + x_G \dot{r}) = Y \tag{3.4}$$

$$I_Z \dot{r} + m x_G (\dot{v} + U_0 r) = N \tag{3.5}$$

where v is the velocity along the y axis and r is the turning rate around the z axis assuming the sign conventions of a direct frame. The direct frame chosen is the frame illustrated on Figure (3-1). The following linear decomposition of the hydrodynamic forces and moments is used, keeping only the first order terms:

$$Y = Y_{\dot{v}} \dot{v} + Y_{\dot{r}} \dot{r} + Y_v v + Y_r r + Y_\delta \delta_R \tag{3.6}$$

$$N = N_{\dot{v}} \dot{v} + N_{\dot{r}} \dot{r} + N_v v + N_r r + N_\delta \delta_R \tag{3.7}$$

where δ_R is the rudder angle, **positive if the rudder is turned to port**. The rudder angle sign is illustrated on Figure (3-2).

The yaw-sway equations can also be written in the following matrix form:

$$\mathbf{M}\begin{bmatrix} \dot{v} \\ \dot{r} \end{bmatrix} + \mathbf{N}\begin{bmatrix} v \\ r \end{bmatrix} = \mathbf{b}\delta_R \tag{3.8}$$

the matrices being :

$$\mathbf{M} = \begin{bmatrix} m - Y_{\dot{v}} & mx_G - Y_{\dot{r}} \\ mx_G - N_{\dot{v}} & I_Z - N_{\dot{r}} \end{bmatrix}, \quad \mathbf{N} = \begin{bmatrix} -Y_v & mu_0 - Y_r \\ -N_v & mx_G u_0 - N_r \end{bmatrix}, \quad \mathbf{b} = \begin{bmatrix} Y_\delta \\ N_\delta \end{bmatrix} \tag{3.9}$$

From those equation, the **state-space model** of yaw-sway movements is:

$$\mathbf{x} = \mathbf{A} \cdot \mathbf{x} + \mathbf{b_1} \cdot \delta_R \tag{3.10}$$

where $\mathbf{x}$ is the state-space vector $\mathbf{x} = [v, r]^T$ and $\mathbf{A}$ and $\mathbf{b_1}$ are defined below:

$$\mathbf{A} = -\mathbf{M^{-1}} \cdot \mathbf{N}, \qquad \mathbf{b_1} = \mathbf{M^{-1}} \cdot \mathbf{b} \tag{3.11}$$

3.2 The Models of Nomoto

For more details about the models of Nomoto, references [10], [3] and [21] can be consulted.

3.2.1 Nomoto's Second Order Model

To obtain a direct relationship between the rudder angle δ_R and the turning rate r, the sway velocity can be eliminated in the two-variable Equations (3.4) and (3.5).
Thus, the Nomoto's second order transfer function between r and δ_R can be obtained:

$$\frac{r}{\delta_R}(s) = \frac{K_R(1 + T_3 s)}{(1 + T_1 s)(1 + T_2 s)} \tag{3.12}$$

The parameters K_R, T_1, T_2 and T_3 of Nomoto's equation are defined by the following equations:

$$T_1 T_2 = \frac{det(M)}{det(N)} \tag{3.13}$$

$$T_1 + T_2 = \frac{n_{11}m_{22} + n_{22}m_{21} - n_{12}m_{21} - n_{21}m_{12}}{det(N)} \tag{3.14}$$

$$K_R = \frac{n_{21}b_1 - n_{11}b_2}{det(N)} \tag{3.15}$$

$$K_R T_3 = \frac{m_{21}b_1 - m_{11}b_2}{det(N)} \tag{3.16}$$

with m_{ij} and n_{ij} and b_i are the elements of the matrices **M**, **N** and **b** defined in Equation (3.9). Now, looking at how the angles have been defined (cf Figure (3-2)), a positive rudder deflection implies a negative turning rate. However, the remote control system of the ship model was designed such that the rudder angle is positive when the two rudders are turned to starboard, so that when the rudder angle is positive the turning rate of the boat is also positive. Consequently, in order to design a controller that is compatible with those requirements, the following modified model will be used:

$$K = -K_R, \qquad \delta = -\delta_R \tag{3.17}$$

The time domain equation for the turning rate r is:

$$T_1 T_2 \ddot{r} + (T_1 + T_2)\dot{r} + r = K(\delta + T_3\dot{\delta}) \tag{3.18}$$

The transfer function between r and δ is:

$$\frac{r}{\delta}(s) = \frac{K(1 + T_3 s)}{(1 + T_1 s)(1 + T_2 s)} \tag{3.19}$$

The transfer function between δ and the heading angle ψ ($\dot{\psi} = r$) is:

$$\frac{\psi}{\delta}(s) = \frac{K(1 + T_3 s)}{s(1 + T_1 s)(1 + T_2 s)} \tag{3.20}$$

Consequently, Nomoto's second order model is represented mainly by 4 coefficients:

- **three time constants**: T_1, T_2 and T_3. Usually, T_1 is bigger than T_2 and T_3. Also, T_2 and T_3 are of the same order.

- **one turning ability** coefficient K.

3.2.2 Nomoto's First Order Model

The simplification of the previous model was made by Nomoto and al. on the assumption that steering motions of ships are substantially **first order phenomena**. Consequently, the unique time constant T has to be chosen so that the first order simulating system coincides with the ultimate phase of the second order model. Nomoto and al. (cf. [10]) showed that the resulting simulation is satisfactory for a ship with relatively small T_1.
The goal of this first order model is to describe the steering qualities of ships with only two fundamental indices:

- an index of **turning ability** (K),
- an index of **quick response in steering and the dynamic stability** on course (T)

Nomoto's first order model is simply obtained by approximating the previous model using the **effective time constant** $T = T_1 + T_2 - T_3$. The equations of this model are:

- **Time domain equation**:

$$T\dot{r} + r = K\delta \qquad \text{or} \qquad T\ddot{\psi} + \dot{\psi} = K\delta \tag{3.21}$$

- **Transfer function equation**:

$$\frac{r}{\delta}(s) = \frac{K}{Ts+1} \qquad \text{or} \qquad \frac{\psi}{\delta}(s) = \frac{K}{s(Ts+1)} \tag{3.22}$$

However, according to [3], the first order model should only be used at low frequencies.

The models of Nomoto are very simple models and thus very useful to describe the heading as a function as the rudder angle. The next step in building the controller is to find the K and T coefficients using the hydrodynamic coefficients of the model DDG51 and experiments realized in [17].

3.3 Hydrodynamic Coefficients

The Nomoto model coefficients can be obtained in two ways:

- using Slender Body Theory (SBT) to compute the Nomoto's coefficients,
- using the data from tests performed on the ship model at Hanscom swimming pool.

Another way to obtain the ship model coefficients would be to use the hydrodynamic coefficients of the real ship, given in [14] and [18]. The real ship data are summarized in Appendix A.

3.3.1 Nomoto's Coefficients from SBT

The hydrodynamics parameters of the ship model can be estimated using **Slender Body Theory** (SBT) was used to find estimations of the parameters. For more details on SBT, see [21] and [9]. A brief summary of SBT and the methods used to obtain the hydrodynamic coefficients is given in Appendix E.
The formulae used to compute SBT approximations are:

$$Y_v = -Um_a(x_t) \tag{3.23}$$

$$Y_{\dot{v}} = -m_{22} \tag{3.24}$$

$$Y_r = -Ux_t m_a(x_t) \tag{3.25}$$

$$Y_{\dot{r}} = m_{26} \tag{3.26}$$

$$N_v = -U(x_t m_a(x_t) + m_{22}) \tag{3.27}$$

$$N_{\dot{v}} = m_{26} \tag{3.28}$$

$$N_r = -U(x_t^2 m_a(x_t) - m_{26}) \tag{3.29}$$

$$N_{\dot{r}} = -m_{66} \tag{3.30}$$

Actually, there are three ways to compute the hydrodynamic coefficients of the ship model:

1. using the full SBT, which means use the approximation of SBT to compute m_{26} and m_{66} and the stern added mass $m_a(x_t)$. This method will be referred to as method 1,
2. using equipment weight and position inside the boat to evaluate m_{26}, m_{66} and $m_a(x_t)$ and then use SBT equations to determine the hydrodynamics coefficients (method 2),
3. using the real ship hydrodynamic coefficients (given in Appendix A), and non-dimensionalize them using the method presented in Appendix F.

ND Coefficient	Method 1	Method 2	Error [1]	Real Ship	Error [2]
x'_G	-0.00625	-0.00625	0 %	-0.0059842	4.3 %
m'	0.005249	0.005249	0 %	0.005876	12 %
I_{zz}	0.00041723	0.00041723	0 %	0.00078364	88 %
$(Y_v/U)'$	-0.0069029	-0.0044922	35 %	-0.010816	56.7 %
$(Y_{\dot{v}})'$	-0.0069029	-0.0038452	44.3 %	-0.0047567	31.1 %
$(Y_r/U)'$	0.0035593	0.0023163	35 %	0.0028569	19.7 %
$Y'_{\dot{r}}$	0	0	0 %	0	0 %
$(N_v/U)'$	-0.0033436	-0.00125289	54.3 %	- 0.0010017	70 %
$N_{\dot{v}'}$	0	0	0 %	0	0 %
$(N_r/U)'$	-0.0018353	-0.0011943	35 %	-0.0009756	46.8 %
$N'_{\dot{r}}$	-0.00057524	-0.00028014	53 %	-0.00027083	52.9 %
Y_δ/U^2	0.0023969	0.0023969	0%	0.0025008	4.34 %
N_δ/U^2	-0.0011984	-0.0011984	0%	-0.0011802	1.52 %
C'[3]	$8.19 \cdot 10^{11} > 0$	$4.68 \cdot 10^{-12} > 0$	—	$8.014 \cdot 10^{-11} > 0$	—

Table 3.1: Values of Dimensional and ND Hydrodynamic Parameters of the Scaled Boat

However, in case one and two, the values of the mass m, the rotational moment of inertia I_{zz} and the position of the center of gravity x_G were computed using the weight and position of each element of the boat system. The values of the dimensional and non-dimensional (ND) coefficients can then be computed. The results are presented in Table (3.1). In the same table is also presented the value of the **non-dimensional stability parameter** defined as follows:

$$C' = (I'_{zz} - N'_{\dot{r}})Y'_{v,U}(m' - Y_{\dot{v}})(N_{r,U} - m'x'_G) - \left[N_{\dot{v}'}Y'_{v,U} + (m' - Y'_{\dot{v}})N'_{v,U}\right] \cdot \ldots$$
$$\ldots \left[-(I_{zz} - N_{\dot{v}})(m' - Y'_{r,U}) + Y'_{\dot{r}}(N'_{r,U} - m'x'_G)\right] \quad (3.31)$$

where $Y'_{r,U} = (Y_r/U)'$ and so on. Using the fact that for the three models both $Y_{\dot{r}} = 0$ and $N_{\dot{v}} = 0$:

$$C' = (I'_{zz} - N'_{\dot{r}})(m' - Y'_{\dot{v}})\left[Y'_{v,U}(N'_{r,U} - m'x'_G) + (m' - Y'_{r,U})N'_{v,U}\right] \quad (3.32)$$

The stability of the ship requires $\mathbf{C' > 0}$.

The comparison between Nomoto's non-dimensional second and first order models are shown on Figures 3-3 for both the ship model (coefficients from method 1) and the full-size ship. In

[1]Error between full SBT and SBT+Estimation
[2]Error between the full SBT method and the Real ship non-dimensional coefficients
[3]Non-dimensional stability parameter

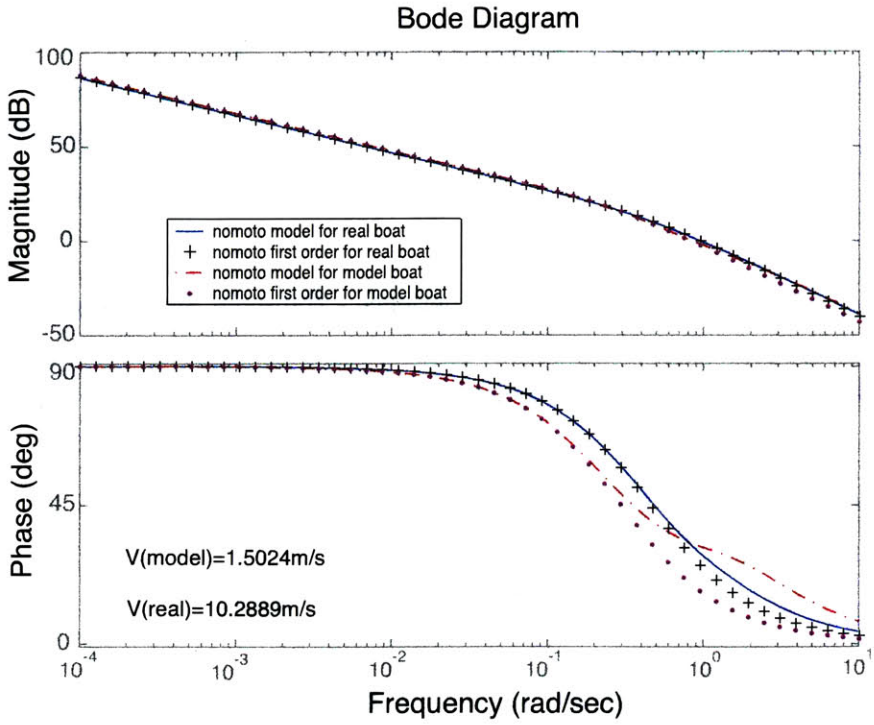

Figure 3-3: Comparison between the first and second order Nomoto models

fact, as The coefficients used for the ship model are the full SBT coefficients. The difference between the first and the second order model appears at high frequencies, which do not influence much the boat behavior.

3.3.2 Nomoto's Coefficients from Model Experiments

The Data from the experiments carried out at the Hanscom Swimming Pool (cf. [17]) were used. The experiments used here are: boat going going straight for $0 < t < t_1$, at $t = t_1$ the rudder is turned of an angle $\delta = \delta_1$ and at $t = t_{end}$ the boat is stopped around 10 seconds after the the rudder started turning (there was not enough place in the swimming pool for the boat to turn completely). Those experiments were carried out for different values of RPM's and different rudder angles (cf. Figure (3-4)).
The list of the experiments used for evaluating the Nomoto's coefficients are given in Table (3.2).

The yaw rate data given by the DMU was used to find the transfer function $r(s)/\delta(s)$. It is supposed that at $t = t_1$ the rudder angle is given a step input: $t \leqslant 0 \quad \delta = 0, \quad t \geqslant 0 \quad \delta = \delta_1$,

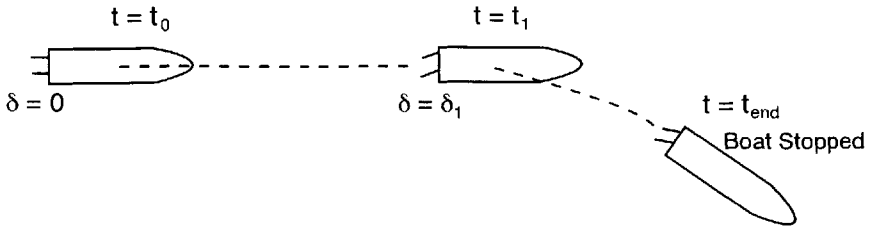

Figure 3-4: Ship Model Experience - Hanscom Swimming Pool

which can be written using transfer function: $\delta(s) = \frac{\delta_1'}{s}$, where here $\delta_1' = \delta_1$ but δ_1' is in deg/s or rad/s.

Using Nomoto's first order transfer function (Equation (3.22)):

$$r(s) = \frac{K \cdot \delta_1'}{s(Ts+1)} \quad \rightarrow \quad r(t) = K\delta_1(1 - e^{-t/T}) \tag{3.33}$$

Plots of the yaw rate were analyzed and a curve fitting with $r(t) = K_1(1 - e^{t/K_2})$ was done on the yaw rate plot of each experiment described in Table (3.2). K and T are easily obtained: $K = \frac{K_1}{\delta_1}$ and $T = K_2$. Since the yaw rate plots are in deg/s, K_1 is also in deg/s. The yaw rate plots are presented in Appendix G. The values of K an T are summarized in Table (3.2). The non-dimensional first order Nomoto model is compared to the first and second order models for the real ship on 3-5. Since only the coefficients of the first order Nomoto model could be estimated from the experiments, only the first order Nomoto model for the ship model is presented on the figure.

3.4 Designing the Heading Controller

3.4.1 Choice of the Type of Controller

A heading controller is also called a course-keeping autopilot. This autopilot uses feedback from a sensor which measures the actual heading of the ship and then compares it to the desired heading. The controller output is a position command for the rudder. The working of the controller is illustrated on Figure (3-6) . The sensor could either be the GPS or the magnetometer. The magnetometer was chosen because GPS signals are not received in the Towtank or in the MIT pool.

First a PID controller was built. PID stands for **P**roportional-**I**ntegral-**D**erivative. This type of

List of the experiments			
RPM	Rudder angle	t_1 (s)	t_{end} (s)
400	10	10	15
400	20	10	20
500	10	8	16
500	20	8	16
500	30	8	16
500	40	8	16
600	20	15	30
600	30	15	30
800	10	15	30
800	20	15	30
800	30	10	25

Values of K and T					
RPM	δ_1 (deg.)	K_1	K_2	**K**	**T**
400	10	1.9	4.5	**0.190**	**4.5**
400	20	3.7	3.5	**0.185**	**3.5**
500	10	2.6	5	**0.260**	**5.0**
500	20	4.7	3.5	**0.235**	**3.5**
500	30	5.9	2.4	**0.197**	**2.4**
500	40	7.5	1.9	**0.185**	**1.9**
600	20	6.2	2.1	**0.310**	**2.1**
600	30	8.4	2.1	**0.280**	**2.1**
800	10	5	2.5	**0.500**	**2.5**
800	20	8.6	1.6	**0.430**	**1.6**
800	30	9.5	1.5	**0.475**	**1.5**

Table 3.2: Experimental evaluation of the K ans T coefficients

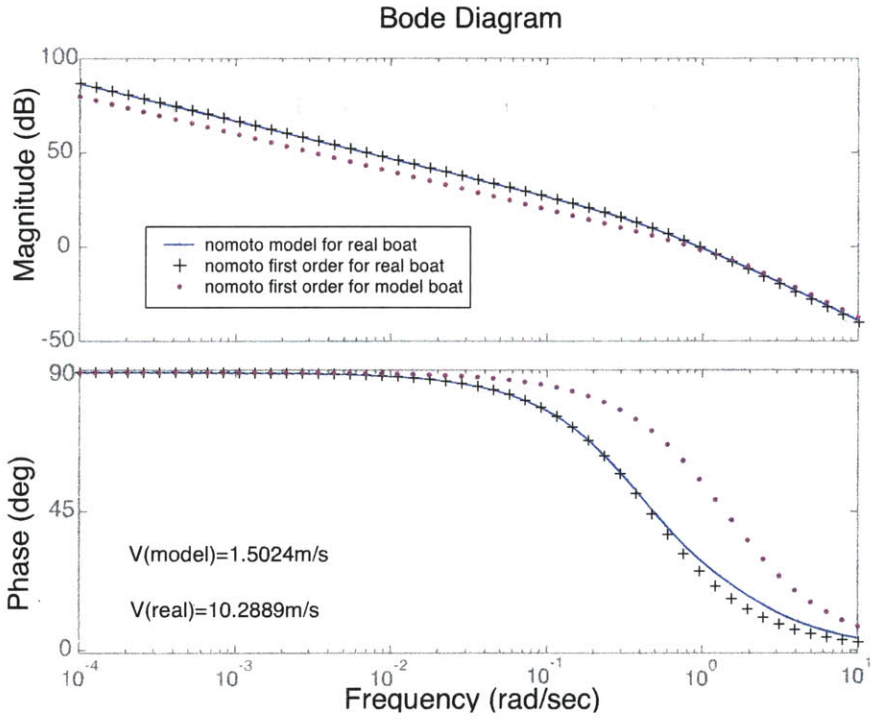

Figure 3-5: Comparison between the first and second order Nomoto models

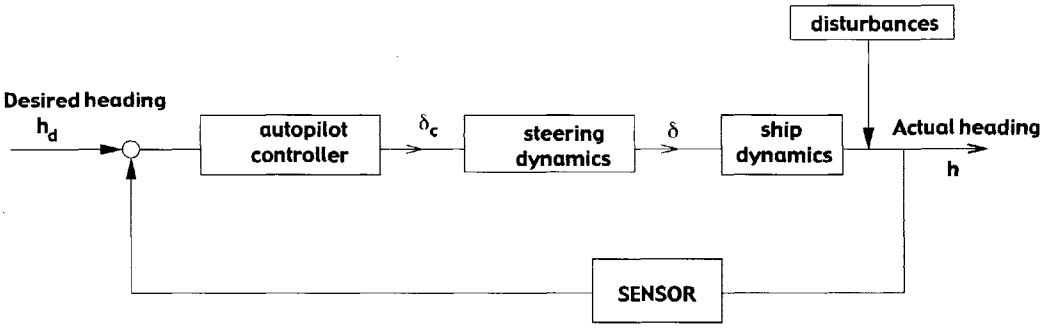

Figure 3-6: Heading controller

controller is one of the most basic and consequently can be implemented very easily, especially on a computer.

3.4.2 Controller Equations and Parameters

The time-domain equation representing the dynamics of the controller can be written in the following form:

$$\delta = K_p(\psi_d - \psi) - K_d\dot{\psi} + K_i \int_0^t (\psi_d - \psi(\tau))d\tau \tag{3.34}$$

where $K_p > 0$, $K_d > 0$ and $K_i > 0$ are respectively the proportional, derivative and integral **gain.**

The transfer function of the controller can also be obtained, as shown in *equation 3.35*:

$$\delta = K_p(1 + \tau_d s + \frac{1}{\tau_i s})(\psi_d - \psi) \tag{3.35}$$

where $\tau_d = K_d/K_p$ and $\tau_i = K_i/K_p$ are respectively the derivative and time constants.

The principal asset of the PID controller compared to more simple controller like P or PD controllers is that the integral part allows to get rid of **steady disturbances** due to wind, current and wave drift.

The most difficult part is of course choosing adequately the three proportional constants so that the controller stabilizes the boat. K_p and K_d can be computed using a PD controller model (cf. [3]):

$$K_p = \frac{T\omega_n^2}{K}; \qquad K_d = \frac{2T\zeta\omega_n - 1}{K} \tag{3.36}$$

where the relative damping ratio ζ is chosen such a $0.8 \leq \zeta \leq 1.0$. As for the natural frequency, it is limited by the bandwidth of the rudder noted ω_δ (rad/s) and by the ship dynamic frequency 1/T (rad/s), T being the Nomoto time constant:

$$1/T \quad < \quad \omega_b = \omega_n \sqrt{1 - 2\zeta^2 + \sqrt{4\zeta^4 - 4\zeta^2 + 2}} \quad < \quad \omega_\delta \tag{3.37}$$

ω_b being the closed-loop bandwidth.
A rule of thumb given by [3, section 6.3] can be used to determine K_i:

$$\frac{1}{T_i} \approx \frac{\omega_n}{10} \tag{3.38}$$

where ω_n is the natural frequency of the system.

3.5 Adapting the Controller

The goal of this section is to show how the controller can be adapted to specific operating conditions.

3.5.1 Gain Scheduling

The yaw-sway dynamics of the boat change with the operating conditions, mainly the forward velocity and the rudder angle. However, a standard heading controller as described above is designed for specific operating conditions. A good way to compensate for variations in process parameters is to changing the parameters of the controller by monitoring the operating conditions. This method is called **gain scheduling**. It is a non-linear feedback of special type : it has a linear controller whose parameters are changed as a function of the operating conditions. One of the advantage of gain scheduling is that it is particularly easy to implement in a computer controlled system. Gain scheduling is a type of **adaptative controller**, it can be viewed as a feedback control system in which the feedback gains are adjusted using feedforward compensation, as illustrated in Figure (3-7). Gain scheduling is the foremost method used for handling parameters variations in flight control systems. For more details on Gain Scheduling see [20] and [15].

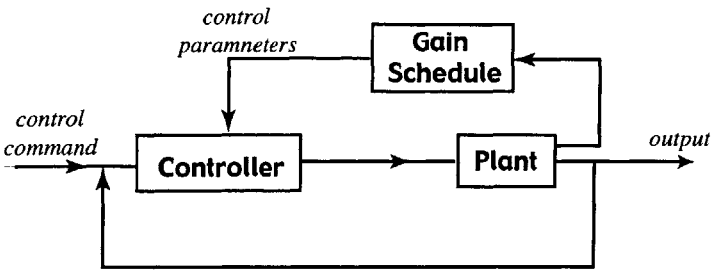

Figure 3-7: Gain scheduling controller

3.5.2 The Parameters Which Influence the Controller

In the case of the heading controller, the controller regulates the yaw rate of the boat and is defined for a given velocity and rudder angle. Consequently, the three controller PID gains should be written: $K_p(U, \delta_0)$, $K_d(U, \delta_0)$ and $K_i(U, \delta_0)$. To obtain those coefficients, the boat linearized equations around the operating point (U, δ_0) are needed.
Moreover, when the rudder angle is not zero, r and v are also affected:

$$r = r_0 + r' \quad \text{with } v' \ll v_0 \quad \text{and } v_0 = \frac{N_v Y_\delta - Y_v N_\delta}{N_v(mU - Y_r) - Y_v(mx_g U - N_r)} \cdot \delta_0 \tag{3.39}$$

$$v = v_0 + v' \quad \text{with } r' \ll r_0 \quad \text{and } r_0 = \frac{(mx_g U - N_r)Y_\delta + (Y_r - mU)N_\delta}{N_v(mU - Y_r) - Y_v(mx_g U - N_r)} \cdot \delta_0 \tag{3.40}$$

where r_0 and v_0 are respectively the steady yaw rate and the steady sway velocity produced by the rudder angle δ_0.
The equations of motions linearized around (U,v_0, r_0,δ_0) have the same form as the ones linearized around ($U, r = 0, v = 0, \delta_0 = 0$) except that the Y and N hydrodynamic coefficients are different, they are the derivatives around $v_0 \neq 0$ and $r_0 \neq 0$:

$$(m - Y_{\dot{v}_0})\dot{v} + (mx_G - Y_{\dot{r}_0})\dot{r} - Y_{v_0}v + (mU - Y_{r_0})r = Y_{\delta_0}\delta \tag{3.41}$$

$$(mx_G - N_{\dot{v}_0})\dot{v} + (I_{zz} - N_{\dot{r}_0})\dot{r} - N_{v_0}v + (mx_G U - N_{r_0})r = N_{\delta_0}\delta \tag{3.42}$$

If more data were available, the hydrodynamic coefficients mentioned above could be computed using the non linear derivatives, as shown below for Y_v:

$$Y_{v_0} = Y_{v=0} + v_0 \cdot Y_{vv(v=0)} + r_0 \cdot Y_{v=0,r=0} \tag{3.43}$$

As a consequence, only the influence of the forward velocity U on the controller coefficients was studied.

3.5.3 Study of the Influence of the Forward Velocity

Going back to Equation (3.9), the matrix N can be rewritten in the following form:

$$\mathbf{N} = U \cdot \begin{bmatrix} -\frac{Y_v}{U} & m - \frac{Y_r}{U} \\ -\frac{N_v}{U} & mx_G - \frac{N_r}{U} \end{bmatrix} \tag{3.44}$$

where all the coefficients inside the matrix are now independent of U, if the hydrodynamic coefficients Y_v, Y_r, N_v and N_r are supposed linear function of U as it is teh case in this study. As for the matrix **b** of Equation (3.9), it can be rewritten:

$$\mathbf{b} = U^2 \cdot \begin{bmatrix} \frac{Y_\delta}{U_2} \\ \frac{N_\delta}{U^2} \end{bmatrix} \tag{3.45}$$

The Nomoto's coefficients of Equation (3.13) to Equation (3.16) can be rewritten:

$$T_1 T_2 = \frac{1}{U^2}(T_1 T_2)_0 \tag{3.46}$$

$$T_1 + T_2 = \frac{1}{U}(T_1 + T_2)_0 \tag{3.47}$$

$$K_R = U \cdot K_{R_0} \tag{3.48}$$

$$K_R T_3 = (K_R T_3)_0 \tag{3.49}$$

where $(T_1 T_2)_0$, $(T_1 + T_2)_0$, K_{R_0} and $(K_R T_3)_0$ are variables independent of the forward velocity U.

Consequently, the two Nomoto's first order parameters have an explicitly dependence on U:

$$K = U \cdot K_0, \qquad T = \frac{T_0}{U} \tag{3.50}$$

Parameter	Real Ship	Ship Model		
		Method 1	Method 2	Exp.
Second Order Model				
T_1'	2.346	3.789	18.393	—
T_2'	0.6686	0.4686	0.4698	—
T_3'	0.8160	0.8894	1.1958	—
First Order Model				
T'	2.098	3.3682	17.667	0.994
K'	2.136	2.398	12.3298	0.714

Table 3.3: Non-dimensional values of K and T for different models

where K_0 and T_0 are independent of U.

To compare different ships, the non dimensional values of K and T have to be computed:

$$K' = \frac{L}{U} \cdot K, \qquad T' = \frac{U}{L} T \tag{3.51}$$

3.5.4 Finding the Parameters K_0 and T_0

The values of the two Nomoto's first order "modified" coefficients K_0 and T_0 can be obtained using the data of Table (3.5). However, the velocity of the boat as a function of the motors RPM has to be known. The RPM vs velocity values are presented in Table (3.4), the measurements where made during experiments at the MIT Towing Tank done by Stoffel. The RPM velocity curve was approximated by the following equation:

$$U \text{ [m/s]} = 7.6 \times 10^{-7} \cdot \text{RPM}^2 + 0.0011 \cdot \text{RPM} \tag{3.52}$$

The values of K_0 and T_0 were obtained by taking the mean of the different K_0 and T_0 values computed from the data of Table (3.5). The different K_0 values are relatively constant with a slight tendency to decrease when the rudder angle δ increases. As for T_0, the deviation from the mean value is more important than for K_0 and it is clear that T_0 decreases significantly when δ increases. However, not enough data was available to quantify the dependence on the rudder angle.

Consequently, for the rest of the controller design process, it was supposed that K_0 and T_0 are

RPM	Velocity (m/s)			
	Test 1	Test 2	Test 3	Mean
300	0.386	0.495	0.437	**0.439**
400	0.649	0.624	0.592	**0.622**
500	0.744	0.736		**0.740**
600	0.903	0.980		**0.942**
700	1.156			**1.156**
800	1.430			**1.430**

Table 3.4: RPM - Forward Velocity Correspondence

RPM	δ_1 (deg.)	v (m/s)	K_0	T_0
400	10	0.62	0.3065	2.79
400	20	0.62	0.2984	2.17
500	10	0.74	0.3514	3.7
500	20	0.74	0.3176	2.59
500	30	0.74	0.2658	1.78
500	40	0.74	0.25	1.41
600	20	0.94	0.33	1.97
600	30	0.94	0.263	1.97
800	10	1.43	0.35	3.57
800	20	1.43	0.30	2.28
800	30	1.43	0.33	2.15
Mean			**0.306**	**2.32**

Table 3.5: Nomoto's constants from experiments

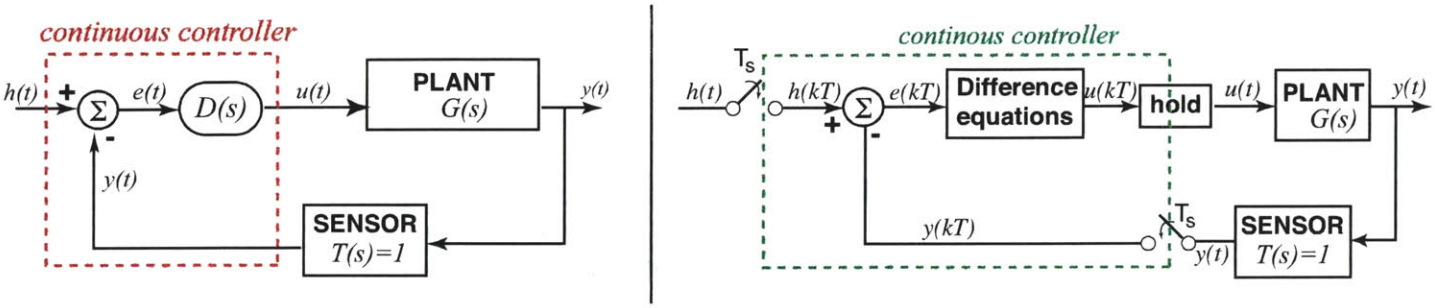

Figure 3-8: Difference between a continuous and a digital controller

independent of the rudder angle and:

$$K = U \cdot K_0 = U \cdot 0.306, \qquad T = \frac{T_0}{U} = \frac{2.32}{U} \tag{3.53}$$

Knowing the values of K and T as a function of the RPM, the three controller gains are then obtained using the Equations (3.36) and (3.38).

3.6 Discrete Controller

3.6.1 Why Discretize the Controller?

The heading controller designed for the boat depends on the heading data given by the magnetometer. However, the magnetometer is sampled at the certain rate (maximum rate being 100 Hz). Consequently, the signal feeding the controller is discretized every T_s, if T_s **is the sampling period**. Moreover, the controller being implemented on the PC104 is a digital controller by nature and thus uses **difference equations**. The differences between a continuous and a **digital controller** are illustrated on Figure (3-8).

The discrete signal coming out of the controller is seen by the continuous plant as **"hold"** in between the discrete values. The discretization and holding process is illustrated in Figure (3-9).The sampling and holding process is illustrated on Figure (3-9).

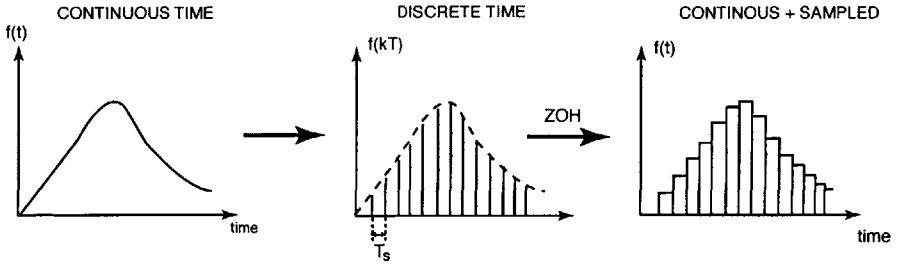

Figure 3-9: Sampling and Holding Process

3.6.2 Equations for the Discrete Controller

The time-continuous transfer function of a PID controller being:

$$C(s) = K_p + K_d s + \frac{K_i}{s} = K_p(1 + \tau_d s + \frac{1}{\tau_i s}), \qquad \tau_d = \frac{K_d}{K_p}, \quad \tau_i = \frac{K_p}{K_i} \tag{3.54}$$

The discrete-time transfer function of the same controller is:

$$C(z) = K_p^d + \frac{K_i^d}{1 - z^{-1}} + K_d^d(1 - z^{-1}) \tag{3.55}$$

where the superscript d stands for discrete. The discrete gains K_p^d K_p^d and K_p^d are related to the time-continuous gains by the following relations:

$$K_p^d = K_p - K_i^d \tag{3.56}$$

$$K_i^d = \frac{K_p T_s}{T_i} = K_i T_s \tag{3.57}$$

$$K_d^d = \frac{K_p T_d}{T_s} = \frac{K_d}{T_s} \tag{3.58}$$

where T_s is the sampling time of the discrete controller.

3.7 Evaluating the Controller Robustness

Due to the great uncertainties on the plant model, the design of the controller has to be **robust**. Robustness will assure that the controller will be adapted even if the real plant differs from the plant model.

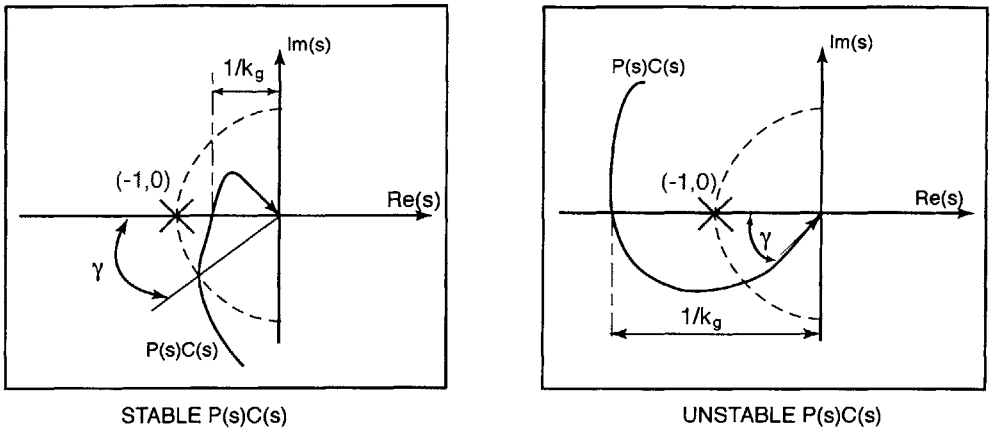

Figure 3-10: Gain and Phase Margin Definitions

3.7.1 Measures of the Robustness

There are two measures of the robustness of a system, both using the **Nyquist plot**. The Nyquist plot is a plot of the open loop transfer function $P(s)C(s)$ ($P(s)$ transfer function of the plant and $C(s)$ transfer function of the controller): $\mathcal{I}m(P(s)C(s))$ is plotted versus $\mathcal{R}e(P(s)C(s))$ when $s = i \cdot \omega$, $\omega \in [-\infty + \infty]$.
For robustness, the $P(s)C(s)$ curve needs to stay away from the **critical point** $(-1, 0)$. This can be expressed in terms of magnitude and angle using the two following definitions:

- the **gain margin** $\mathbf{k_g}$, which is a measure of the magnitude of $|P(s)C(s)|$ when the angle is 180°,
- the **phase margin** γ, which is a measure of the angle of $P(s)C(s)$ when the magnitude of $|P(s)C(s)|$ is 1.

Both are illustrated on Figure (3-10).

The requirements for robustness on the values of k_g and γ differ if the transfer function P(s)C(s) is stable or not:

- **Stable P(s)C(s)**: $k_g \geq 2$ and $\gamma \geq 30°$
- **Unstable P(s)C(s)**: $k_g \geq 0.5$ and $\gamma \geq 30°$

The robustness was checked modeling the controller on Matlab. For the model to be fully accurate, not only matlab function for discretizing need to be used but also the steering plant needs to be modeled and added to the Nomoto plant to form the full plant system.

3.7.2 Implementing Rudder Limitations

The rudder angle limitation is implemented in several ways: first there is a **mechanical limitation** on the rudder system itself, which prevents the rudders to bump into the propellers. This mechanical limitations is around 75° from both sides of the 0° position.
There are also three **software limitations**: the first one is a position limitation put on the MEI card axis controlling the rudder angle. The second one is implemented on the graphical interface: the rudder command sent to the MEI card is in the range [-35 , 35] degrees. The limiting values were chosen according to the limitations on the real ship rudder angle. The third limitation is in the heading thread-code: the output of the discrete controller equations is checked and a [-35 , 35] degrees limitation is implemented on the output of the controller.

As for the rudder rotation rate, it is set by the parameters sent to the MEI card when the rudder is remote controlled. The velocity used for the rudder rotation movements is counts/s; the velocity used for the rudder movements is 50000 counts/s i.e. 25 rps. Moreover, a rate limitation also has to be implemented in the heading controller, between two consecutive rudder angle commands.
Reference [3] gives the following limitations (for full scale ships):

$$\frac{2}{3} \leq \dot{\delta}_{max} \leq 7 \quad [\text{deg./s}], \qquad \dot{\delta}_{min} = 132.9\frac{U}{L} \quad [\text{deg./s}] \tag{3.59}$$

The limitations can be scaled using:

$$\dot{\delta}_{\text{ship model}} = \sqrt{\lambda} \cdot \dot{\delta}_{\text{real ship}}, \qquad U_{model} = \frac{U_{real}}{\sqrt{\lambda}} \tag{3.60}$$

The limitations are given in Table (3.6).

3.7.3 Analysis of the Matlab Program for Testing the Controller

The program proceeds as follows:

	Real Ship	Ship Model
$\dot{\delta}_{max}$	$0.67 \leq \dot{\delta}_{max} \leq 7$ [deg./s]	$4.6 \leq \dot{\delta}_{max} \leq 48$ [deg./s]
$\dot{\delta}_{min}$	$\dot{\delta}_{min} = 0.94 \cdot U_{real}$	$\dot{\delta}_{min} = 44.18 \cdot U_{model}$

Table 3.6: Rudder rotation rate limitations

Velocity (m/s)	0.38	0.75	1.13	1.5	1.88	2.25
$T_s = 0.5$ s						
k_g	66.8	27.3	15.3	10.1	7.3	5.7
ϕ (deg.)	108	102	93.3	84.3	74.4	64.7
$T_s = 0.1$ s						
k_g	331	138	74.1	45.7	29.9	21.1
ϕ (deg.)	109	104	97.3	90.4	83	75.7

Table 3.7: Ship Model Controller Robustness Characteristics

- enter the forward velocity U and compute Nomoto parameters K and T along with the plant TF P(s),
- compute the K_i, K_d and K_p continuous controller gains using Equations 3.36 and 3.38 and the controller TF C(s),
- compute the **steering plant TF** :

$$S(s) = \frac{\delta_{max}}{\frac{\dot{\delta}_{max}}{\delta_{max}} s + 1} \tag{3.61}$$

- compute the continuous close-loop transfer function S(s)P(s)C(s)/(1+S(s)P(s)C(s)),
- discretize each component to obtain the discrete transfer functions C(z) and S(z)P(z). C(z) is obtained using Equation (3.55), S(z)P(z) is computed using the "c2d" Matlab command with the "zoh" option.

The results are shown in the form of a step-response comparison between the continuous and the discrete close-loop models. The robustness and poles are obtained using the "sisotool" and "LTIviewer" Matlab toolboxes. Robustness is summarized in Table (3.7) and the poles are listed in Table (3.8). In those two tables the velocities corresponds to real ship velocities of 5, 10, 15, 20, 25 and 30 knots.

U (m/s)	$z = e^{T \cdot s}$, $s = -\omega_n\zeta \pm \omega_n\sqrt{1-\zeta^2}$											
	pole 1			pole 2			pole 3			pole 4		
	z	ω_n	ζ	z	ω_n	ζ	z	ω_n	ζ	z	ω_n	ζ
$T_s = 0.5$ s												
0.38	-0.00125	13.4	1	0.619	0.96	1	0.933	0.14	1	0.988 *pm* 0.0139i	0.04	0.65
0.75	-0.00219	12	1	0.628	0.93	1	0.879	0.26	1	0.978 *pm* 0.0284i	0.07	0.61
1.13	-0.00379	11.15	1	0.631	0.92	1	0.836	0.36	1	0.962 *pm* 0.0448i	0.12	0.64
1.5	-0.00508	10.56	1	0.622	0.95	1	0.812	0.42	1	0.948 *pm* 0.0627i	0.17	0.63
1.88	-0.00644	10.1	1	0.601	1.02	1	0.804	0.44	1	0.934 *pm* 0.0839i	0.23	0.61
2.25	-0.00778	9.71	1	0.571	1.12	1	0.806	0.43	1	0.922 *pm* 0.108i	0.28	0.57
$T_s = 0.1$ s												
0.38	$-4.46 \cdot 10^{-5}$	20.04	1	0.907	0.195	1	0.986	0.028	1	0.998*pm*0.0028	0.007	0.58
0.75	$-8.84 \cdot 10^{-5}$	18.7	1	0.908	0.193	1	0.975	0.051	1	0.995±0.00573	0.015	0.67
1.13	-0.000134	17.8	1	0.907	0.195	1	0.965		1	0.992 ±0.00904	0.024	0.66
1.5	-0.000178	17.3	1	0.904	0.202	1	0.959	0.084	1	0.99±0.0126	0.032	0.62
1.88	-0.000224	16.8	1	0.896	0.220	1	0.956	0.09	1	0.987±0.0169	0.04	0.61
2.25	-0.000269	16.4	1	0.887	0.240	1	0.956	0.09	1	0.985±0.0216	0.053	0.57

Table 3.8: Ship Model Controller Close-Loop Poles

3.8 Summary

This chapter presented the heading controller design procedure. The first step was to find a model which would represent accurately the **yaw dynamics** of the ship model. The model chosen was **Nomoto's first order model**.

Then, the second step was to evaluate the parameters of Nomoto's yaw rate model. Since the two parameters which define the yaw rate model are function of the ship hydrodynamic coefficients, the theoretical evaluation of these hydrodynamic coefficients was the first method investigated. Several ways of evaluation were compared, and since they did not led to good enough results another method was used. The experimental data obtained by Stoffel during tests in Hansom Air Force Base Swimming Pool were analyzed and the parameters of Nomoto's model were **extrapolated from yaw rate graphs.**

The final step was to actually build the heading controller. A simple **PID controller** was designed and then discretized and thus could be implemented easily on the on-board PC104. The final point was to make sure that the controller was **robust** enough to withstand some differences between the real yaw dynamics and the modeled dynamics.

Chapter 4

IMPLEMENTATION OF THE HEADING CONTROLLER

4.1 Boat Operating System

4.1.1 System Overview

The boat operating system is described in detail in [17]. Some modifications have been made to meet the requirements of heading control, and a brief summary of the modified system is given here.

The boat is controlled remotely from a laptop working under **Linux Redhat version 2.2.14** using **Real-Time Linux version 2.2** (called RTLinux in the following). The laptop exchanges commands and data with the PC104 (also operated under Linux Redhat and RT linux) located on the boat. The PC104 distributes the motor commands to the MEI motion control board which output voltage is amplified by amplifiers before finally being executed by the motors. All three motors are equipped with encoders, which allows the MEI motion control board to perform a PID close-loop control on the motors velocity and position.

The main modification that has been made is the **heading and rudder angle display** on the GUI. The heading visualization is very important for heading control but it was also necessary to perform such tests as the zigzag maneuver (cf. section 6.3.4). Moreover, the raw DMU data could also have been displayed on the GUI in real-time, but data transfer might slow

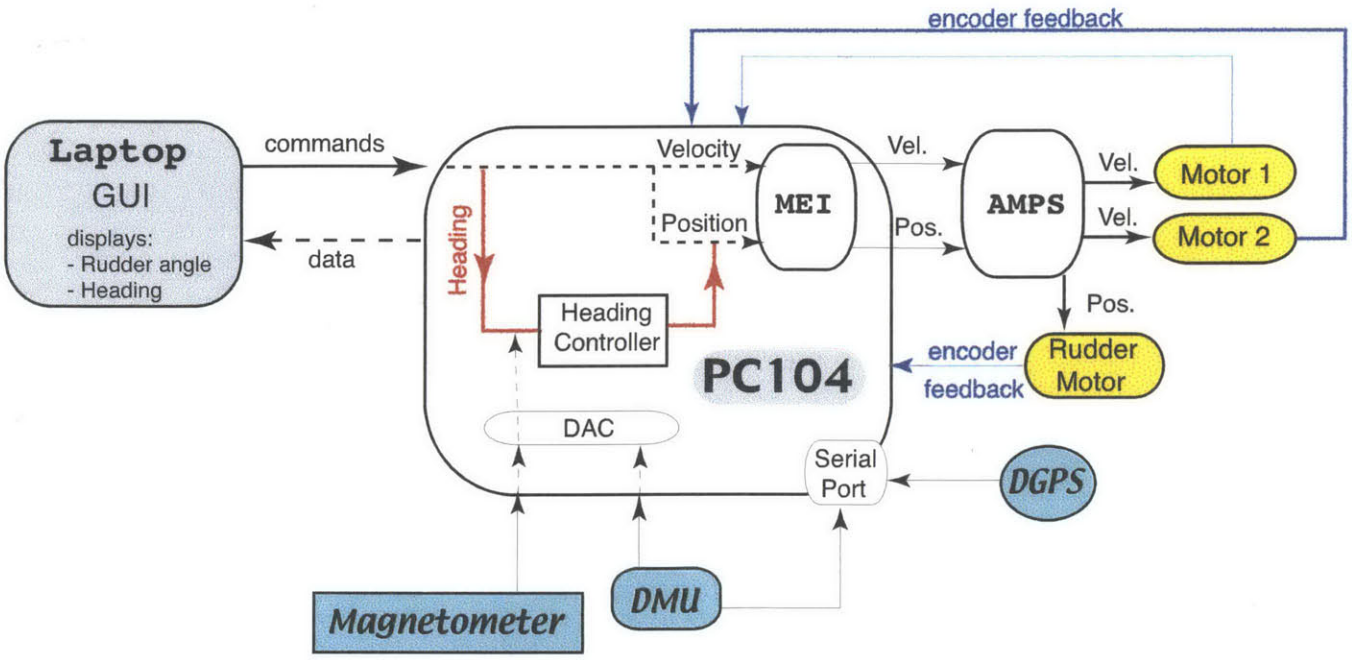

Figure 4-1: Boat Global Operating System

down the GUI and increase the risk of connection breaks between the Laptop and the PC104. The global operating system is illustrated on Figure (4-1).

4.1.2 System Components Description

Laptop GUI

The GUI running on the laptop was built using the developer program **KDevelop 1.2**. The GUI was written in C++ which brings all the easiness and flexibility of class design. The **Qt library** incorporated to KDevelop was also used, this library makes available very useful pre-designed classes such as radio-buttons, push-buttons, checkboxes and text-display devices. Those were widely used in the design of the GUI.

The transfer of data between the GUI and the PC104 uses **wireless communication** and **Real-Time (RT) Fifo's**. Both are described in the next paragraph.

The GUI has three working modes:

- **standard remote control mode**: the user can set remotely both the two motors RPM and the rudder angle. The two motors can be driven separately if needed, but actually this feature was never used. In this mode, the actual heading of the boat is displayed continuously on the GUI (the heading data come from magnetometer data).
- **heading control mode**: the user can set the two motors RPM and the heading of the boat. This mode uses the heading controller implemented on te PC104. While the heading control is on, the rudder angle cannot be changed by the operator.
- **macro mode**: the user can record a sequence of events, each event containing RPM commands for both main motors and either a rudder angle command or a heading command. Compared to the GUI of [17], an important feature was added: a macro could be written in advance in a standard text file and loaded from the GUI. This functionality saves time when many tests have to be performed: the operator does not have to enter by hand the macro just before each test.

The GUI window is shown on Figure (4-2). The heading is displayed in the circle on the right of the window like in a compass. he previous GUI built in [17] has also been kept operational and can be used as a spare application. The window of this GUI is shown on 4-3.

Real-Time Linux

Three important features of RT Linux were used:

- **Real Time Fifo's**: **F**irst **I**n **F**irst **O**ut queues that can be read from and written to by Linux processes and RTLinux threads. Fifo's are **unidirectional**, however a pair of Fifo's can be used for bi-directional data exchange. They are used to buffer data between one process and another. Normally, a fifo is open for *read* by one process and for *write* by another. When the *write* process is ready to add data to the buffer it does so without having to wait for the *read* process to be ready.

  RT Fifo's are Linux character devices with a major number of 150. Device entries in /dev are created during system installation. The device file names are **/dev/rtf0** through **/dev/rtf63**.

  Before a real-time Fifo can be used, it must be created and once it is not needed anymore, it must be destroyed. Fifo's can only be created and destroyed from RT process.

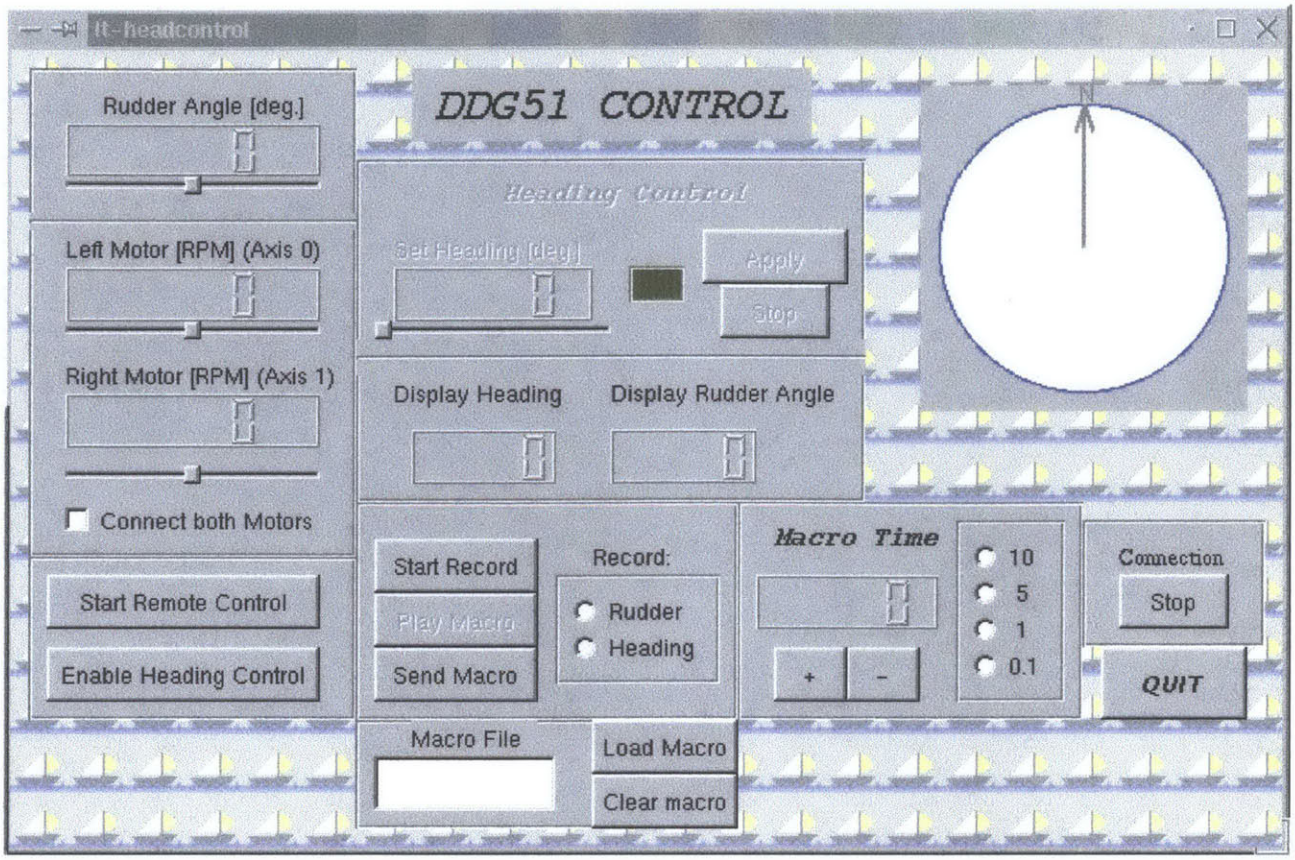

Figure 4-2: Ship model Graphical User Interface (on Laptop)

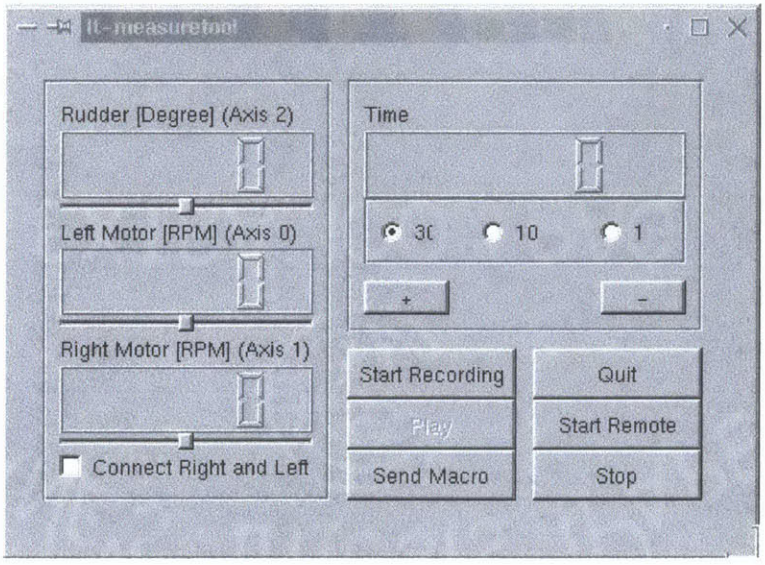

Figure 4-3: Ship model GUI from [17]

Fifo's are accessed by standard Linux processes using the read and write functions and they are accesses by RT processes using the rtf_get and rtf_write processes.
A Fifo can be linked to a **handler function** which will be called each time data is written in the Fifo.
All the Fifo's are described in Table (4.2) (Laptop Fifo's) and Table (4.3) (PC104 Fifos).

- **Thread**: threads are light-weight processes which share a common address space. A thread represents a RT task. When a thread is created, it is linked to its **thread function**, which contains all the operations the RT task has to perform.

- **Modules**: a module is simply an object file created from a .c file. However, the usual main function of the .c file is replaced by:

  - an init_module function where the Fifo's and threads are created and liked to their handler function or thread function,
  - a clean_module function where all Fifo's and threads are deleted.

  A module is loaded using the insmod modulename.o command and removes using the rmmod modulename.

Data Exchange

First, the wireless connection enables the operator to launch a "ssh" session on the Laptop and to log on remotely on the PC104. The PC104 can thus be controlled via a window terminal on the Laptop.
Fifo's are exchanged via the wireless cards and the use of cat and netcat programs. cat simply reads a file and writes the content in the default standard output (the terminal) or to a specified output; netcat works the same way but via the wireless connection. Sending a command from computer A (outgoing side) to computer B (incoming side) is done as follows:

- **Outgoing side**: cat /dev/rtf15 | netcat computerB 7015 reads the file /dev/rtf15 on computer A and the output is used as input of netcat which send the content of /dev/rtf15 to computerB using the port # 7015 of computerA

- **Incoming side**: netcat -l -p 7015 computerA >> /dev/rtf15 means computerB listens to port 7015 of computerA and copy all data transfered through this port to the file

/dev/rtf15 on computerB. The ">>" sign makes sure that new data is added to the already existing file amd do no overwrite the previous data.

Data exchange is initialized via **two main shell scripts**, one on the PC104 and one on the Laptop. The actions performed by the shell scripts are illustrated on Figures 4-4 and 4-5. The shell scripts do all the necessary initialization procedures and especially call the secondary shell scripts. Each of the **secondary shell scripts** are responsible for a fifo exchange, using the commands explained above. Each of the scripts on one computer is related to a script on the other computer. The list of all the secondary shell scripts on each computer is given in Table (4.1), along with their mirror shell scripts on the other computer.

Data Acquisition

Data acquisition is made possible through the use of **Comedi** (Comedi and Measurement Device Interface). Comedi is a collection of hardware drivers, a common kernel interface and a support library for data acquisition. **kcomedilib** is the library used for RT tasks. This library is loaded the same way a RT module is.
Data logging is started when the main program is started from the PC104. The main program used is main.cpp is no GPS data are logged, maingps.cpp is GPS data are logged. There are four types of logfiles:

- Logfile 1: data from GPS,
- Logfile 2: data from the DAC, i.e. data from accelerometers, gyros and from the magnetometer,
- Logfile 3: actual position, velocity, acceleration and jerk of the two main motors and the rudder motor,
- Logfile 4: Position, velocity, acceleration and jerk commands send to the MEI card (via the GUI on Laptop)

All logfiles include in their name a number which is the time in seconds since January, 1*st* 1970. This number is also displayed on the PC104 terminal when the main program(main.cpp or maingps.cpp) is launched on the PC104 .

Laptop shell script	Data transferred	**PC104 shell script**
Outgoing		**Incoming**
allrcmdsat	/dev/rtf16 (Motors commands)	allrcmddest
allwdsat	/dev/rtf15 (Watchdog messages)	allwddest
allheadsat	/dev/rtf31 (heading messages)	allheaddest
allheadCsat	/dev/rtf36 (heading commands)	allheadCdest
Incoming		**Outgoing**
allremdisat	/dev/rtf17 (data from DAC)	allremddest
allremmisat	/dev/rtf18 (data from MEI card)	allremmdest

Table 4.1: Shell scripts for data transmission

RTF #	Fifo name	Nature	Description	Dual
Graphical User Interface				
rtf1	fdmei	outgoing[1]	Motors[2] commands	mei_ci_fifo (wdrmod)
rtf3	fdmod	outgoing	Watchdog message	hand_fifo
rtf19	remd	incoming	DAC data	remd_fifo
rtf20	remm	incoming	MEI data	remm_fifo
rtf30	fheadmod	outgoing	Heading message	headm_fifo
rtf35	headmesg	outgoing	Heading commands	headc_fifo
wdrmod module				
rtf1	mei_ci_fifo	incoming (GUI)	Motors commands	fdmei (GUI)
rtf2	get_fifo	internal	Watchdog message	hand_fifo
rtf3	hand_fifo	incoming (GUI)	Watchdog message	fdmod (GUI)
rtf4	gethead_fifo	internal	Heading message	headm_fifo
rtf5	myget_fifo	internal	Watchdog message	hand_fifo
rtf15	wd_fifo	outgoing(PC104)	Watchdog message	wd_fifo (PC104)
rtf16	mei_co_fifo	outgoing (PC104)	Motors commands	rcmd_fifo (PC104)
rtf17	remd_fifo	outgoing (GUI)	DAC data	remm (GUI)
rtf18	remm_fifo	outgoing (GUI)	MEI data	remd (GUI)
rtf19	das_in_fifo	internal	DAC data	remd_fifo
rtf20	mei_in_fifo	internal	MEI data	remm_fifo
rtf30	headm_fifo	incoming (GUI)	Heading message	fheadmod (GUI)
rtf31	htransmit_fifo	outgoing (PC104)	Heading message	headm_fifo (PC104)
rtf35	headc_fifo	incoming (GUI)	heading commands	headmesg (GUI)
rtf36	htransc_fifo	outgoing (PC104)	Heading commands	headc_fifo (PC104)

Table 4.2: Laptop Fifo's list and description

RTF #	Fifo name	Nature	Description	Dual
all_in_one_module module				
rtf1	outd_fifo	outgoing (log.[3])	DAC data for logfiles	allStruct.ddata (log.)
rtf5	myget_fifo	internal		hand_fifo
rtf10	outm_fifo	outgoing (log.)	MEI data for logfiles	allStruct.mdata (log.)
rtf11	get_fifo	internal		hand_fifo
rtf12	hand_fifo	incoming (log.)	Command message	allStruct.ctl (log.)
rtf13	cmd_fifo	incoming (log.)	MEI command (not used)	allStruct.cmd (log.)
rtf14	done_fifo		Successfully executed commands of rcmd_fifo	allStruct.cmdlog (log.)
rtf15	wd_fifo	incoming (Lap.[4])	Watchdog message	wd_fifo (Lap.)
rtf16	rcmd_fifo	incoming (Lap.)	Motor commands	mei_co_fifo (Lap.)
rtf17	remd_fifo	outgoing (Lap.)	Data from DAC	remd_fifo (Lap.)
rtf18	remm_fifo	outgoing(Lap.)	Data from MEI card	remm_fifo (Lap.)
rtf31	headm_fifo	incoming (Lap.)	Heading message	headm_fifo (Lap.)
rtf33	mygethead_fifo	internal	Heading message	headm_fifo
rtf36	headc_fifo	incoming (Lap.)	Heading message	htransc_fifo (Lap.)
allcontroll.cpp (data logging)				
rtf1	allStruct.ddata	incoming (wdrmod)	DAC data for logfiles	outd_fifo (wdrmod)
rtf10	allStruct.mdata	incoming (wdrmod)	MEI data for logfiles	outm_dido (wdrmod)
rtf14	allStruct.cmdlog	incoming (wdrmod)	Successfully Executed motors commands	done_fifo (wdrmod)
rtf12	allStruct.ctl	outgoing (wdrmod)	command message[5]	hand_fifo (wdrmod)
rtf13	allStruct.cmd	outgoing (wdrmod)	MEI command (not used)	cmd_fifo (wdrmod)

Table 4.3: PC104 Fifo's list and description

Watchdog

The watchdog verifies every 0.01 second if the connection between the PC104 and the Laptop is operational. If it detects a connection break, the rudder angle and both main motors RPM's are set to zero. The watchdog is part of the threadtask thread implemented in the all_in_one_module module (cf. Appendix H) and it also uses a Fifo's.

The organization of the boat software is shown for the PC104 in Figure (4-4) and for the laptop in Figure (4-5).

[1]The destination of all the outgoing Fifo's of the GUI is the wdrmod module, and all the incoming fifo to the GUI comes from the wdrmod module.

[2]Commands for the two main motors and for th ruder motor.

[3]Lap.=Laptop

[4]log.= data logging program (allcontrol.cpp)

[5]Command to initialize/start/stop remote control

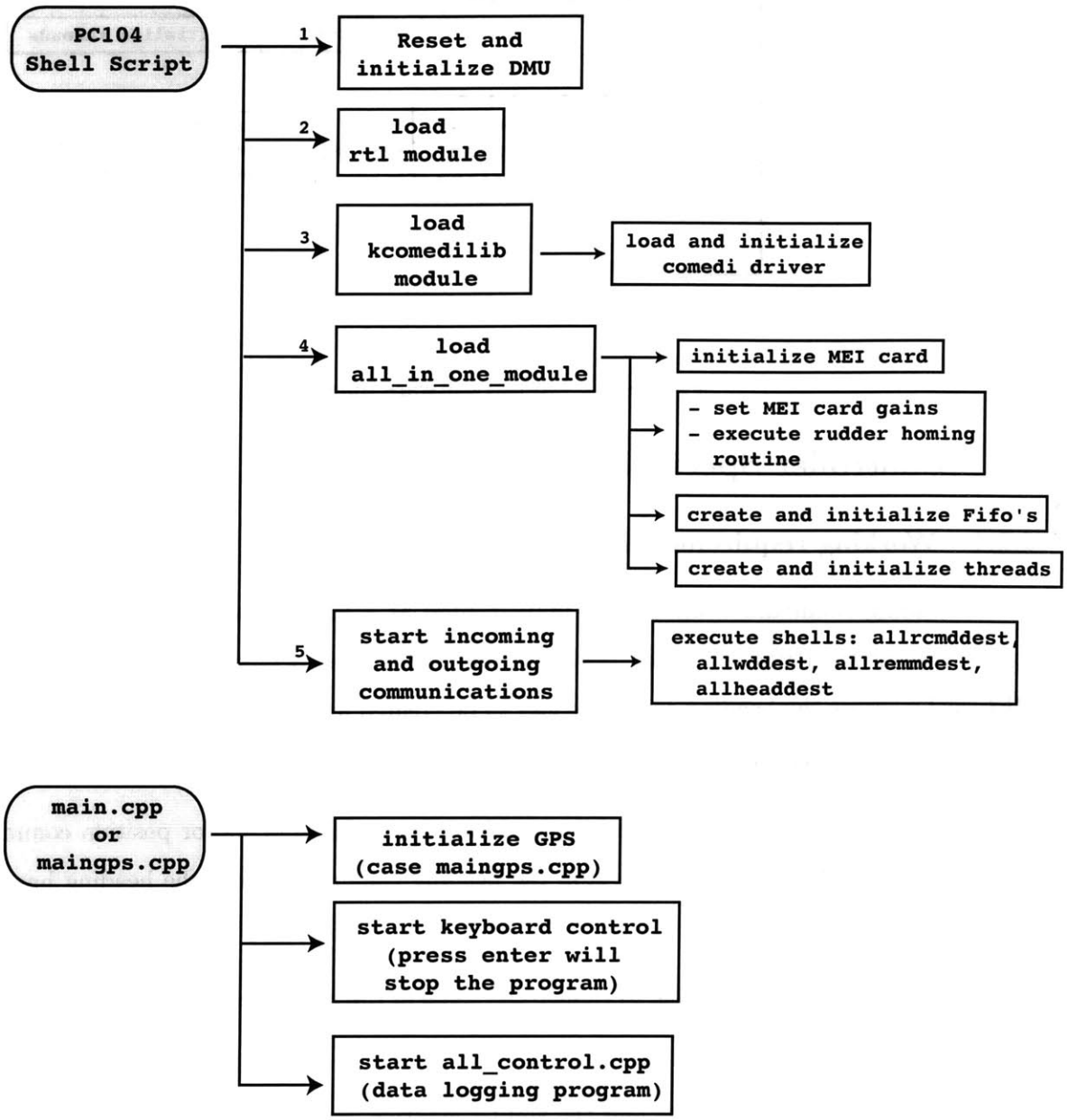

Figure 4-4: PC104 software diagram

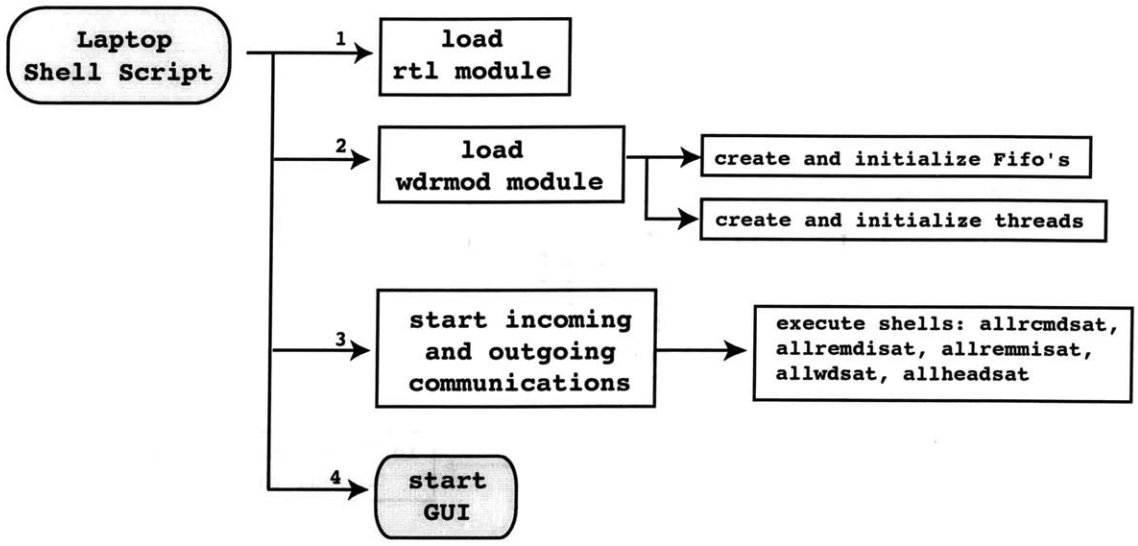

Figure 4-5: Laptop software diagram

4.2 Controller Specificities

4.2.1 Working requirements

The heading command could not be implemented as a RPM or a rudder angle command simply because the RPM and motor position command is directly closed-loop controlled by the MEI card whereas the heading controller had to be created and included in the remote control module. The working requirements for the heading controller are the following:

- The command taking much longer to achieve than a RPM or motor position command, the operator should be able to stop the heading command before the heading has been reached,
- The operator should be able to change the value of the desired heading before it has even been reached by the boat.
- Moreover, the rudder angle and the rudder rotation rate had to be limited just as it is the case in a real boat. The rudder angle limitation serves as an anti-windup device.

4.2.2 Implementation

The working requirements given above were achieved using a **separate thread** in the PC104 control module for heading control. This thread has its own triggering message: initialization is

done when the Laptop GUI is launched, the thread is woken up each time a heading command is sent from the GUI and the thread is suspended when the heading command is stopped, whether the desired heading has been reached or not. The thread is a periodic thread with a period equal to 0.1 seconds. When the thread receives a "start" message from the GUI, the thread performs the following tasks during each period:

- Checking the **desired heading** sent from the GUI, so that the heading command can actually be changed while in process.
- Get and process data from the magnetometer, making sure the heading is in the [0, 360] degrees interval.
- Computing the **heading error** using data from the magnetometer. The error has to be in the [-180, 180] degree interval for the boat to take the shortest path to go to the desired heading. If the initial error is greater than 180, it is replaced by (180-error) and if the initial error is less than -180, it is replaced by (error+180).
- Checking if the **desired heading has been reached** with a tolerance of two degrees. If this is the case, a real-time message is displayed on the terminal but the controller does not stop.
- Implementing the **discrete heading controller equations** designed with a sampling time of T_s=0.1s, using as an input the heading error (in radian).
- Sending the **rudder angle output** by the controller to the MEI board.

The heading thread is implemented in the `all_in_one_module` module. The heading controller is written as a procedure which inputs are the actual error and the errors of the two previous steps and which output is the rudder angle command. This procedure checks the RPM's of the two main motors via the MEI card, use the RPM's to compute the ship model velocity (using first the approximation of Equation (3.52) and later Equation (7.1)) and compute Nomoto's K and T parameters before implementing the discrete equations of the heading controller.

4.3 Summary

In this chapter, the ship model system and software was rapidly described. All the major features were presented: Graphical User Interface, Real-Time Linux, Fifo's, Threads, data exchange, and emphasis was laid on the description of the numerous Fifo's which allow data exchange between the user operated GUI and the ship model on-board PC104 computer.
The ship model system is based on two **main shell scripts** (one on the PC104 and one on the Laptop) doing the necessary initializations, starting data exchange between the two computers, loading all the RT modules (which declare and initialize the threads and the Fifo's) and launching the GUI.
Finally, the implementation of the heading controller on the PC104 was described.

Chapter 5

TRACK KEEPING

5.1 Introduction

In this chapter, a track keeping (or ship guidance) system will be studied, it uses a position feedback on top of a heading controller and can make the boat follow a predefined path. Since it is based on the heading controller, building a track keeping system is a natural extension of the work presented in the previous chapter.
First, the kinematics for track keeping and guidance by Line Of Sight (LOS) will be studied. Then a simple Matlab program implementing those tow concepts will be presented. Finally, the implementation of such a controller in the boat system will be discussed. The main difference in the implementation is that the position of the boat do not have to be computed using equations but is directly given by the DGPS sensor.

5.2 Kinematics for track keeping

In order to design a track keeping system, it is necessary to have at any moment the position of the boat in an Earth base reference frame: the inertial frame described in Section 2.1.2.
As for the design of the heading controller, the track keeping system will also be designed supposing the boat stays on the horizontal $x - y$ plane.

Thus, in the $x-y$ plane of the IF, the ship kinematics are described by the following equations:

$$\dot{x} = u\cos(\psi) - v\sin(\psi) \tag{5.1}$$

$$\dot{y} = u\sin(\psi) + v\cos(\psi) \tag{5.2}$$

$$\dot{\psi} = r \tag{5.3}$$

with ψ being the heading angle and r being the turning rate of the ship.
However, since the equations are nonlinear in u, v and ψ, they are not easy to use directly. In order to be able to linearize Equation (5.1) and Equation (5.2), the Earth-fixed coordinate system can be rotated such that the desired heading is $\psi_d = 0$. Moreover, the origin of the IF will be taken such that it coincides with the starting point of the boat $\big(x_d(t_0), y_d(t_0)\big)$. Consequently, the heading angle ψ of the ship will be small during track control. Hence, the two following approximations can be made:

$$\sin(\psi) \approx \psi \qquad\qquad \cos(\psi) \approx 1 \tag{5.4}$$

Moreover, it can also be assumed that the ship stays at constant velocity U and that $u \approx U$. As a consequence, the Equations (5.1), (5.2) and (5.3) can be transformed into the following linear equations:

$$\dot{x} = U + d_x \qquad\qquad \dot{y} = U\psi + v + d_y \tag{5.5}$$

where d_x and d_y describe the errors due to the linearization and environmental disturbances.

5.3 Guidance by Line of Sight

The boat is given a set of N way points (noted WP from now on), the coordinates of WP number i being (x_d^i, y_d^i), i=1...N. If the boat has passed the WP number $i-1$ and is heading toward WP number i, the desired heading angle, noted ψ_d^i is then the angle between the ship and WP number i, and since it depends on the actual position of the boat it is a function of time. ψ_d^i is defined in *equation 5.6*:

$$\psi_d^i(t) = tan^{-1}\Big(\frac{y_d^i - y(t)}{x_d^i - x(t)}\Big) \tag{5.6}$$

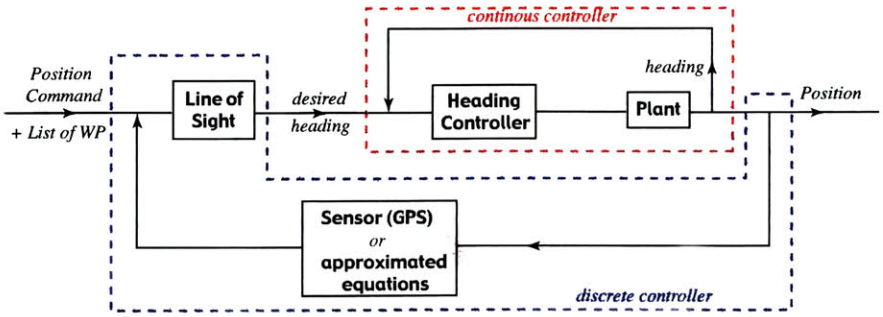

Figure 5-1: Coupled position and heading controller

Due to the use of the function tan^{-1}, a quadrant check must be performed on ψ_d.
When the boat begins to be "too close" to WP number i, the destination has to be changed from WP number i to WP number $i+1$. The term "too close" can be understood as the ship being in a circle of **acceptance of radius** ρ_0 around WP number i. According to [3], this radius should be chosen such as $\rho_0 = 2L$, L being the length of the ship. That means that if:

$$\left[x_d^i - x(t)\right]^2 + \left[y_d^i - y(t)\right]^2 \leq \rho_0^2 \tag{5.7}$$

then the next WP should be chosen.

5.4 Matlab Program for Track Keeping system

5.4.1 Overall Structure

To model the boat behavior, the first order Nomoto model designed in Chapter 3 is used. More precisely, the K and T experimental values of Equation (3.53) are chosen to model the boat. The steering machine model and the PID controller used are the same as the one designed for the Matlab test for the robustness of the controller cf. section 3.7 of chapter 3.
The program uses the two interwoven controllers: a continuous controller for heading control and a discrete controller for position control, as shown in Figure (5-1)

5.4.2 Analyzis of the program

The initial parameters are:

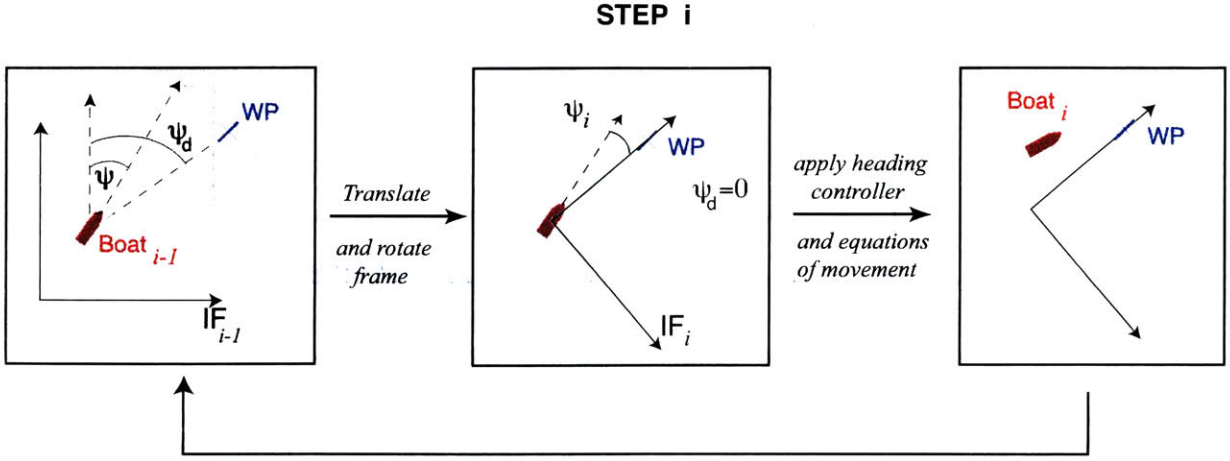

Figure 5-2: Step of the autopilot Matlab program

- initial position of the boat taken as the center of a IF in which x axis points towards East and y axis points toward the geographical North,
- initial heading of the boat in the IF defined above,
- list of way points defining the path the boat has to follow,
- value of the radius of the circle of acceptance,
- time step for position check, called T_s.

The program is based on a loop which do the following actions at each step:

- Defining which is the WP to go to, using the definition of circle of acceptance,
- Computing the angle between the boat-WP line and the y axis of the frame, this angle is called the "desired heading" and noted ψ_d.
- Translating the origin of the IF so that the new origin coincides with the position of the boat and modifying the coordinates of all the WP's in consequence.
- Rotating the axes if the IF so that the new y axis coincides with the boat-desired WP vector, modifying all the WP's coordinates in consequence and computing the actual heading in this new frame.
- Applying the controller so that the heading should tend to zero.

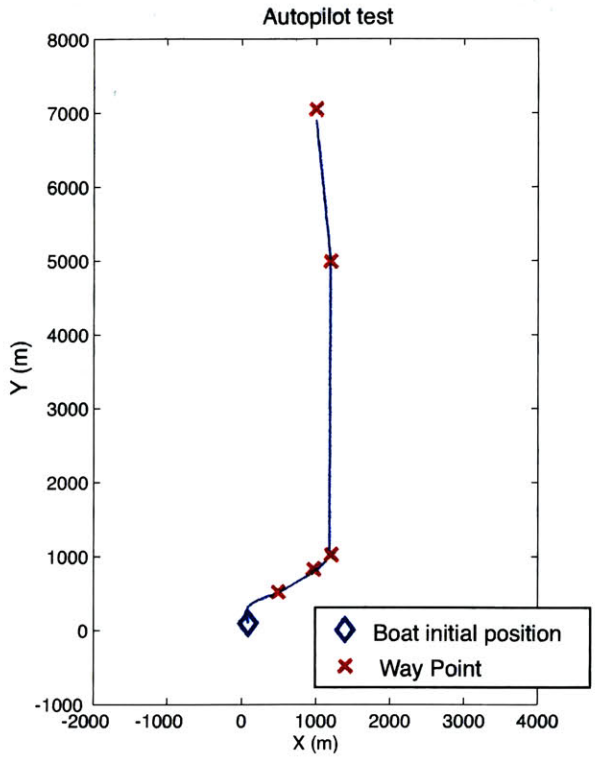

Figure 5-3: Result of the Matlab autopilot program

- The heading at the end of the step is taken equal to the response of the controller after T_s seconds, position variations during the T_s seconds are computed integrating equations 5.5.

  The path is plotted using the position of the boat in the local IF at each step and translating and rotating backwards to find the position of the boat at each step in the initial IF.

The actions executed at each step are described on Figure (5-2).

Results

It was supposed that there is no external disturbances, so that $d_x = 0$ and $d_y = 0$.

The condition at each WP is that the boat approach the WP by a distance of at least the radius of the circle of acceptance. No specification was given on how the boat should approach the WP (leaving it at starboard or port) and no obstacles were present on the road.

5.5 Implementing the Position Controller

Once the heading controller design described at Chapter 3 is ready and has been tested and refined, implementing a position controller on the ship model operating system is easy. Though there are no doubt many methods to implement it, a method will be suggested in the following.

The first step of the implementation of the heading controller is to create a new thread in the `all_in_one_module` module on the PC104. The task of this thread will be to check every T_{pos} seconds the position of the ship model by sampling the GPS via the serial port. This thread will then write the GPS position data in a Fifo created beforehand in the `init_module` function of `all_in_one_module`. This means that a special data structure will have to be added to the ones described in Section H.1 of Appendix H to be able to transmit the position data. This fifo will be open for read by the heading thread `headingtask` and checked at each period of `headingtask` thread. As soon as the position is picked up by the thread, the LOS desired heading to reach the point is computed. Then the heading error is computed and sent as an input of the PID controller function which output the rudder angle command. The same desired heading is used until a new position is measured by the GPS.
For the period of the position thread, a value around 10 seconds can be used.
Of course, the desired path of the ship model will have to be first decomposed into a set of way points, which coordinates have to be given in longitude and latitude.

5.6 Summary

This chapter has presented a method to use the heading controller to built a position controller. The method consists of **nesting two control loops**: the outer loop is the position control as uses the GPS as the position sensor, the inner loop has a smaller period than the position control loop and is in charge of the heading control. From the location of the ship model and the desired position the LOS heading is computed and used as the input of the heading controller.

Chapter 6

TESTING THE BOAT

6.1 Testing Locations

An important part of this project was to do extensive testing. The ship model as already been tested in a swimming pool (tests at the swimming pool of Hanscom Air Force Base, see [17]). However, as a consequence of the size of the model, testing in a swimming pool was very limited for the two following reasons:

1. high turning radius
2. distance needed for the boat to reach a steady state

Testing in the towing tank could not been carried out, except for velocity test for low velocities. The ship model being larger than the MIT towing tank, no other test could be done.

Evaluating the turning radius (cf. Section 6.3.6) highlighted the facts that testing in a swimming pool would be limited to velocity test and short turning maneuver. Even circle maneuver at high speed and maximum rudder angle was not possible.
In order to testing the boat in open water or at least not in a swimming pool the following points had to be taken into account:

1. Securing all items on the boat,
2. Decreasing to a minimum the time to prepare the boat,
3. Protecting the boat from water projection

These points will be studied in the next section.

6.2 Preparing the Boat for Outdoors Testing

The model hull was built for doing resistance tests in a towing tank and consequently was **not built with a scaled free-board** compared to the real boat: the ship model is very low on the water when fully loaded. So even with only 5cm waves on the Charles river it is too dangerous for the boat to be on the water. As a consequence, the trials had to be very early in the morning when the water is completely flat. However, as the boat was first put into the water manually, it had to be almost completely unloaded to reduce stress on the hull before put into the water. That means the boat had to be assembled in the morning, just before testing. It proved to take a lot of time and the waves were usually too high when the boat was ready for testing.

All items had to be secured inside the boat in case the boat would capsize. Wood cases were built for both the magnetometer, the DMU and the midships battery. As for the PC104 and the bow batteries, they were tied to one of the wooden bars of the hull structure. The DGPS was attached to the hull using a vertical rod that could be screwed on one end on the DGPS itself and on the other end to a piece of wood glued to the hull.

Decreasing the amount of time to prepare the hull being a very important factor, quick connectors were installed. This also proved to be a necessary step in increasing the reliability of the boat. To protect the boat system from splashes, a plastic cover was used. This proved not to be enough because the boat was really too low on the water. Consequently, increasing the free board of 15 cm using polyethylene foam of density 36.84 kg/m^3 (2.3 lbs/cu ft) and using a semi-rigid polyethylene sheet to cover the boat was considered but never realized.

6.3 Presentation of the tests

In order to evaluate the stability and maneuvering characteristics of the model boat, the following tests are carried out:

1. Velocity tests
2. Simple turning tests
3. Dieudonné spiral maneuver
4. Zigzag maneuver

5. Circle maneuver (full turns)

6. Tight turns tests

7. Heading test to test the heading controller

Most of the tests are described in details in the following sections.

6.3.1 Velocity Tests

Velocity tests are very important because having an accurate RPM-Velocity relation is necessary to build an speed-adaptive controller. Velocity data presented in Table (3.4) lacks data for speed above 600 RPM and especially at high speed, which data are important to determine the trend of the RPM versus velocity curve.

6.3.2 Simple Turning Tests

They play also a major part in the controller design. Data from turning tests will help to refine the values of the K and T parameters and especially their dependence upon speed and the rudder angle.

6.3.3 Dieudonné spiral maneuver

Spiral Maneuver for Full Scale Ship

This test allows to identify the **directional stability characteristics** of the boat. Therefore, this test needs to be carried out before any other tests and especially the controllability tests. The test consists of the following:

- $t = 0$: set the speed to $U = U_0$ and wait approximately 1 minute until steady speed is achieved. this speed will stay constant during all the test,
- $t = 1\text{min}$: set $\delta = \delta_R = 20\text{deg}$ (i.e. 20 degrees to starboard) and wait 1 minute until $\dot{\psi}$ reaches a steady value,
- $t = 2\text{min}$: set $\delta = \delta_R = 15\text{deg}$ and wait 1 minute until $\dot{\psi}$ reaches a steady value,
- and so on, decreasing the value of δ by 5 degrees at each step and until $\delta = -20\text{deg}$ and then coming back to $\delta = 20\text{deg}$.

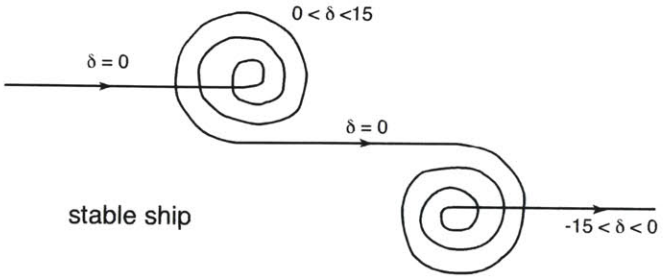

Figure 6-1: Path during a Dieudonné Spiral Maneuver (Stable Ship)

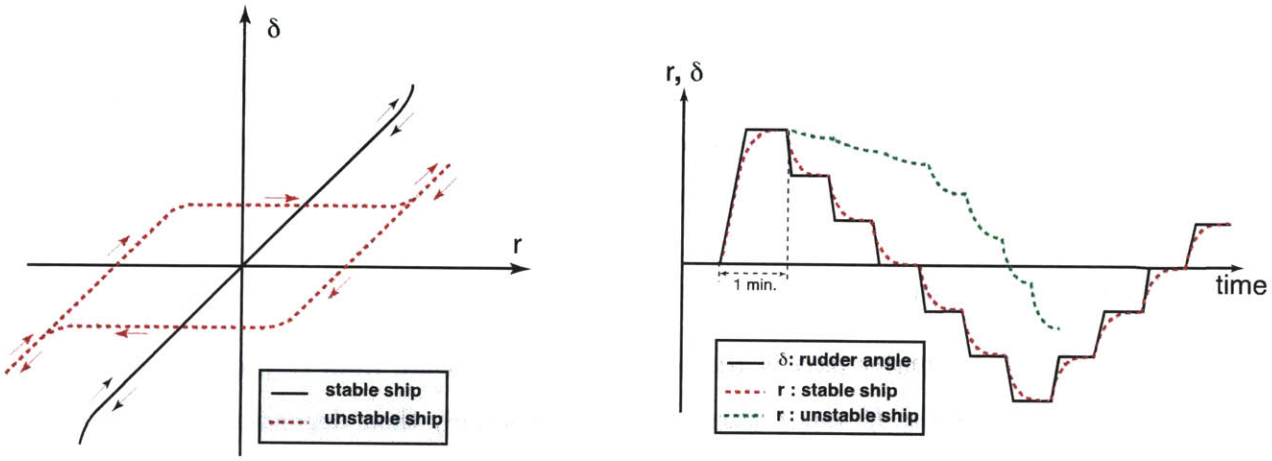

Figure 6-2: Relation between rudder angle and yaw turning rate

For a stable ship, the path should be as illustrated on Figure (6-1).

The directional stability of the boat is evaluated through the relation between the rudder angle δ and the yaw rate r. For a stable ship, δ as a function of r is a straight line. For an unstable ship, an **hysteresis** phenomenon appears and as a consequence, the boat can turn the opposite side as what is expected. The relation between δ and r for stable and unstable ships is illustrated in Figure (6-2).

Adapting The Spiral Maneuver to the Model Boat

The test procedure is the same for the model boat except that the time scale is modified using the scaling relation:

$$t_{model} = \frac{t_{real}}{\sqrt{\lambda}}, \qquad t_{real} = 1\text{min} \quad \rightarrow \quad t_{model} \sim 8.75s \tag{6.1}$$

t_{model}=10s will be used for the smaller velocities and t=9s or 8s will be used for higher velocity.

6.3.4 ZigZag Maneuver

This test is also called the Kempf overshoot or the "Z" maneuver. The goal of this test is mainly to determine the control characteristics of the boat and in particular the **ability of the rudder to control the boat.**

The test consists of the following sequence of events:

- $t = 0$: set the speed to $U = U_0$ and wait until the boat reaches steady speed,
- deflect the rudder angle to a pre-selected angle δ_R (usually chosen equal to 20deg.) at the maximum speed $\dot{\delta}$ and wait until the heading ψ reaches a preselected change of heading $\Delta\psi$ (usually equal to 20deg.),
- then changes the rudder at maximum $\dot{\delta}$ to the opposite angle $-\delta_R$ and hold until the heading ψ changes by -$\Delta\psi$,
- then to complete the zigzag test, deflect again δ to δ_R at maximum speed
- the four previous steps can be repeated to do several continuous zigzag tests.

The result of an overshoot and zigzag maneuver is shown on Figure (6-3).

The following 3 parameters characterize the **control stability** of the boat and are important operational parameters:

1. **Time to reach the second execute yaw**: is a direct measure of the ability of the ship ro rapidly change course,
2. **Overshoot yaw angle**: is a numerical measurement of the **counter-maneuvering ability**, it indicates how much anticipation is required for maneuvering the boat
3. **Overshoot width of path**: is also a measurement of the counter-maneuvering ability.

The results of the Zigzag maneuver are **speed dependent**:

- the time to reach decreases with increasing speed
- the overshoot yaw angle and the overshoot width of path increase with increasing speed,
- the non-dimensional time to reach ($t' = \frac{t \cdot V}{L}$) increases with increasing speed.

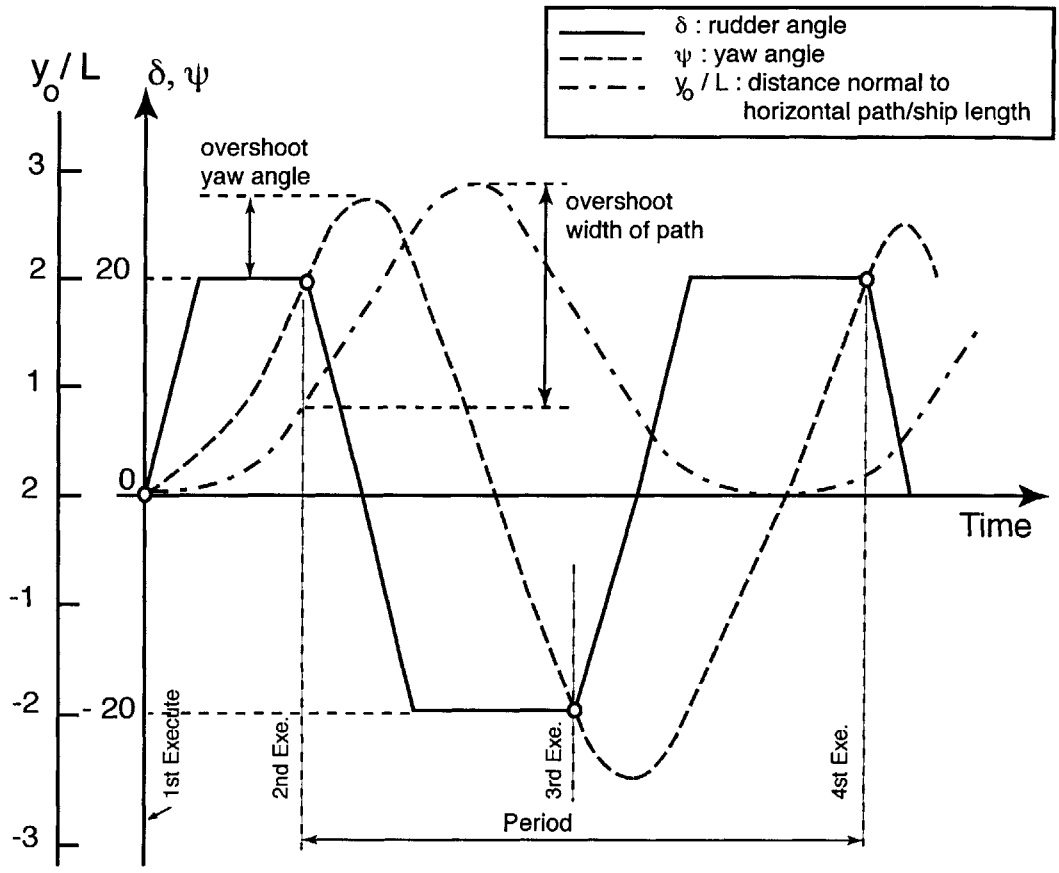

Figure 6-3: Overshoot and zigzag maneuver

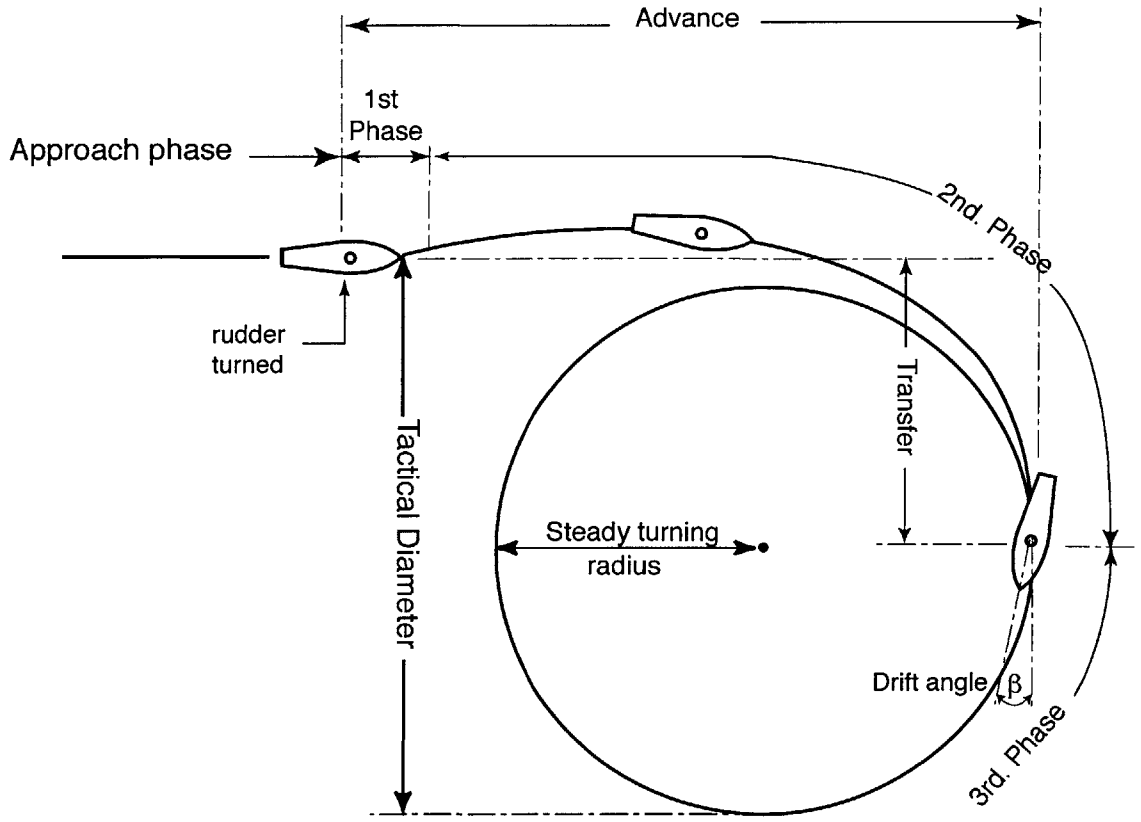

Figure 6-4: Turning Test

6.3.5 Circle Maneuver

Test Description

The most important goal of the circle maneuver is to determine the ship **tactical diameter**. The tactical diameter of a ship is a measure of the space needed for the ship to turn. It is illustrated along with the three phases of a turn on Figure (6-4).
The three phases of a turn are:

- **Phase 1**: it starts when the rudder starts to turn and ends when the rudder has reached the desired deflection angle. During this short phase, the accelerations dominate in the yaw-sway coupled equations,
- **Phase 2**: during this phase, acceleration and velocity terms are comparable in the yaw-sway equation,
- **Phase 3**: the boat reaches equilibrium and the boat settles down to a turn of constant

radius. Only the velocity terms remain in the yaw-sway equations.

Using Equation (3.8), and keeping only the velocity terms in the left hand sides, the equations for the third phase of the the turning test are:

$$-Y'_v v' - (Y'_r - m')r' = Y'_\delta \delta_R \tag{6.2}$$

$$-N'_v v' - (N'_r - m' x'_G)r' = N'_\delta \delta_R \tag{6.3}$$

which implies:

$$\begin{bmatrix} v' \\ r' \end{bmatrix} = \frac{\delta}{-Y'_v(m'x'_G - N'_r) + N'_v(m' - Y'_r)} \begin{bmatrix} (m'x'_G - N'_r) + (Y'_r - m')N'_\delta \\ N'_v Y'_\delta - Y'_v N'_\delta \end{bmatrix} \tag{6.4}$$

Knowing that $r' = r \cdot \frac{L}{U}$ where U is the velocity of the boat (always tangent to the circle in the steady phase) and that $U = R \cdot r$ where R is the steady turning radius: $r' = \frac{L}{R}$ or $R = \frac{L}{r'}$. Using equation Equation (6.4) for r', the expression for the study turning radius R can be obtained:

$$\frac{R}{L} = -\frac{1}{\delta_R}\left[\frac{Y'_v(N'_r - m'x'_G) - N'_v(Y'_r - m')}{Y'_v N'_\delta - N'_v Y'_\delta}\right] \tag{6.5}$$

The **drift angle** β is defined by $v = -U\sin(\beta) \quad \rightarrow \quad v' = -\sin(\beta)$. Since the drift angle can be considered small, the approximation $v' = -\beta$ can be made:

$$v' = -\beta = \delta_R\left[\frac{N'_\delta(Y'_r - m') - Y'_\delta(N'_r - m'x'_G)}{Y'_v(N'_r - m'x'_G) - N'_v(Y'_r - m')}\right] \tag{6.6}$$

6.3.6 Evaluating the Tactical Diameter Before Testing

Having an estimation of the tactical diameter of the model boat before any test is very useful because it helps in determining how much space is needed for the testing, and if the test could be carried out in a swimming pool.
However the prediction of a ship tactical diameter is complex, especially in the case of the model boat since few data were available. A detailed discussion on the means to predict the tactical diameter of a ship is presented in [6]. The methods discussed in the paper are all based on regression analysis.

As for the model boat, two methods can be used to predict the tactical diameter:

	Real ship	Model boat
Velocity	20 knots	1.5 m/s
Rudder angle (deg)	Turning radius (m)	
10	505	11
20	255	5.4
30	160	3.4
35	75	1.6

Table 6.1: Turning radius according to [14]

	Method 1	Method 2.	Real Ship coefficients scaling
$R = -\frac{k \cdot L}{\delta}$	k= -0.4171	k=-0.183611	k=-0.493294
rudder angle	R (m)		
10	7.8	3.42	9.2
20	3.9	1.71	4.6
30	2.6	1.14	3.1
35	2.2	0.98	2.6

Table 6.2: Turning radius according using hydrodynamic coefficients

- scaling the results presented in [14, p. 24] for the turning simulation of the real boat, the results are presented in Table (6.1)
- using the non-dimensional coefficients given by SBT to compute the turning radius using Equation (6.5).

However, the results shown in the two tables mentioned above correspond to a ship model velocity of 100) RPM, which seems a bit too high for turning test.

Chapter 7

RESULTS AND ANALYSIS

Due to a lack of time and the low availability of suitable places to test the boat, not all the tests described in Chapter 6 could be carried out. Only the velocity tests, turning tests and circle maneuver tests could be done.

7.1 Velocity Tests

Velocity tests were performed both at the MIT Alumni Pool and at the Towing Tank. Many more low velocities tests were performed at the Towing Tank than at the pool mainly due to a lack of testing time at the pool. Velocity tests in the Towing Tank at higher than 600 RPM are not reliable due to the size of the tank and thus were not performed.

For all the tests described below a stopwatch was used to time the boat. The testing lengths used to compute the velocities are: **13 yards** in the MIT Alumni Pool and **11 yards** in the Towing Tank.

The results of the velocity tests are presented in Table (7.1) and plotted on Figure (7-1). The results are similar to the one obtained in previous tests and presented Table (3.4).

The RPM-Velocity relation can be approximated by the following equation:

$$U\ [\mathrm{m/s}] = 1 \times 10^{-7} \cdot RPM^2 + 0.0015 \cdot RPM^2 - 0.0129 \tag{7.1}$$

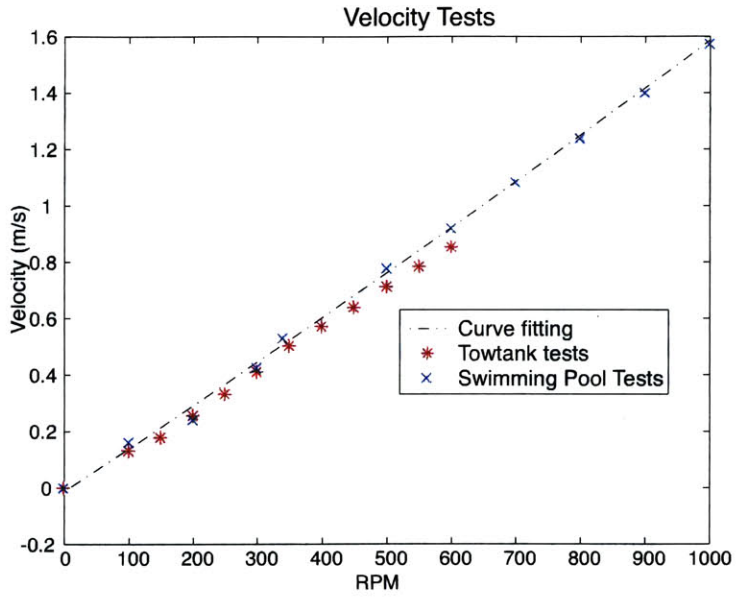

Figure 7-1: Velocity Tests at the MIT pool and Towing Tank

7.2 Turning Tests

7.2.1 Tests Description

All the test presented in this section were performed at the MIT swimming pool. However, the pool was too narrow for the ship model to do full turns. Also, no GPS data could be received. All the turning experiments are turns to **starboard**, using a **positive rudder angle command**.

7.2.2 Values of K_0 and T_0

As explained in Section **??**, the turning tests give information about the yaw dynamics of the boat and lead to an experimental approximation of the r/δ Nomoto first order transfer function. The K_0 and T_0 parameters defined in Section 3.5.3 are obtained using the velocity data of the velocity tests presented in Section 7.1.The yaw-rate graphs and the curve fitting are presented for all tests in Appendix I and the experiments and curve fitting results are presented in Table (7.2). From this table, the approximations for the K and T Nomoto's first order model parameters are:

$$K = U \cdot K_0 = U \cdot 0.330, \qquad T = \frac{T_0}{U} = \frac{1.672}{U} \tag{7.2}$$

Velocity Tests in the MIT Alumni Pool					
RPM	Velocity (m/s)				
	Test 1	Test 2	Test 3	Test 4	**Mean**
100	0.154				**0.154**
200	0.241				**0.241**
300	0.370	0.425	0.481		**0.426**
400	0.564	0.638	0.579		**0.594**
500	0.783	0.763	0.786		**0.777**
600	0.919	0.909	0.932		**0.920**
700	1.064	1.106	1.080		**1.083**
800	1.237	1.251	1.1227		**1.238**
900	1.405	1.431	1.382		**1.400**
1000	1.590	1.602	1.566	1.530	**1.574**

Velocity Tests in the Towing Tank					
RPM	Velocity (m/s)				
	Test 1	Test 2	Test 3	Test 4	**Mean**
100	0.132	0.135	0.141		**0.136**
150	0.174	0.178	0.182		**0.178**
200	0.257	0.257	0.255		**0.256**
250	0.333	0.333	0.330		**0.332**
300	0.404	0.423	0.404	0.422	**0.410**
350	0.504	0.503	0.499		**0.502**
400	0.568	0.582	0.562		**0.571**
450	0.642	0.636	0.636		**0.638**
500	0.709	0.715	0.710		**0.711**
550	0.806	0.770	0.775		**0.783**
600	0.857	0.850	0.853		**0.853**

Table 7.1: RPM - Forward Velocity Correspondence

7.2.3 Analysis of a Turn

In this section, **the analysis will be made for the test done at 600 RPM and a rudder angle of 30 deg**, where the velocity and rudder angle are high enough for the effects to be spotted very clearly. The results of all the other tests are presented in Appendix J, and they are very similar to the results of the 600 RPM and 30 deg. tests. However, they will be referred to here when they present a special pattern. For each run, the following data are presented: a graph of the three linear accelerations, a graph of the three rotation rates, a graph of the stabilized pitch and roll angles, a graph of the heading (from magnetometer and integrated yaw rates), a graph of the surge and sway velocities and finally the path obtained integrating the DMU data. All the figures in this section and in Appendix J represent quantities in the **boat body-fixed frame**, described in Figure (3-1), except the heading and the path.

Each turning test will be referenced to by the RPM and the rudder angle in degrees:

[RPM, rudder angle (deg.)].

In the following, all data presented on the graphs are studied and commented:

1. **X Acceleration**:

   As expected, a forward acceleration appears when the boat starts moving, the acceleration decreases slowly to zero when the boat reached steady state (cf. Figure (7-3)).

   A backward acceleration can also be noticed when the boat is stopped,

2. **Y Acceleration**: when the boat turns, the y axis of the gyro measures the centripetal acceleration $a_c = m\frac{U_r}{R}$ directed towards the turning center, where R is the turning radius

List of the experiments			
RPM	δ	t_1 (s)	t_{end} (s)
200	10	15	30
200	20	15	30
200	30	20	40
200	35	20	40
300	10	20	40
300	20	20	40
300	30	20	40
400	10	15	30
400	20	15	30
400	30	15	30
400	35	20	40
500	20	15	30
500	30	15	30
500	35	15	30
600	10	15	25
600	20	15	25
600	30	15	25
600	35	15	25
700	20	10	20
700	30	10	20
700	35	10	20
800	10	10	20
800	20	10	20
800	30	10	20
800	35	10	20

Values of K and T						
RPM	δ_1 (deg.)	K_1	$K_2 = T$	K	$\mathbf{K_0}$	$\mathbf{T_0}$
200	10	1.3	6	0.13	**0.539**	**1.446**
200	20	2.2	3.5	0.110	**0.456**	**0.843**
200	30	2.6	3.5	0.087	**0.360**	**0.843**
200	35	2.0	2.5	0.057	**0.237**	**1.566**
300	10	2.6	2.5	0.260	**0.610**	**1.064**
300	20	2.7	2.2	0.135	**0.317**	**0.936**
300	30	4.5	2.3	0.160	**0.352**	**0.979**
400	10	2.4	2	0.24	**0.404**	**1.188**
400	20	4.3	3.2	0.215	**0.362**	**1.900**
400	30	6.1	2.5	0.203	**0.342**	**1.485**
400	35	7.1	2.5	0.203	**0.342**	**1.485**
400	35	5.2	3.5	0.150	**0.250**	**2.078**
500	20	5.4	3.4	0.27	**0.348**	**2.641**
500	30	5.6	1.6	0.193	**0.240**	**1.243**
500	35	6.7	1.2	0.191	**0.246**	**0.93**
500	35	8	1.8	0.191	**0.294**	**1.398**
600	10	4.5	2	0.45	**0.489**	**1.840**
600	20	6.1	2.8	0.305	**0.332**	**2.576**
600	30	9	1.4	0.267	**0.290**	**1.288**
600	35	10	1.7	0.271	**0.295**	**1.564**
600	35	8	1.7	0.271	**0.248**	**1.564**
700	20	6.2	3	0.310	**0.286**	**3.250**
700	30	9	1.7	0.300	**0.277**	**1.841**
700	35	10	1	0.286	**0.264**	**1.083**
700	35	9.5	1.2	0.271	**0.251**	**1.300**
800	10	3	2.8	0.3	**0.242**	**3.467**
800	20	9	2.8	0.450	**0.363**	**3.467**
800	30	10	1.4	0.333	**0.269**	**1.734**
800	35	11.2	1.2	0.320	**0.258**	**1.486**
Mean					**0.330**	**1.672**

Table 7.2: Experimental evaluation of the K ans T coefficients

and U_r the boat velocity: $U_r = \sqrt{U^2 + v^2}$. Since all the turns were starboard turns, the centripetal acceleration is always positive in the boat frame as seen on Figure (7-3).

3. **Pitch**: from the stabilized angles plot presented on Figure (7-4), the **list angle** of the boat at rest can be evaluated (around -0.7 degree, i.e. boat pitches forward).
   When the boat starts moving forward, the stern of the boat pitches (from Figure (3-1), positive pitch means the ship pitches astern): it is a well know effect for all motor boats. When the boat stops, the bow pitches momentarily forward, before returning to the steady pitch angle.

4. **Roll**: from the stabilized angles graph (Figure (7-4)), the **heel angle** at rest can be determined: around 1.3 degrees (heel to starboard). Then, when the boat starts turning to starboard, the roll has a positive peak and then becomes smaller than the value at rests. This can be explained by the fact that if the heel angle is zero when the boat is at rest, the boat first rolls **inward** the turn (i.e. roll is positive on Figure (3-1)), and then **outward** the turn. This effect is most easily spotted when both the velocities and the rudder angle are high. For small velocities and rudder angle, the decrease in the roll angle during the turn is not enough to make the boat really roll outwards the turn but for high velocities and rudder angles, the boat does roll outwards (negative roll) as can be seen for [700,30] on Figure (J-31), [700,35] on Figure (J-32), [800,30] on Figure (J-31), [800,35] on Figure (J-36).

5. **Yaw rate**: the yaw rates increases as soon as the boat start to turns as it can be seen on Figure (7-5)). Since the boat could not fully turn in the pool, the steady yaw rate could never be achieved.

6. **Heading**: the heading obtained by the magnetometer and the one obtained by integrating the yaw rate have a similar shape. At $t = 0$, the heading coming from the yaw rate is taken equal to the heading given by the magnetometer. The comparison between the two headings is given in Figure (7-7). It corresponds well to the orientation of the boat in the swimming pool during the trials. However, the two following observations can be made:

   - there is a **drift** in the yaw rate integration, coming from the drift of the sensor itself and from the fact that all the disturbances and noise are integrated.

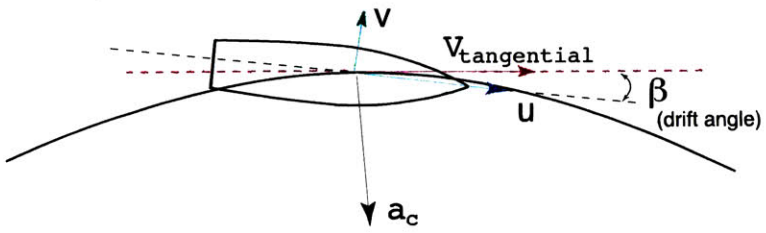

Figure 7-2: Velocities and Acceleration during a turn

- the magnetometer curves present a **non-linearity** above 200 degrees (cf. [400,35] on Figure (J-9) and [500,20] on Figure (J-23) tests for example).

Consequently, obtaining a value of the heading as close to reality as possible is not that easy because both sensors have drawbacks: the integrated yaw rate drifts fast and anyway a direct measurement of the heading is needed at one point; the magnetometer seems to present non-linearities in its behavior and is very sensitive to any magnetic disturbances. However, one can suppose that while the boat is on the water the magnetic disturbances are very small. The conclusion here is that the magnetometer is most probably more reliable than the integrated yaw rate.

7. **Surge and Sway Velocities**: the direction of the sway velocity is shown on Figure (7-2). So a negative sway velocity is expected when the boat turns. The forward velocity is also expected to drop compared to a straight line path for the same RPM. The results given by the method explained in Appendix D are not very convincing, because all the disturbances are integrated despite the filtering of the acceleration data. The values are off within a small amount of time. On Figure (7-6), a drop in the surge velocity can be noticed and the sway velocity is also becoming negative when the boat starts turning but this is not true on for all the other tests. [500,20] on Figure (J-23) and [500,30] on Figure (J-24) are the only runs which have velocity graphs in conformity with the [600,30] and so with what is expected.

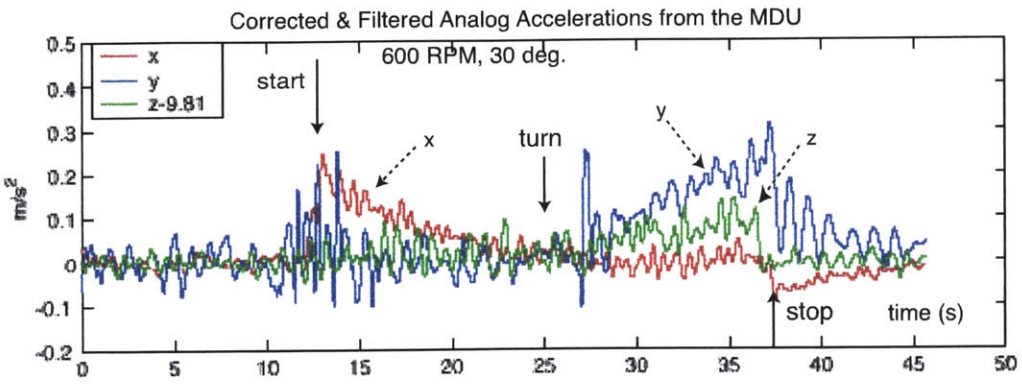

Figure 7-3: X, Y and Z accelerations measured by the DMU

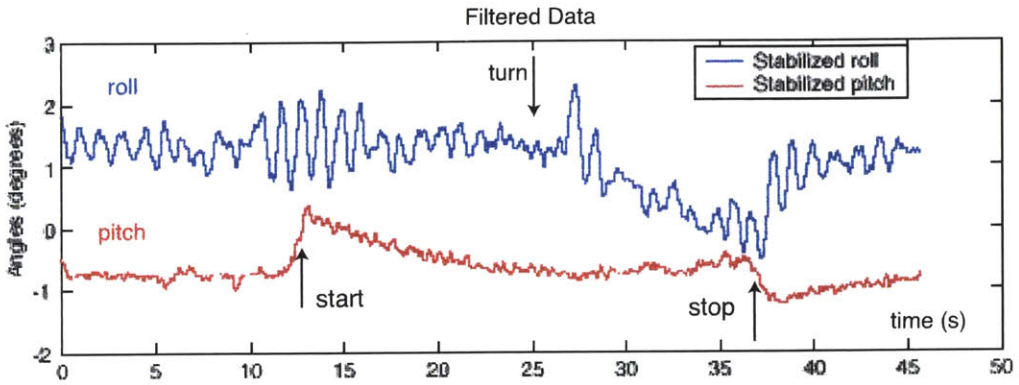

Figure 7-4: Stabilized Pitch and Roll angles measured by the DMU

8. **Boat's path** the path of the boat is computed using the method of Appendix D. It is presented on Figure (7-6). The results are even worse than for the velocities because now the disturbances are integrated twice. Sometimes the method will lead to acceptable results ([300,10] on Figure (J-3) and [300,30] on Figure (J-5), [400,35] on Figure (J-9) for example) and some other times the result is just completely off the path of the ship model during the tests ([400,30] on Figure (J-8), [700,30] on Figure (J-31)).

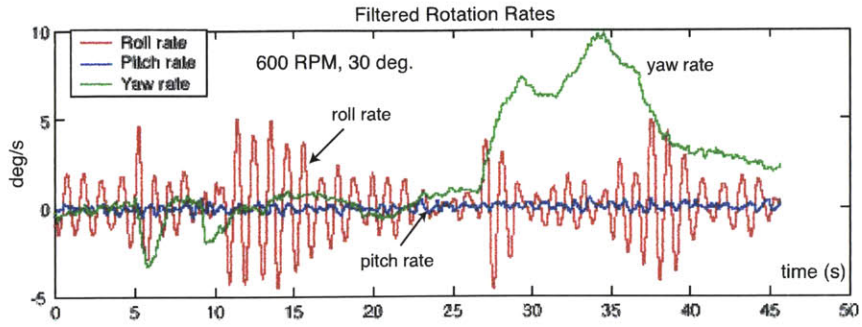

Figure 7-5: Roll, Pitch and Yaw Rotation rates measured by the DMU

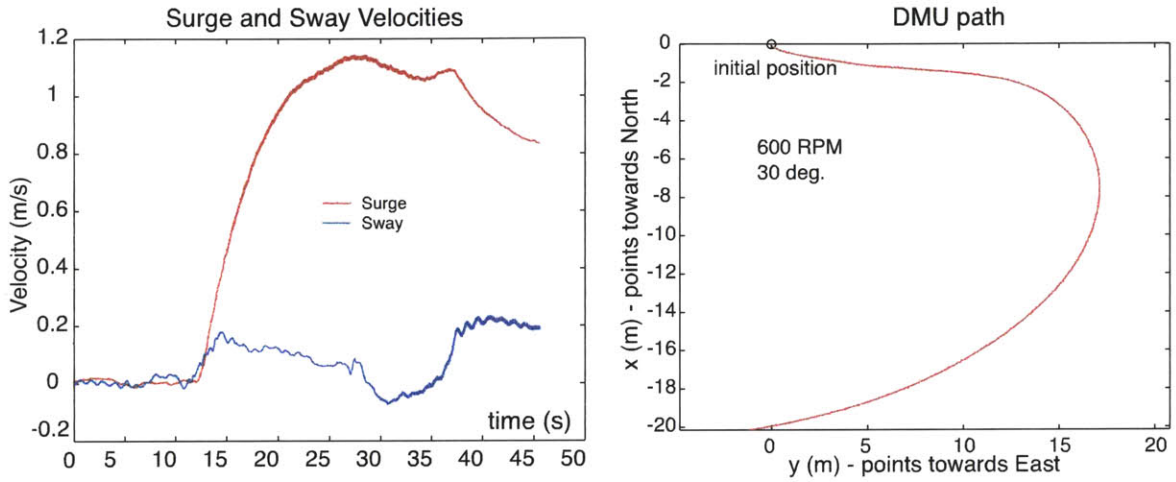

Figure 7-6: Surge and Sway Velocities using DMU data

7.3 Results of the Circle Maneuver Tests

7.3.1 Description of the Tests

All the circle maneuver tests presented in this section were done in BAE Systems Open Water Test Facility in Braintree. The test facility is an old quarry of approximately 100 ft diameter surrounded by granite walls and was large enough for the ship model to do full circles even at low speed. Considering the little amount of time available for testing, only one low speed (300 RPM), one medium speed (500 RPM) and one high speed (700 RPM) were each tested for three different rudder angles : 10, 20 and 30 degrees.

GPS data were available, and although the differential signal could not be received, the precision seemed high enough.

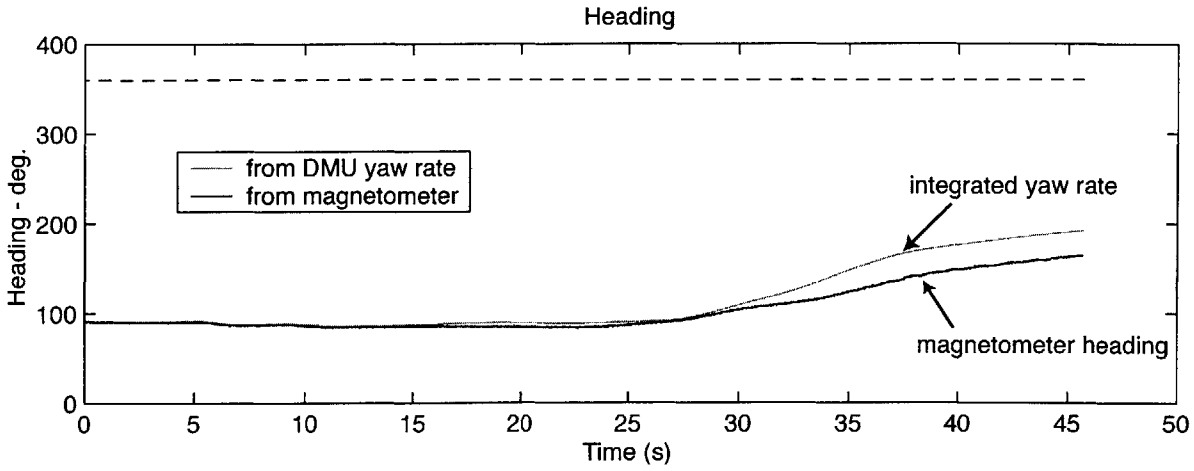

Figure 7-7: Comparison between the magnetometer heading and the yaw rate integration

The macro used for the circle maneuver tests are presented in Table (7.3), where each point of the macro is a vector [time, $RPM_{\text{left motor}}$, $RPM_{\text{right motor}}$, rudder angle (deg.)]. In the following a circle maneuver tests will be referred to by its RPM and its rudder angle:

[RPM,rudder angle(deg.)].

RPM, deg.	Point 1	Point 2	Point 3	Point 4	Point 5
300, 10	[0, 0, 0, 0]	[10, 300, 300, 0]	[30, 300,300, 10]	[310, 300, 300, 0]	[320, 0, 0, 0]
300, -20	[0, 0, 0, 0]	[10, 300, 300, 0]	[30, 300,300, -20]	[310, 300, 300, 0]	[320, 0, 0, 0]
300, -30	[0, 0, 0, 0]	[10, 300, 300, 0]	[30, 300,300, -30]	[310, 300, 300, 0]	[320, 0, 0, 0]
500, -10	[0, 0, 0, 0]	[10, 500, 500, 0]	[30, 500,500, -10]	[310, 500, 500, 0]	[320, 0, 0, 0]
500, -20	[0, 0, 0, 0]	[10, 500, 500, 0]	[30, 500,500, -20]	[310, 500, 500, 0]	[320, 0, 0, 0]
500, -30	[0, 0, 0, 0]	[10, 500, 500, 0]	[30, 500,500, -30]	[310, 500, 500, 0]	[320, 0, 0, 0]
700, -10	[0, 0, 0, 0]	[10, 700, 700, 0]	[27, 700,700, -10]	[210, 0, 0, 0]	
700, -10	[0, 0, 0, 0]	[10, 700, 700, 0]	[30, 700,700, -20]	[310, 700, 700, 0]	[320, 0, 0, 0]
700, -10	[0, 0, 0, 0]	[10, 700, 700, 0]	[22, 700,700, -30]	[210, 0, 0, 0]	

Table 7.3: Circle Maneuver Macros

7.3.2 Analysis of The Tests

For each run, the data analyzed are the following: path given by the GPS, the three linear accelerations, the three rotation rates, the stabilized pitch and roll angles, the headings measurements (from GPS, from magnetometer and from integrated yaw rate) and finally the measurements of the velocity (the one directly given by the GPS and the one computed from

the GPS position measurements). All the graphs are presented in Appendix K. The GPS path for all the runs are presented together and then the other data are presented test by test.

The data of all the tests described in Table (7.3) were usable, however, some data sets have time periods where no data from the data acquisition card were logged (cf. [700,-10] around 220 seconds on Figure (K-9) and [700,-30] around 100 seconds on Figure (K-11) for example). It is due to the data logging program which is sometimes blocked. This phenomenon often appears at the beginning of the logging session, so it can usually be removed without damaging the data (providing that the modification is also taken into account in the GPS logfile), but when it is in the middle of the data logging file it cannot be removed without modifying the data.
Moreover, the logfiles of the data logged from the acquisition card (DMU data + magnetometer data) were very long because the sampling rate is 100 Hz and most of the tests lasted more than 5 minutes. Consequently, processing them took too much time. The solution was to use only part of the data: the data processed had actually a sampling rate of 20 Hz (one over five measurements was kept). This led to a much faster processing without loosing any information. As for the GPS logfiles, the sampling rate being 1 Hz, no processing problem was encountered.

Turning Diameters

The GPS positioning is used to determine the tactical diameter a(s defined in Chapter 6) and the steady turning diameter. The diameters are presented in Table (7.4). The ship paths for the different experiments are presented on Figures K-1 and K-2.

RPM	δ deg.	Tactical Diameter (m)	Steady Turning Diameter (m)	Steady Yaw Rate (deg/s)
300	10	28.2	27.8	1.9
300	-20	20.7	20.7	-2.7
300	-30	14.1	14.1	-3.6
500	-10	35	34.4	-4.2
500	-20	19.6	19	-4.7
500	-30	14.75	13.2	-5.8
700	-10	34.4	33.9	-4.2
700	-20	19	19	-7.6
700	- 30	13.8	13.5	-8.1

Table 7.4: Tactical and steady turning diameters and steady yaw rates for circle maneuvers

GPS Heading and Velocity

The heading and velocity measurements given by the GPS are computed internally by the sensor and their computation seems to be triggered only starting at a certain speed. Heading and velocity measurements were not available for the 300 RPM runs (cf. the heading and velocity graph for [300,10] on Figure (K-3), [300,-20] on Figure (K-4) and[300,-30] on Figure (K-5)). GPS Velocity was available for all higher RPM's, however the GPS heading data do not seem to be stable: heading is not computed during several small time intervals for [500,-20] on Figure (K-7) or during a long time period ([500,-30] on Figure (K-8), [700,-10] onFigure (K-9) and [700,-30] on Figure (K-11)).

Another observation is that when the GPS is giving heading and velocity signals, even though the velocity signal seems to be almost synchronized with the boat real movements (that can be seen from the comparison of the velocity computed using the GPS position and the GPS velocity signal) the heading seems to have a lag. For example, for [500,-10] on Figure (K-6), the GPS heading has a lag of about more than 10 seconds compared to the magnetometer signal, and for [700,-10] on Figure (K-9) a lag a little smaller can be spotted.

The best way to spot the GPS lag in heading and in velocity is to plot the velocity and heading direction vector on the GPS path plots for the 500 and 700 RPM tests. This will be discussed in the analysis of the drift angle at the end of this section.

Ship Model Velocity

As described in Section 2.3.2, the model ship velocity can also be computed using GPS positions, which are always available whatever the ship speed is. The time step between two GPS position measurement is 1 second.

From the different GPS velocity graphs, the values of the steady velocity are distributed with $\pm$ 0.1 m/s, whatever the speed is. When compared to the direct GPS velocity (when available), the computed velocity is always higher, the direct velocity bottoming the curve of the computed velocity. The velocity measurements during the tests are compared to the straight line velocity in Table (7.5). As expected, the velocity during a turn is less than the straight line velocity for equal RPM's and the higher the rudder angle is the higher the drop in velocity is. The values of the computed velocity seem closer to the straight line velocity than the direct GPS velocity and knowing that the boat movements are much too swift for their dynamics to be captured

Test	Straight Line Vel.	GPS Vel. (m/s)	Computed Vel. (m/s)	v_{GPS}
300,10	0.426	- - -	0.46	v+0.032
300,-20	0.426	- - -	0.44	v-0.046
300,-30	0.426	- - -	0.4	v-0.061
500,-10	0.777	0.78	0.78	v-0.071
500,-20	0.777	0.672	0.75	v-0.080
500,-30	0.777	0.57	0.67	v-0.098
700,-10	1.083	1.04	1.11	v-0.071
700,-20	1.083	0.88	1.07	v-0.129
700,-30	1.083	0.68	0.92	v-0.137

Table 7.5: GPS Velocity and Variation in sway velocity for the GPS

by the GPS velocity measurements, it is probably more reliable to compute the velocity using the position.

Moreover, the velocity (given by the GPS or computed) is the velocity of the boat section located at the abscissa of the GPS (0.97m in front of the ship Cog). If the sway velocity of the boat (in the boat frame) is noted v and the yaw rate is r, the sway velocity of the GPS sensor is:

$$v_{GPS} = v + x_r \cdot r \tag{7.3}$$

where $x_r = 0.97m$ is the position of the GPS in the boat frame. To get an idea of the perturbation in the sway velocity, it can be compared to the value of the forward velocity, taken from the velocity tests results presented in Section 7.1. The yaw rate r is taken from Table (7.4). The variations in sway velocity are presented in Table (7.5), the variations can reach up to 15 % of the forward velocity.

Ship Model Heading

Considering the three ways to compute the heading, the following observations can be made. First, the integrated yaw rate is not reliable as a measurement of heading variation at a long term. The best illustration is on Figure (K-10): from the GPS position graph on Figure (K-2), the boat makes 5 turns. This is confirmed by the GPS and magnetometer data. However, the integrated yaw rate leads to 6 turns. On the other graphs, compared to the magnetometer data, the integrated yaw rate is either ahead ([300,-20] on Figure (K-4), [300,-30] on Figure (K-5), [500,-10] on Figure (K-6), [700,-10] on Figure (K-9)) or behind ([500,-20] on Figure (K-7), [500,-

30] on Figure (K-8), [700,-30] on Figure (K-11)). The integrated yaw rate signal integrates all the noises and errors so it cannot be as reliable as the magnetometer measurements which are punctual and clearly need less processing. Moreover, even if the magnetometer is perturbed by some noise or disturbance at one point, this will not affect the following measurements as it does for the integrated yaw rate method.

As for the magnetometer signal, there exist a **non-linearity** for the heading measurements between 200 and 360 degrees. The non-linearity can be spotted on almost all the heading graphs, and it confirms the observations made during the turning experiments in the Alumni Pool.

Finally, for the tests where GPS heading was available, the heading signal is late compared to the magnetometer in two cases: [500,-20] on Figure (K-7) and [700,-10] on Figure (K-9). The signal is way ahead for the [700,20} test on Figure (K-10)). For [500,-10], magnetometer and GPS heading seem to be synchronized.
What is expected is a GPS signal late compared to the magnetometer: the GPS heading is computed internally using the position data and a **lag** of the GPS heading compared with the actual heading is expected. As for the case where the GPS is ahead of the magnetometer, it is probably due to a lag of the GPS logfile itself: the GPS and magnetometer data come from **two different logfiles** and thus have two different time vectors. The time vector of the magnetometer is given by the PC104 and the time vector of the GPS is given by the satellites in use.

Ship Model Accelerations

The acceleration signals during the circle maneuver tests have more noise than the acceleration signals during the test in the swimming pool. A positive x acceleration peak can be observed when the boat starts and a negative peak can be spotted when the boat stops if the velocity is high enough and the noise not too loud: it can be seen for [500,-30] (Figure (K-8)).

As for the acceleration on the y axis, the **centripetal acceleration** starts to appear when the boat starts turning: for [300,10] the rudder angle is positive so a positive turning rate and a positive centripetal acceleration is expected. This effect can be seen in Figure (K-3).
For all the other tests, since the rudder angle was negative, a negative centripetal acceleration

is expected. The effect is too small to be spotted on any of the 300 RPM test, but it exists for the [500,-10] (Figure (K-6)). As for the [500,-20] test, a sway perturbation before the movement starts (due to positioning the boat properly by hand before the test) affects the measurement of the sway acceleration during the first 10 seconds where the boat it supposed to be at rest.Since those 10 seconds are used to compute the mean sway offset at rest, the graph is then biased. The negative y centripetal acceleration can also be identified for [500,-30] on Figure (K-8), for [700,-10] on Figure (K-9) for [700,-20] on Figure (K-10) and for [700,-30] on Figure (K-11).

Ship Model path

Only the GPS path was plotted and not the path computed using the DMU data. The noise on the accelerations was too high and the duration of the test was too long for the double integration to lead to good results .

A interesting phenomena on the GPS path is the **drift** of the trajectory in the direction of the initial 20 seconds of straight trajectory. It seems that even after several minutes and turns, the ship model is still under the influence of the initial momentum.

Pitch and Roll Angles

The stabilized pitch and roll graphs gives the steady **list** and **heel** angles when the boat is at rest, they are listed in Table (7.6).

Moreover, the same phenomena as the ones described in the analysis of the turning test in Section 7.2.3 exist: when the boat starts moving, a positive peak in the pitch angle can be spotted, this means the stern of the boat is pitching. This is visible for all the tests, even the ones at 300 RPM. The second phenomenon is that the boat rolls outward the turn just at the beginning of the turn and inward the turn during the steady part of the turn. The [300,10] test is the only one for which the rudder angle is positive, what is expected is a small positive peak before the roll decreases below the steady value and stabilizes for all the rest of the turn. However, the velocity and rudder angle of the turn are too small for the positive peak to be spotted on Figure (K-3), but the second effect is visible (steady roll is -0.7 deg. compared to the -0.5 deg. of heel at rest).

As for all the other runs, what is expected is a negative peak of roll just when the turn starts and then the roll increasing to a steady value above the heel angle. The negative peak can be seen on the stabilized angles graph of [500,-30] on Figure (K-8) and [700,-20] on Figure (K-10).

The values of the steady roll during the turn are given for all runs in Table (7.6).

Test	List (deg.)	Heel (deg.)	Roll during turn
300,10	-1.2	-0.5	-0.7
300, -20	-1.2	- - -	-0.3
300, -30	-1.2	-0.5	-0.2
500, -10	1.2	-0.5	0.1
500, -20	1.2	-0.4	0.25
500, -30	1.2	-0.4	0.3
700, -10	-1.2	- - -	0.5
700, -20	-1.2	-0.5	0.9
700, -30	-1.2	-0.5	1
Mean Value	**-1.2**	**-0.5**	- - -

Table 7.6: List and Heel at rest, Steady Roll angle during a turn

Drift Angle

The drift angle β during the turn is illustrated on Figure (7-2), it is the angle between the tangent to the boat path and the heading of the boat. As explained in Section 6.3.5, knowing the drift angle allows to know the sway velocity: $v = U\sin(\beta)$, v directed outward the turn. The drift angle can be computed easily using the GPS data: at the time t_i, it is defined as the angle between the vector $(\vec{X}_{pos,i} - \vec{X}_{pos,i-1})$ and the vector $\vec{V}_{head,i}$ oriented along the **true heading**. However, the only problem in this method is that the GPS heading data for t_i is given with a lag compared to the position data at t_i. This lag can be evaluated by plotting the heading direction vector at each position $\vec{X}_{pos,i}$: since all runs start with a straight line during 20 seconds, the heading data given by the GPS should start as soon as the boat moves and the heading vector should be aligned with the straight line trajectory. Even if an estimation of the GPS lag can be obtained during this method, the error made on the lag is an error of one or two seconds but it makes the estimation of the drift angle vary between 5 and 10 degrees. The results of the measurements on the graphs are given in Table (7.7).

7.4 Summary

This chapter has presented the results and analysis of the three following types of testing: first the **velocity tests** preformed at the MIT ALumni Pool and MIT Towing Tank, then the

Test	GPS Lag (s)	Drift angle (deg)
500,-10	11	15
500,-20	9	23
700,-10	9	12
700,-20	8	25

Table 7.7: GPS lag and drift angle

results of the (partial) **turning tests** performed at the MIT pool and finally the results of the **circle maneuver tests** done at the BAE open water testing facility.

RPM vs Velocity relation was updated with the new results and the Nomoto parameters for the yaw dynamics model were also compute with the new data.

For the turning tests and circle maneuver, all the data types logged were thoroughly analyzed: accelerations, rotation rates, pitch and roll stabilized angles, heading, velocities and ship model path.

For almost all tests, the measurements are in conformity with what is expected from such tests. However, certain parameters like the noise and disturbances seen by the inertial unit and the GPS lag have to be taken into account and cause difficulties for data processing.

Chapter 8

CONCLUSION

8.1 Thesis Summary

This work accomplished the following objectives:

- getting a good understanding of the sensors which equip the boat,
- modeling the yaw-sway dynamics of ship model in order to design a robust heading controller ,
- understanding the existing remote control system of the boat and modifying it in order to implement the heading controller,
- presenting a way to implement with a minimum work a position controller using the heading controller previously and the GPS position data,
- do as many maneuvering tests as possible on the ship model and analyze all the data logged in order to get a maximum of information on the ship model maneuvering capabilities and characteristics.

  Unfortunately, not all the tests planned could be carried out and especially the heading controller could not be tested. The test carried out were: velocity tests which led to a RPM versus velocity relation, turning tests which led to a refinement of the yaw dynamics model and finally circle maneuver tests which allowed to determine notably tactical diameters, steady yaw rates and an evaluation of drift angles.

8.2 Conclusions

This section will summarize the most noteworthy points which appeared over the course of this study:

1. Positioning accurately the sensors and taking into account the position of the different sensor frames with respect to the boat frame is a key point to data analysis. The DMU is positioned very close to midships, so the DMU data reflect the behavior of the ship itself but the DGPS is located at the bow, one meter away from midships so the GPS position data are not exactly the position of midships. This was not taken into account in this study.

2. There are two main problems in the ship model system. The first one is the reliability of the connectors. Carrying the boat back and forth for testing put a high wear not only on the hull itself but on all the connectors. Even though the connectors were redone several times, one of them may eventually break at one point.
   The second problem is the wireless connection between the PC104 and the Laptop: it can break from time to time. Even if the watchdog is there to check any connection break and to reset it, the whole system may break and all connection lost with the only solution left being to reboot the PC104. One of the reason the connection may break is the quantity of data transmitted. Consequently, the implementation of the heading controller was designed so that to keep data transfer to a minimum between the two computers.

3. The comparison between the three measurements of the heading leads to the conclusion that the magnetometer heading is probably the most reliable source of heading measurements. Actually, the GPS lag is unpredictable and the eventual offset between the DAC logfile and the GPS logfile may worsen the measurements. As for the integrated yaw rate, it is simply not reliable for long term runs, any error at one point will bias all the next heading data.

4. The weak point of this thesis is the lack of data. Testing the boat takes an incredible amount of time and unfortunately testing locations suitable for the boat are not often available.

8.3 Recommendation for Future Work

The ship model system is fully operational and the method described in this work to design and implement the heading controller can in fact be used to design any type of controller, so many other tests and developments can be done with the ship model system presented in this work. The most important in the author's mind can be summarized as follows:

1. The first step of any future work should be to perform more tests on the ship model and especially the ones described in Chapter 6. Even if the objectives of the next project using the ship model hull implies modifying the system and eventually removing some components, more tests on the system as it is should be done to get a maximum of data. Particularly, the Dieudonné spiral and zif-zag maneuver would bring a lot of information on the maneuverability and behavior of the model ship. Spanning a large range of RPM's and rudder angle is also very important to fully characterize the boat.
   Actually, data on US Navy ships are not made public and the sources of any available data often unclear. So the best way to have any data on the ship model is to get them by extensive testing. The importance of not using the data of the real ship for the model ship if possible is justified by the fact that if the same system is used for a boat which maneuvering capabilities are known it would allow a comparison between the real ship and the model ship. This could demonstrate if a model ship at the scale of the DDG51 model can be accurate to predict the maneuverability capabilities of the full scale ship, which is unclear at the date of today.

2. Testing implies finding a good testing location which is seen by the author as the most urgent task for a future project with this hull. The Charles River proved to be not so good a choice and swimming pools are too small for the boat to fully turn or to reach steady state. Finding a location where the hull could be left overnight and where currents and waves are minimal would be the best solution.

3. A first start for a future work would be to build a more complex heading controller (like a LQG) a compare its performance to the PID heading controller.

4. Moreover, any future work should take advantage of the existing boat operating system to implement the position controller. The DGPS being connected directly to the PC104

via a serial port, getting GPS data in Real-time from the `all_in_one_module` RT module should be simple. The method to process the GPS data to obtain the positions in meters is already implemented in the Matlab GUI built to process data and can be translated into C without any problem.

5. Of course, the same method as the one using to implement on the PC104 the heading controller could be used to implement even a quite different controller such as a surge dynamic controller to simulate the LM2500 gas turbine dynamics of the real ship.

Appendix A

DDG51 Characteristics

This chapter gives a summary of the real DDG51 US Navy Destroyer characteristics. All the parameters presented in Table (A.1) are taken from the matlab codes of R. Quezada and M. Taylor (cf. references [14] and [18]).

Parameter	Value
Length (LBP)	142.04
Beam	17.98
Mass (T)	8,630.0 10^3
I_{zz} (kg.m^3)	23.22 10^9
x_G (m)	-0.85
A_w (m^2)	2,777.2
Rudder Area (single rudder) (m^2)	14.15
Rudder Aspect Ratio	1.18
Rudder Drag Coefficient	0.085
Midships-Rudder distance (m)	- 67.3
Rotational Moment of Inertia I_p	129.765512 10^3

Table A.1: Real DDG51 Parameters

In Table (??), b_1 and b_2 are the coefficients of the linearization of the thrust coefficient K_T with respect to the ratio of advance J:

$$K_T = b_1 - b_2 \cdot J, \qquad J = \frac{V_{ship}(1-w)}{n_p D} \tag{A.1}$$

n_p being the rotational speed of the propeller and D the diameter of the propeller.

In Table (??), γ_1 and γ_2 are the coefficients of the linearization of the open-water torque

Propeller Parameters	
Parameter	Value
Number of prop.	2
Type	CRPP
Number of blades	5
D (m)	7.21
w	0.22
P/D	1.38
η_R	0.984
b_1	0.8831
b_2	0.05
γ_1	0.1474
γ_2	0.0076
Propeller position x_p (m)	-63.81

LM2500 Gas Turbine	
Parameter	Value
a	0.830
b	0.258
c	2.088
d	0
f_m	5.3175
Q_m	101,965
n_m	60

Table A.2: Propeller and LM2500 Characteristics

coefficients K_{Q_0}:

$$K_{Q_0} = \gamma_1 - \gamma_2 \cdot J \tag{A.2}$$

For more details on the propeller [8, Vol. II, Chap. 6] can be consulted.

The coefficients a, b, c and d are related to the gas turbine characteristics. Those four coefficients appear in the propeller Torque Q_p equation:

$$Q_p = \eta_R \eta_G \lambda Q_m \Big(- (a\frac{f}{f_m} + b) \cdot \lambda \cdot \frac{n_p}{n_m} + c \cdot \frac{f}{f_m} + d \Big) \tag{A.3}$$

where η_R is the relative rotative efficiency, η_G is the gearbox efficiency, n_p is the propeller rotation rate, f is the fuel rate, f_m is the maximum fuel rate, n_p is the rotation rate of the propeller, n_m is the maximum rotation rate of the propeller, $\lambda = n_e/n_p$ where n_e is the engine rotation rate, Q_p is the propeller torque and Q_m is the maximum propeller torque.
More details on the DDG51 LM2500 gas turbine can be found in reference [13]

Parameters	Dimensional Value	Dimension	Non-Dimensional Parameters
Y_v/U	-1.1185 10^5	kg.m^{-1}	-0.010816
$Y_{\dot{v}}$	-6.986 10^6	kg	-0.0047567
Y_r/U	4.1959 10^6	kg	0.0035593
$Y_{\dot{r}}$	0	kg.m	0
N_v/U	1.4712 10^6	kg	-0.0033436
$N_{\dot{v}}$	0	kg.m	0
N_r/U	-2.0352 10^8	kg.m	-0.0009756
$N_{\dot{r}}$	-8.025 10^9	kg.m^2	-0.00027083
Y_δ/U^2	2.5858 10^4	kg.m^{-1}	0.0025
N_δ/U^2	-1.7333 10^6	kg	-0.0012
I_{zz}	2.322 10^{10}	kg.m^3	0.00078364
x_G	-0.85	m	-0.0059842

Appendix B

SHIP MODEL PAYLOAD

Element	Position[6] (m)	Weight (kg)	Moment of Inertia (kg.m^2)
Left Main Motor	- 0.73	7.43	3.96
Right Main Motor	-0.73	7.43	3.96
Main Motors Support Plate	-0.65	1.5	0.63
Rudder Motor + support	-1.38	2.1	4.0
Bow battery[7] + support	0.80	11.9	7.61
Midships Battery + support	-0.18	11.48	0.37
DMU box + support [8]	-0.01	4.18	0.00042
DGPS+ support[9]	0.97	1.178	1.11
Magnetometer box +support [10]	0.97	1.68	2.64
PC104 box	0.40	10.54	1.69
Amplifier Box	-0.38	10.72	1.55
Payload Center of Gravity (m)	-0.058	- - -	- - -
Total Payload (kg)	- - -	70.2	- - -
$I_{payload}$ (kg.m^2)	- - -	- - -	27.52
Ship Model Center of Gravity (m)	-0.025	- - -	- - -
Total Ship Model Weigth (kg)	- - -	86	- - -
I_{total} (kg.m^2)	- - -	- - -	65.6

Table B.1: Weight and position fo the equipment

[1]Position is referenced to midships, position is negative if the piece of equipment is aft of midships
[2]Weight of one battery alone is 10.73kg
[3]Weight of DMU sensor alone is 475 g
[4]Weight of DGPS alone is 0.678
[5]Weight of magnetometer sensor alone is 30 g

Appendix C

DMU TESTING

C.1 Test Bench

The two testing configurations are illustrated on Figures C-1 and C-2.

The testing macro is defined in terms of time and the RPM of the motor that drives the shaft. The left motor was used (Axis 0 of the MEI card). The macro is described quantitatively in Table (C.1).

Macro 2	
RPM	Time (s)
0	0
-1	10
0	19
-1	24
0	33

Table C.1: Macro Description

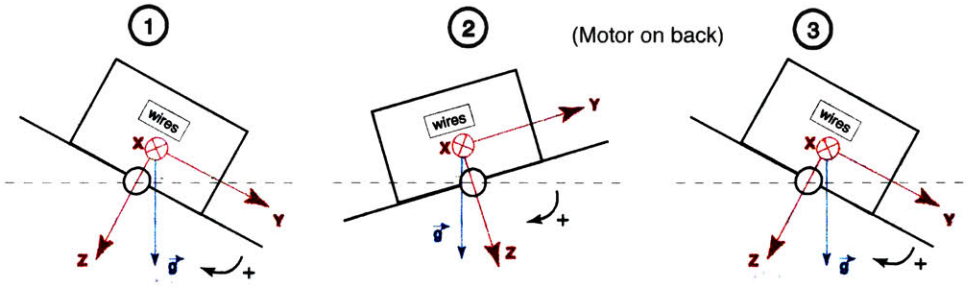

Figure C-1: Testing Configuration 1 for DMU Test Bench

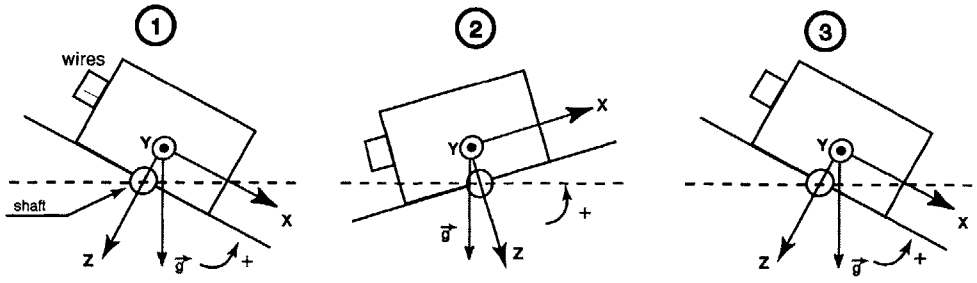

Figure C-2: Testing Configuration 2 for DMU Test Bench

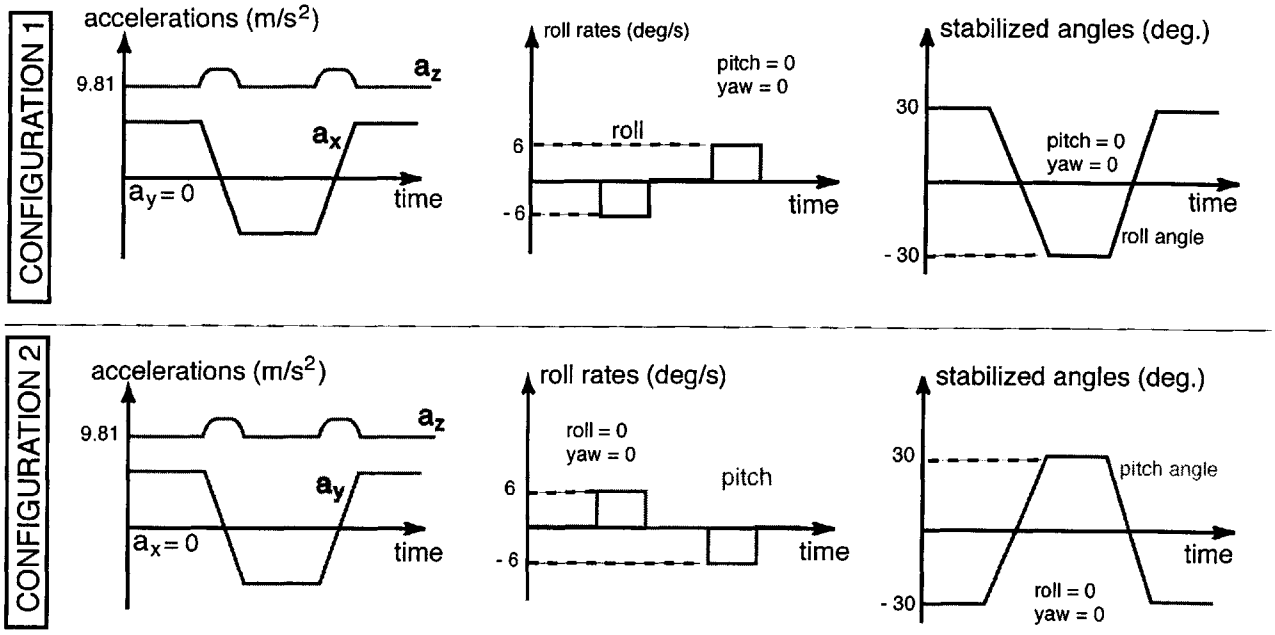

Figure C-3: Expected Measurement from the DMU

During the tests, the DMU is not submitted to any direct acceleration. However, the **gravity** $\vec{g}$ is present and the axes of the DMU frame see the components of this vector.
In state 1, the DMU platform touches the ground when inclined, so the angle between the DMU platform and the horizontal can be deduced from the platform dimension (approximately 30 degrees). The RPM of the motor was chosen such that the DMU rotates slowly enough: 1 RPM makes the DMU rotate of 6 degrees per second.
Consequently, the stabilized angles measured by the DMU when inclined should be around 30 degrees and the rotation rate should be 6 deg/s. The measurements that are expected from the DMU in each testing configuration are illustrated in Figure (C-3).

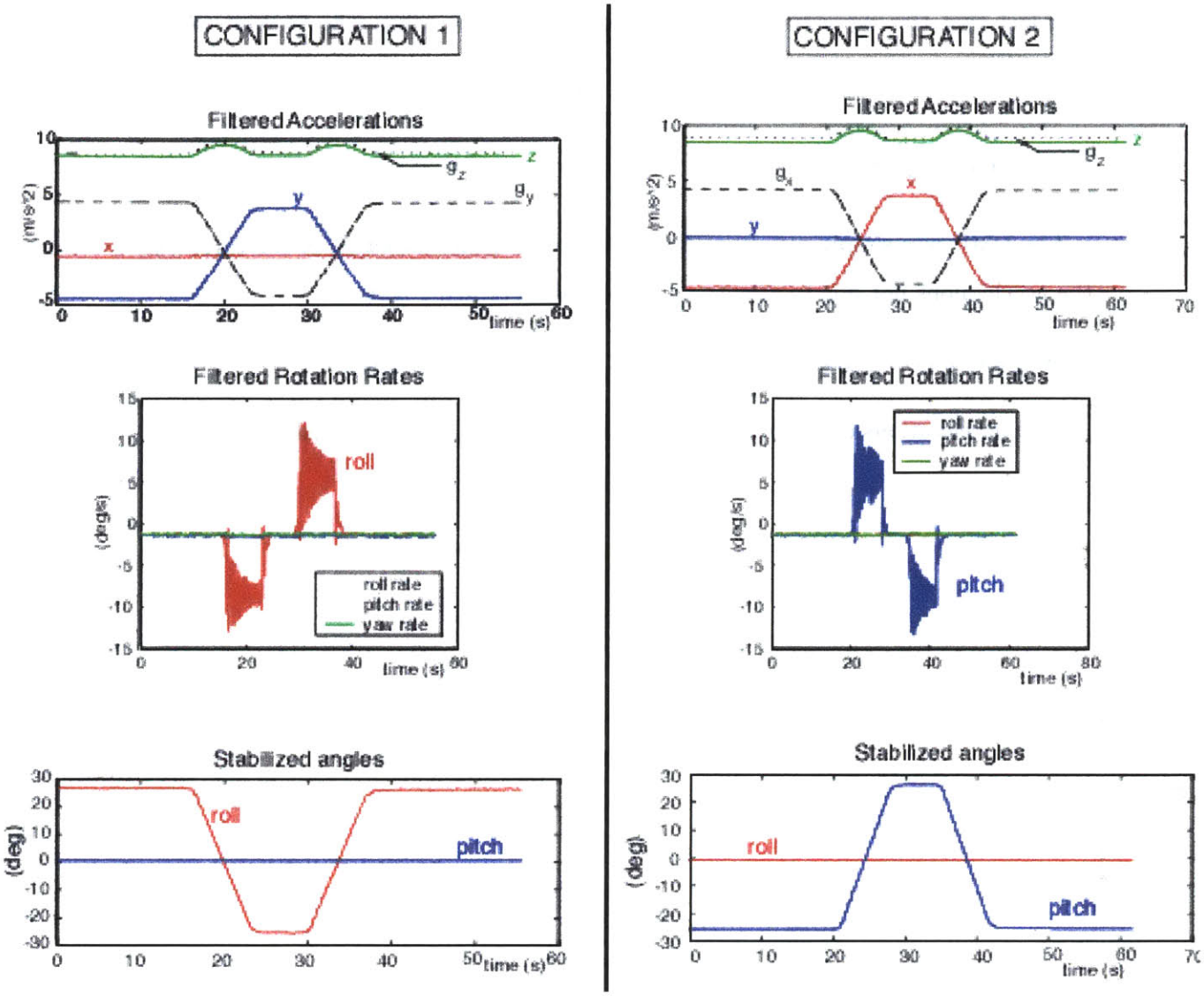

Figure C-4: Experimental Data from DMU

The data from the experiments are presented on Figure (C-4) for both configurations. The data are filtered to remove noise.

The differences between the expected and actual measurements are the following:

- the rotation of the DMU is not smooth and some vibrations can be seen on the rotation rate plot,
- the values of both the x and the y gravity components are opposite compared to the expected values.

The fact that the opposite values are opposite has to be taken into account when data from the DMU are processed.

C.2 Other Tests

The DMU was simply put on a table and moved in the diredtion of the three axis to verify the acceleraions not due to gravity. The conclusion of many tests is:

- x and y accelerations not due to gravity have the right signs
- z accelerations other gravity is opposite compare to the expected values.

Appendix D

SHIP PATH USING DMU DATA

D.1 Method

The data available through the DMU, once modified as explained in Section **??**, give the ship accelerations on the three axis: $a_x = \dot{u}$, $a_y = \dot{v}$ and $a_z = \dot{w}$ and the three rotation rates: roll rate p, pitch rate q and yaw rate r; those six parameters being described on *Figure (3-1)*. The rotation rates can be used to convert the accelerations in the body frame to the accelerations in the fixed frame. Then the accelerations in the fixed frame are integrated twice to find the position. The velocity in the body fixed frame can obtained integrating the three accelerations, using a simple **Euler forward scheme**:

$$u_{i+1} = u_i + \dot{u}_i \cdot \Delta t \tag{D.1}$$

$$v_{i+1} = v_i + \dot{u}_i \cdot \Delta t \tag{D.2}$$

$$w_{i+1} = w_i + \dot{u}_i \cdot \Delta t \tag{D.3}$$

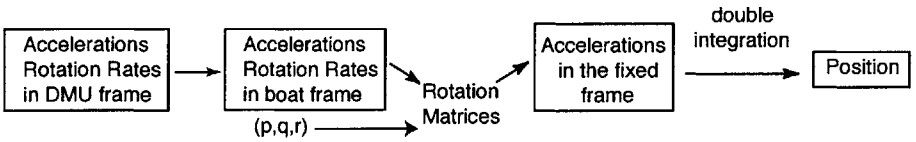

Figure D-1: Method to obtain the ship path using the DMU data

D.2 Matrices Relations

In order to compute the path of the ship in an Earth-based frame using DMU data, it is necessary to introduce the following notations (cf. [3]):

$$\eta = [\eta_1^T, \eta_2^T]^T \qquad \eta_1 = [v_x, v_y, v_z]^T \qquad \eta_2 = [\phi, \theta, \psi]^T \tag{D.4}$$

where η represents the position and velocity vector of the ship in the **Earth frame**. ψ, θ and ψ are the **Euler angles**.

$$\nu = [\nu_1^T, \nu_2^T] \qquad \nu_1 = [a_x^b, a_y^b, a_z^b]^T, \qquad \nu_2 = [p, q, r] \tag{D.5}$$

where ν represents the linear acceleration vector and angular velocity vector in the **Body fixed frame**.

The parameters are illustrated on Figure (3-1), in Chapter 3.

The relation between the position η_1 in the Earth frame and the linear velocity vector ν_1 in the body frame is the following:

$$\dot{\eta_1} = J_1(\eta_2)\nu_1 \quad \rightarrow \quad \nu_1 = J_1^{-1}(\eta_2)\dot{\eta_1} \tag{D.6}$$

where J_1 is a transformation and rotation matrix related to the Euler angles:

$$J_1(\eta_2) = C_{z,\psi}^T C_{y,\theta}^T C_{x,\phi}^T \quad \rightarrow \quad J_1(\eta_2)^{-1} = J_1(\eta_2)^T = C_{z,\psi} C_{y,\theta} C_{x,\phi} \tag{D.7}$$

where $C_{z,\psi}$, $C_{y,\theta}$ and $C_{x,\phi}$ are the **principal rotation matrices**. They are defined by:

$$\mathbf{C_{x,\phi}} = \begin{bmatrix} 1 & 0 & 0 \\ 0 & c_\phi & s_\phi \\ 0 & -s_\phi & c_\phi \end{bmatrix}, \quad \mathbf{C_{y,\theta}} = \begin{bmatrix} c_\theta & 0 & -s_\theta \\ 0 & 1 & 0 \\ s_\theta & 0 & c_\theta \end{bmatrix}, \quad \mathbf{C_{z,\psi}} = \begin{bmatrix} c_\psi & s_\psi & 0 \\ -s_\psi & c_\psi & 0 \\ 0 & 0 & 1 \end{bmatrix} \tag{D.8}$$

where s_α and c_α design respectively the sine and cosine of angle α. Using *Equation (D.8)*, the

final expression for the transformation matrix J_1 is:

$$\mathbf{J_1}(\eta_2) = \begin{bmatrix} c_\psi c_\theta & -s_\psi c_\phi + c_\psi s_\theta s_\phi & s_\psi s_\phi + s_\psi c_\phi s_\theta \\ s_\psi c_\theta & c_\psi c_\phi + s_\phi s_\theta s_\psi & -c_\psi s_\phi + s_\theta s_\psi c_\phi \\ -s_\theta & c_\theta s_\phi & c_\theta c_\phi \end{bmatrix} \tag{D.9}$$

There is a similar relation between the ship rotation rates [p,q,r] and the euler angles variations:

$$\dot{\eta_2} = J_2(\eta_2)\nu_2 \quad \rightarrow \quad \nu_2 = J_2^{-1}(\eta_2)\dot{\eta_2} \tag{D.10}$$

The expression for J_2 is obtained using the following relation:

$$\nu_2 = \begin{bmatrix} \dot{\phi} \\ 0 \\ 0 \end{bmatrix} + \mathbf{C_{x,\phi}} \begin{bmatrix} 0 \\ \dot{\theta} \\ 0 \end{bmatrix} + \mathbf{C_{x,\phi}C_{y,\theta}} \begin{bmatrix} 0 \\ 0 \\ \dot{\psi} \end{bmatrix} = J_2^{-1}(\eta_2)\dot{\eta_2} \tag{D.11}$$

Once again, using *Equation D.8*, the expression for J_2 becomes:

$$\mathbf{J_2}(\eta_2) = \begin{bmatrix} 1 & s_\phi t_\theta & c_\phi t_\theta \\ 0 & c_\phi & -s_\phi \\ 0 & s_\phi/c_\theta & c_\phi/c_\theta \end{bmatrix} \tag{D.12}$$

Finally, combining *Equation (D.6) and (D.10)*, a global relation can be obtained:

$$\begin{bmatrix} \dot{\eta_1} \\ \dot{\eta_2} \end{bmatrix} = \begin{bmatrix} J_1(\eta_2) & 0_{3\times3} \\ 0_{3\times3} & J_2(\eta_2) \end{bmatrix} \cdot \begin{bmatrix} \nu_1 \\ \nu_2 \end{bmatrix} \quad \rightarrow \quad \dot{\eta} = J_\eta \nu \tag{D.13}$$

The same method as described above can be used for $\eta_1 = [x, y, z]^T$ (position vector in the fixed frame) and $\nu_1 = [u, v, w]$ (velocity vector in the boat frame, which is given by the DMU). Integrating the equations twice gives the path of the boat in the boat frame of the first step of the integration (noted BF_0). To be able to compare different tests and especially to compare the DMU path to the GPS path, the path of the boat in BF_0 is rotated using the heading of the boat, so that the path will be given in a (North, East) frame.

The comparison between this method and the position given by the GPS are given in Figure (D-2), for several of the tests performed at Hanscom swimming pool in february 2001. The

DMU method is not very accurate because all the errors and noise are integrated twice.
The surge and sway velocities in the boat frame can be obtained by two means: either by using the accelerations in the boat frame, integrating them once and then rotating them back to the boat frame, or by integrating integrating directly the accelerations in the boat frame. For this last method to be easily used, the roll and pitch can be neglected and only the yaw rate can be taken into account:

$$u_i = (u_{i-1} + a_{x,i-1}) \cdot cos(\phi_i - phi_{i-1}) + (v_{i-1} + a_{y,i-1}) \cdot sin(\phi_i - phi_{i-1}) \quad \text{(D.14)}$$

$$v_i = -(u_{i-1} + a_{x,i-1}) \cdot sin(\phi_i - phi_{i-1}) + (v_{i-1} + a_{y,i-1}) \cdot cos(\phi_i - phi_{i-1}) \quad \text{(D.15)}$$

$$w(i) \sim 0 \quad \text{(D.16)}$$

For more detail on how to get position from an 6 axis inertial unit, [4] and [5] can be consulted.

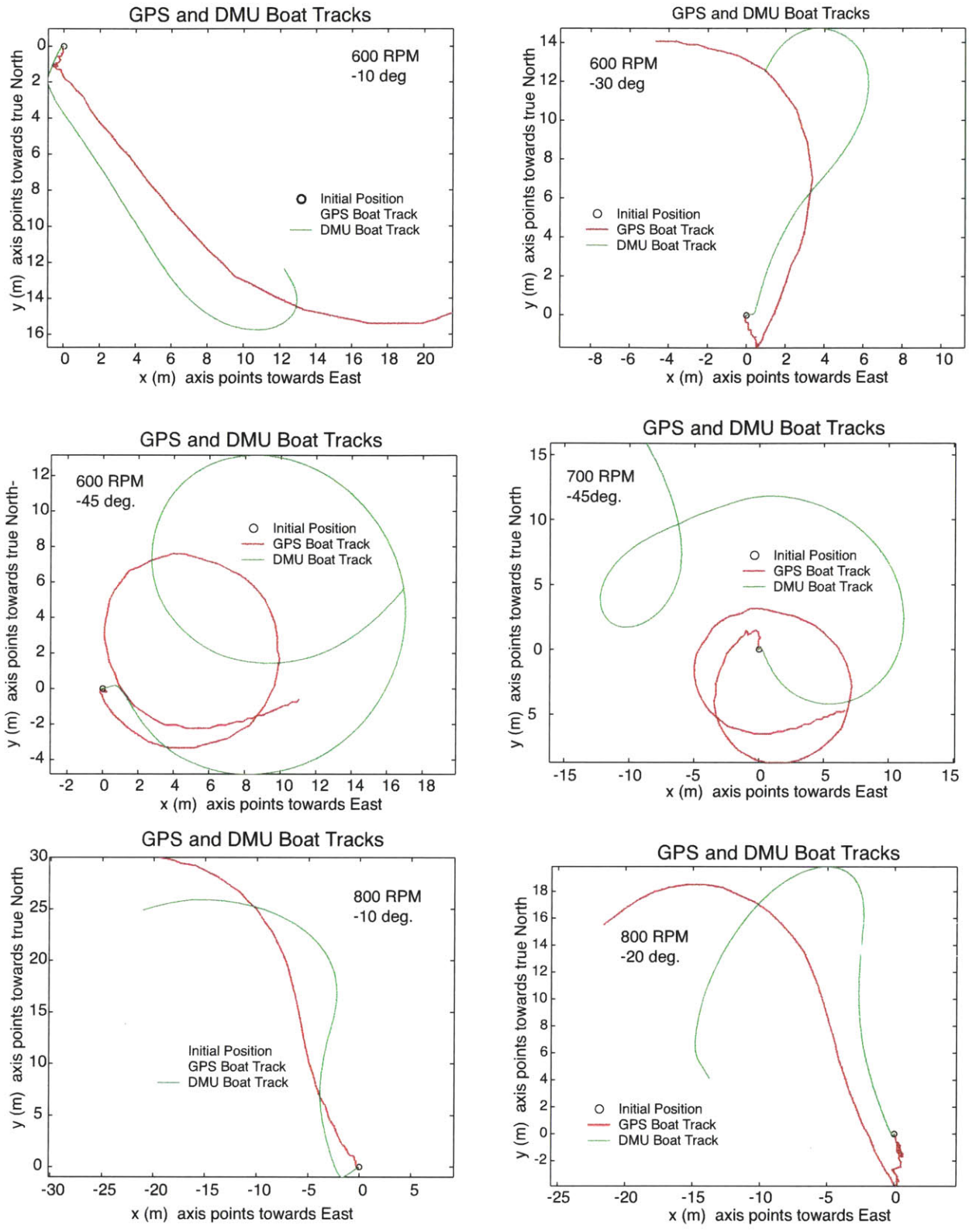

Figure D-2: Comparison between the positions given by the GPS and the DMU method

Appendix E

SLENDER BODY THEORY

A brief revue of important results of **Slender Body Theory** for hydrodynamic coefficients prediction will be given below. The main center of interest being the **yaw-sway** behavior of a boat , this part focuses on how to obtain estimations of the **hydrodynamic derivatives** that appears in the two coupled equations describing yaw and sway, that is to say: Y_v, Y_r, $Y_{\dot{r}}$, $Y_{\dot{v}}$, N_v, N_r, $N_{\dot{r}}$, $N_{\dot{v}}$.

Slender body theory can be applied to bodies for which d$\ll$L, where d is the width of the body and L is its length. $\epsilon = d/l$ is called the **slenderness** parameter.
This applies well to the DDG51 and its model boat, for which $\frac{d}{L} \simeq 0.12$.
For more details on Slender Body Theory, see [9, Chapter 7]. In this appendix, only the final and important results are given.

E.1 Fluid force - Y hydrodynamic coefficients

A rigid body is considered throughout the calculations.

E.1.1 Reference Frame

The body is supposed to be located at position $\vec{X}_{pos} = (X_{pos}, Y_{pos})$ in the inertial frame which at t=0 coincides with midships (which means: $(X_{pos}, Y_{pos})_0 = (0, 0)$). This reference frame will be called $\mathcal{R}$ from now on.
Then, it is supposed that the body is moving at a constant forward velocity U ($\vec{U} = U\vec{x}$), $\vec{x}$ being the x axis unit vector of $\mathcal{R}$. Consequently, a new frame noted $\mathcal{R}'$ can be defined such

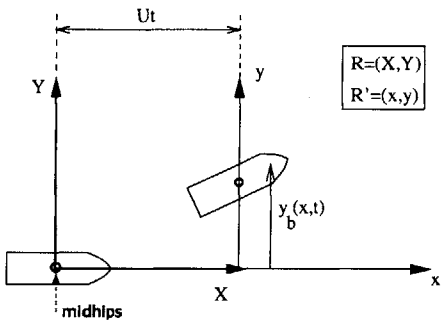

Figure E-1: Coordinate Systems for SBT

that the vector position $\vec{x}_{pos}$ of the body in $\mathcal{R}'$ verifies: $\vec{x}_{pos} = \vec{X}_{pos} - \vec{U} \cdot t$, that is to say $\mathcal{R}'$ is in translation at a constant speed with respect to $\mathcal{R}$. The relation between the two coordinate systems is then:

$$X_{pos} = x_{pos} + Ut \tag{E.1}$$

$$Y_{pos} = y_{pos} \tag{E.2}$$

The two frames are illustrated on Figure (E-1).

E.1.2 Elementary Fluid force

Now, the fluid force exerted on an element of the body of small length dx, located at abscissa X in $\mathcal{R}$ and at abscissa x in $\mathcal{R}'$ has a component along the y axis which is defined as follows:

$$dF_y(x,t) = -\frac{d}{dt}[v_b(x,t)m_a(x)] \cdot dx \tag{E.3}$$

where $m_a(x)$ is the sway added mass (added mass in the y direction) for the body section located at abscissa x, and $v_b(x,t)$ is the lateral velocity **as observed in a fixed reference frame**(like $\mathcal{R}$) at time t of the body section located at abscissa x. If v_b is positive then dF_y is negative and the fluid force tends to oppose the movement.

$v_b(x,t)$ is defined as follows:

$$v_b(x,t) = \frac{dy_b}{dt}(x,t) \tag{E.4}$$

where $y_b(x,t)$ is the y position on the IF (or on the fixed-body frame), x depending on time. Consequently, v_b can be rewritten as follows:

$$v_b(x,t) = \frac{\partial y_b}{\partial t}(x,t) + \frac{\partial x}{\partial t} \cdot \frac{\partial y_b}{\partial x} \tag{E.5}$$

Using *equation (E.1)*:

$$\frac{\partial x}{\partial t} = -U \tag{E.6}$$

and thus:

$$v_b(x,t) = \frac{\partial y_b}{\partial t} - U\frac{\partial y_b}{\partial x} = \underbrace{\left(\frac{\partial}{\partial t} - U\frac{\partial}{\partial x}\right)}_{\text{Fluid derivative}} y_b(x,t) \tag{E.7}$$

Finally, $\frac{\partial y_b}{\partial t}$ can be expressed as follows :

$$\frac{\partial y_b}{\partial t} = v(t) + xr(t) \tag{E.8}$$

where $v(t)$ is the sway velocity and $r(t)$ the yaw rate. For simplicity reasons, $v(t)$ is noted v, $r(t)$ is noted r and $m_a(x)$ might be noted m_a in the following. In Equation (E.3), the derivation with respect to the time t can be replaced by the **fluid derivative** as in Equation (E.4):

$$dF_y(x,t) = -\left(\frac{\partial}{\partial t} - U\frac{\partial}{\partial x}\right)\left(m_a(v+xr)\right)dx = -m_a(\dot{v} + x\dot{r}) + U\frac{\partial}{\partial x}\left(m_a(v+xr)\right) \tag{E.9}$$

E.1.3 Total Fluid force

To obtain the fluid force on all the body, it is necessary to integrate *equation E.9* over the body length. If x_n denotes the position of the nose of the body and x_t is the position of the tail in $\mathcal{R}'$:

$$\begin{aligned} F_y &= -\int_{x_t}^{x_n} ma(x)[\dot{w} + x\dot{q}]dx + U\int_{x_t}^{x_n} \frac{\partial}{\partial x}\big[m_a(x)(v+xr)\big]dx \\ &= -m_{22}\dot{v} + m_{26}\dot{r} + U\big[m_a(x)(v+xr)\big]_{x_t}^{x_n} \end{aligned}$$

where the following added mass definitions have been used:

$$m_{22} = \int_{x_t}^{x_n} m_a(x)dx \tag{E.10}$$

$$m_{26} = -\int_{x_t}^{x_n} x m_a(x)dx \tag{E.11}$$

$$\tag{E.12}$$

If the added mass of the nose is neglected (i.e if the nose of the body is pointed):

$$F_y = -m_{22}\dot{v} + m_{26}\dot{q} - U m_a(x_t)v - U m_a(x_t)x_t r \tag{E.13}$$

E.1.4 Y Hydrodynamic Coefficients

Using *equation E.13*, the estimated formulae of the hydrodynamic coefficients can then be deducted:

$$(F_y)_v = Y_v = -U m_a(x_t) \tag{E.14}$$

$$(F_y)_{\dot{v}} = Y_{\dot{v}} = -m_{22} \tag{E.15}$$

$$(F_y)_r = Y_r = -U m_a(x_t)x_t \tag{E.16}$$

$$(F_y)_{\dot{r}} = Y_{\dot{r}} = m_{26} \tag{E.17}$$

E.2 Fluid Moment

E.2.1 Elementary Fluid moment

The expression of the moment exerted by the fluid on a section of the body is given by the following expression:

$$dN_z = x dF_y \tag{E.18}$$

dN_z being the elementary moment around the z axis. Using the expression of dF_y given in *equation E.9*, the following equation is obtained:

$$dN_z = -x m_a(\dot{v} + x\dot{r}) + U\Big[\frac{\partial}{\partial x}\big(m_a(v + xr)\big)\Big]x \tag{E.19}$$

E.2.2 Total Fluid Force

The total fluid force on the body is obtained integrating E.19:

$$N_z = \int_{x_t}^{x_n} dN_z \tag{E.20}$$

which gives:

$$N_z = -\int_{x_t}^{x_n} [m_a(\dot{v} + x\dot{r})] - U\int_{x_t}^{x_n} \Big(\frac{\partial}{\partial x}\big(m_a(v + xr)\big)\Big)xdx \tag{E.21}$$

Then using the property: $\int_{x_2}^{x_1} \frac{df}{dx}(x)g(x)dx = [f(x)g(x)]_{x_2}^{x_1} - \int_{x_2}^{x_1} f(x)\frac{dg}{dx}(x)dx$:

$$\begin{aligned} N_z &= -\dot{v}\int_{x_t}^{x_n} m_a x dx - \dot{r}\int_{x_t}^{x_n} m_a x^2 dx + U[m_a(v + rx)x]_{x_t}^{x_n} - U\int_{x_t}^{x_n} m_a(v + xr)dx \\ N_z &= m_{26}\dot{v} - m_{66}\dot{r} - Ux_t m_a(x_t)v - Ux_t^2 m_a(x_t)r - Um_{22}v + Um_{26}r \end{aligned}$$

where the yaw added mass m_{66} has been introduced:

$$m_{66} = \int_{x_t}^{x_n} x^2 m_a(x)dx \tag{E.22}$$

Gathering terms:

$$N_z = -U\big(x_T m_a(x_t) + m_{22}\big)v + m_{26}\dot{v} - U\big(x_t^2 m_a(x_t) - m_{26}\big)r - m_{66}\dot{r} \tag{E.23}$$

E.2.3 Hydrodynamic Coefficients

So the hydrodynamic coefficients are:

$$(N_z)_v = N_v = -U\big(x_t m_a(x_t) + m_{22}\big) \tag{E.24}$$

$$(N_z)_{\dot{v}} = N_{\dot{v}} = m_{26} \tag{E.25}$$

$$(N_z)_r = N_r = -U\big(x_t^2 m_a(x_t) - m_{26}\big) \tag{E.26}$$

$$(N_z)_{\dot{r}} = N_{\dot{r}} = -m_{66} \tag{E.27}$$

It can be verified that those coefficients match with the expressions given by Newman, p346, table 7.1.

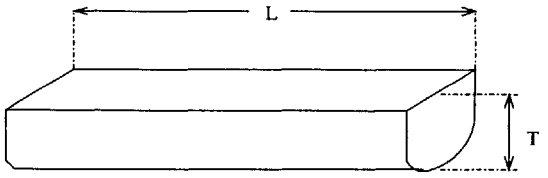

Figure E-2: Ship Approximation

E.3 Computing SBT hydrodynamic coefficients

E.3.1 Elementary added mass

The added mass of a circular element of diameter d and of elementary length dx along the x axis has the following added mass on the x direction:

$$\delta m_a(x) = \frac{\pi}{4}\rho d^2 dx \tag{E.28}$$

This added mass is equal to the mass of fluid displaced by the elementary volume $dV = \frac{\pi}{4}d^2dx$.

E.3.2 "Rectangular Platform" estimation

A first approximation to compute the added mass of a ship is to replace the ship by a half cylinder of radius equal to the draft T of the ship, this radius being supposed constant along the ship length (cf. Figure (E-2)).

That means for any section of the ship located at abscissa x, the added will be obtained integrating Equation (E.28) with $d(x) = 2T$:

$$\forall x \quad m_a(x) = \frac{\delta m_a(x)}{dx} = \frac{1}{2} \cdot \frac{\pi}{4}\rho(2T)^2 = \frac{1}{2}\pi\rho T^2 \tag{E.29}$$

where the factor 1/2 had to be used to account for the fact that the ship is half of a cylinder. Consequently, the added mass of the stern section can be approximated by the following formula: $m_a(x_t) = \frac{1}{2}\pi\rho T^2$

Then the other added mass defined in Equations E.10 and E.32 can be computed as follows:

$$m_{22} = \int_{x_t}^{x_n} m_a(x)dx = \int_{L/2}^{L/2} \frac{\pi}{2}\rho T^2 = \frac{\pi}{2}\rho T^2 L \tag{E.30}$$

$$m_{26} = -\int_{x_t}^{x_n} x m_a(x)dx = 0 \tag{E.31}$$

$$m_{66} = \int_{x_t}^{x_n} x^2 m_a(x)dx = \frac{\pi}{24}\rho T^2 L^3 \tag{E.32}$$

Equation E.31 comes from the fact that the body is supposed to be symmetric about midships, which of course is not true for the real ship.

Consequently, knowing x_t, $m_a(x_t)$, m and U , all the Y and N hydrodynamic parameters can be computed. It can be noted that N_r, Y_r, N_v and Y_v are linear function of the ship velocity of advance U.

E.4 Other ways to compute the hydrodynamic coefficients

E.4.1 Semi-empirical Methods and Regression Analysis

Reference [8, Vol. 3, Section 9, p248] gives an approximate way of computing the hydrodynamic coefficients using only the following parameters: ship length L, ship beam B, ship draft T and block coefficient C_B, from the results of Clarke [1]. Clarke compared empirical formulas developed by Smitt [16], Norrbin [11] and Inoue [7] against scatter plots of velocity derivatives available in the literatures. He used multiple linear regression analysis to develop the following empirical formulae:

$$Y'_{\dot{v}} = -\pi\left(\frac{T}{L}\right)^2\left[1 + 0.16\frac{C_B B}{T} - 5.1\left(\frac{B}{L}\right)^2\right] \tag{E.33}$$

$$Y'_{\dot{r}} = -\pi\left(\frac{T}{L}\right)^2\left[0.67\frac{B}{L} - 0.033\left(\frac{B}{T}\right)^2\right] \tag{E.34}$$

$$N'_{\dot{v}} = -\pi\left(\frac{T}{L}\right)^2\left[1.1\frac{B}{L} - 0.041\frac{B}{T}\right] \tag{E.35}$$

$$N'_{\dot{r}} = -\pi\left(\frac{T}{L}\right)^2\left[\frac{1}{12} + 0.017\frac{C_B B}{T} - 0.33\frac{B}{L}\right] \tag{E.36}$$

$$Y'_{v} = -\pi\left(\frac{T}{L}\right)^2\left[1 + 0.40\frac{C_B B}{T}\right] \tag{E.37}$$

$$Y'_{r} = -\pi\left(\frac{T}{L}\right)^2\left[-\frac{1}{2} + 2.2\frac{B}{L} - 0.80\frac{B}{T}\right] \tag{E.38}$$

$$N'_{v} = -\pi\left(\frac{T}{L}\right)^2\left[\frac{1}{2} + 2.4\frac{T}{L}\right] \tag{E.39}$$

$$N'_{r} = -\pi\left(\frac{T}{L}\right)^2\left[\frac{1}{4} + 0.039\frac{B}{L} - 0.56\frac{B}{T}\right] \tag{E.40}$$

E.4.2 Fossen's approximations

Another way of approximating the hydrodynamic coefficient is to use the formulas presented in [3], supposing the ship is symmetrical:

$$Y'_v = -(\frac{\pi T}{L} - C_{D0}) \quad \text{(E.41)}$$

$$Y'_r = X'_{\dot{u}} + \frac{x_P}{L} Y'_v \quad \text{(E.42)}$$

$$N'_v = -(X'_{\dot{u}} - Y'_{\dot{v}}) + \frac{x_P}{L} Y'_v \quad \text{(E.43)}$$

$$N'_r = \frac{1}{4} Y'_v \quad \text{(E.44)}$$

$$Y'_\delta = \rho \frac{\pi}{4} \frac{A_\delta}{LT} \quad \text{(E.45)}$$

$$N'_\delta = -\frac{1}{2} Y'_\delta \quad \text{(E.46)}$$

where C_{D0} is the drag coefficient of the ship at zero angle of attack (small for slender bodies), A_δ is the rudder area, x_P is the distance between the center of gravity of the boat and the center of pressure. x_P can be approximated by:

$$x_P = x_G \pm 0.1L$$

Then the added mass derivatives that appears in Equations E.41-E.46 can be approximated by:

$$X_{\dot{u}} = -(0.05m \text{ to } 0.10m) \quad \text{(E.47)}$$

$$Y_{\dot{v}} = -(0.70m \text{ to } 1.00m) \quad \text{(E.48)}$$

$$Y_{\dot{r}} = 0 \quad \text{(E.49)}$$

$$N_{\dot{v}} = -(0.01 I_{zz} \text{ to } 0.1 I_{zz}) \quad \text{(E.50)}$$

where:

$$I_{zz} = m x_G^2 + I_r, \qquad I_r = m r^2 \quad \text{where } 0.15L < r < 0.30L$$

Appendix F

SCALING & NON-DIMENSIONALIZATION

F.1 Scaling process

The main goal of model testing is to be able to reproduce the real flow around the model boat. This flow can be characterized by the two following non dimensional numbers;

1. **Froude number**

$$F_r = \frac{V}{\sqrt{g \cdot L}} \tag{F.1}$$

V : velocity of the ship

L : length of the ship

2. **Reynolds number**

$$R_e = \frac{V \cdot L}{\nu} \tag{F.2}$$

ν : kinematic viscosity of the fluid (for the real boat it is salt water, and for the model boat it is fresh water)

For the scale flow to have exactly the same pattern as the flow around the real ship, the following should be verified:

$$(F_r)_{real} = (F_r)_{scaled} \tag{F.3}$$

$$(R_e)_{real} = (R_e)_{scaled} \tag{F.4}$$

By a simple calculation and knowing that sea water has a kinematic viscosity very close to that of the fresh water,it is obvious that the two previous equations cannot be satisfied at the same time.

Froude's assumption is that at equal Froude numbers, the model and full scale ship have the same friction resistance coefficient. So, Froude numbers will be taken as equal. As for Reynolds number, the flow around the real ship being turbulent, special care has to be taken that the flow around the scale ship is also turbulent. This means that the Reynolds number of the ship has to be high enough. Consequently, the laminar flow has to be tripped deliberately with some kind of roughness near the bow. To add roughness on the DDG51 hull, turbulence stimulators were added to the bow.

The scaling ratio between the real boat and the model is defined as follows:

$$\lambda = \frac{L_s}{L_m} \tag{F.5}$$

where subscript s denotes the real ship and subscript m denotes the model ship. For the DDG51 model, this scaling ratio is λ=**46.9**.

According to be able to do more realistic testing, the Froude number of the ship and model are taken to be equal:

$$F_{r_s} = \frac{V_s}{\sqrt{g \cdot L_s}} = F_{r_m} = \frac{V_m}{\sqrt{g \cdot L_m}} \tag{F.6}$$

So consequently:

$$\frac{V_s}{V_m} = \sqrt{\frac{L_s}{L_m}} \tag{F.7}$$

F.2 Non-Dimensionalization

The non-dimensionalization is obtained using the $\frac{\rho}{2}$ and the following formulas:

$$v = U \cdot v' \quad [m \cdot s^{-1}] \tag{F.8}$$
$$\dot{v} = \frac{U^2}{L} \cdot \dot{v}' \quad [m \cdot s^{-2}] \tag{F.9}$$
$$r = \frac{U}{L} \cdot r' \quad [s^{-1}] \tag{F.10}$$
$$\dot{r} = \frac{U^2}{L^2} \cdot \dot{r}' \quad [s^{-2}] \tag{F.11}$$
$$x_G = L \cdot x'_G \quad [m] \tag{F.12}$$
$$m = \frac{1}{2}\rho L^3 \cdot m' \quad [kg] \tag{F.13}$$
$$I_{zz} = \frac{1}{2}\rho L^5 \cdot I'_{zz} \quad [kg \cdot m^2] \tag{F.14}$$
$$Y_{\dot{v}} = \frac{1}{2}\rho L^3 \cdot Y'_{\dot{v}} \quad [kg] \tag{F.15}$$
$$Y_{\dot{r}} = \frac{1}{2}\rho L^4 \cdot Y'_{\dot{r}} \quad [kg \cdot m] \tag{F.16}$$
$$N_{\dot{v}} = \frac{1}{2}\rho L^4 \cdot N'_{\dot{v}} \quad [kg \cdot m] \tag{F.17}$$
$$N_{\dot{r}} = \frac{1}{2}\rho L^5 \cdot N'_{\dot{r}} \quad [kg \cdot m^2] \tag{F.18}$$
$$Y_v = \frac{1}{2}\rho L^2 U \cdot Y'_v \quad [kg \cdot s^{-1}] \tag{F.19}$$
$$Y_r = \frac{1}{2}\rho L^3 U \cdot Y'_r \quad [kg \cdot m \cdot s^{-1}] \tag{F.20}$$
$$N_v = \frac{1}{2}\rho L^3 U \cdot N'_v \quad [kg \cdot m \cdot s^{-1}] \tag{F.21}$$
$$N_r = \frac{1}{2}\rho L^4 U \cdot N'_r \quad [kg \cdot m^2 \cdot s^{-1}] \tag{F.22}$$
$$Y_\delta = \frac{1}{2}\rho U^2 L^2 Y'_\delta \tag{F.23}$$
$$N_\delta = \frac{1}{2}\rho U^2 L^3 N'_\delta \tag{F.24}$$

The non-dimensional velocity being $U' = 1$, the following relations are verified:

$$\left(\frac{Y_v}{U}\right)' = Y'_v \quad , \quad \left(\frac{Y_r}{U}\right)' = Y'_r \quad , \quad \left(\frac{N_v}{U}\right)' = N'_v \quad , \quad \left(\frac{N_r}{U}\right)' = N'_r \tag{F.25}$$
$$\left(\frac{Y_\delta}{U^2}\right)' = Y'_\delta \quad \left(\frac{N_\delta}{U^2}\right)' = N'_\delta \tag{F.26}$$

Appendix G

YAW RATE GRAPHS

Hanscom Swimming Pool- Feb. 2001

The yaw rate results of the tests performed at Hanscom Air Force Base swimming pool in February 2001 are presented here.

Curve fitting along with the equation used to approximate the variation of the yaw rate are both displayed on each graph.

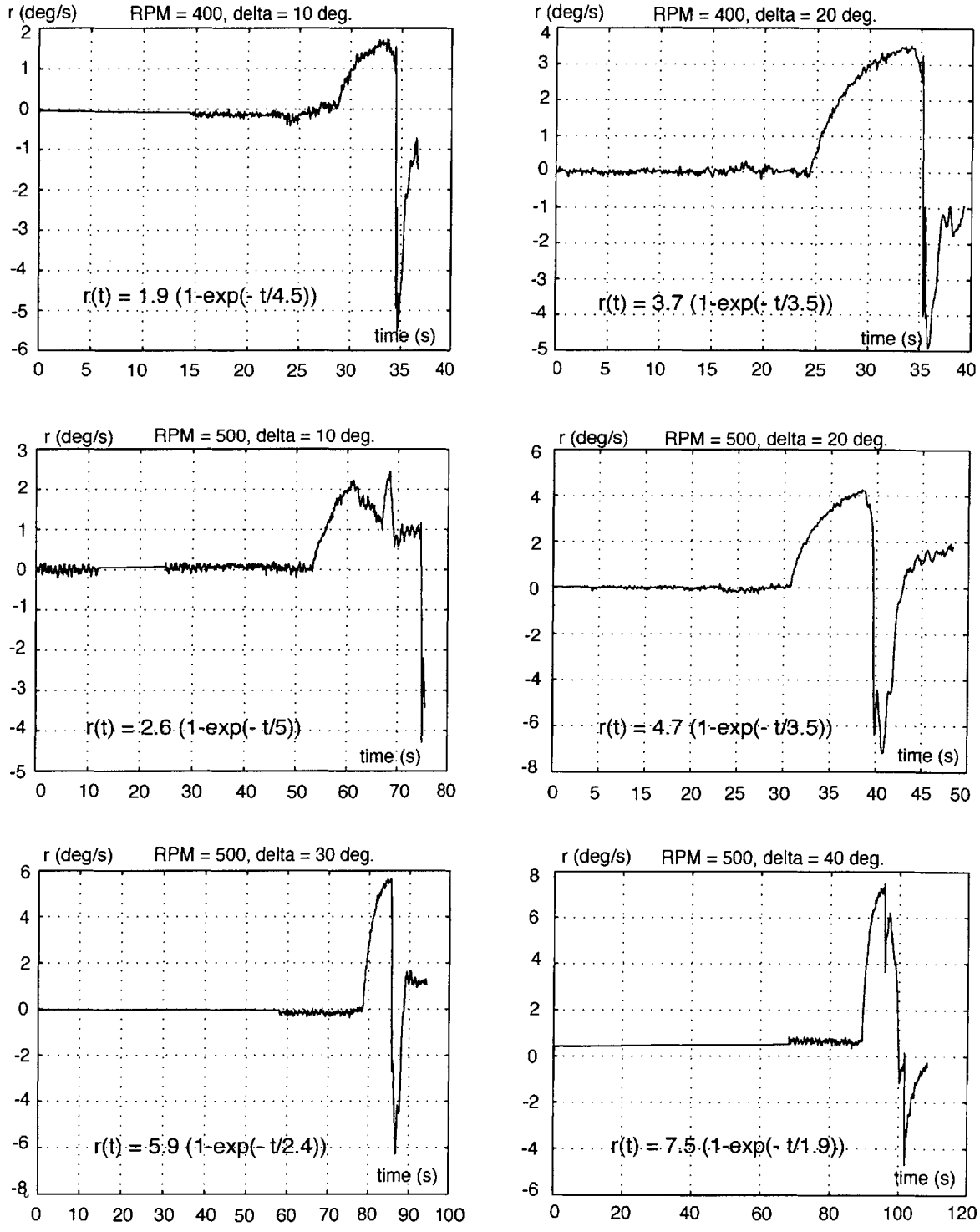

Figure G-1: Experiments in Hanscom Pool - 1/2

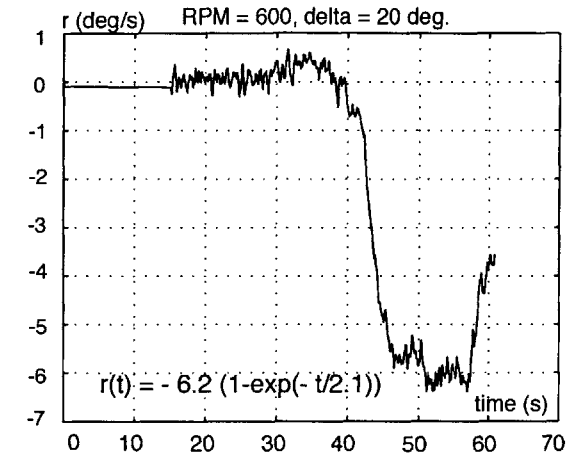

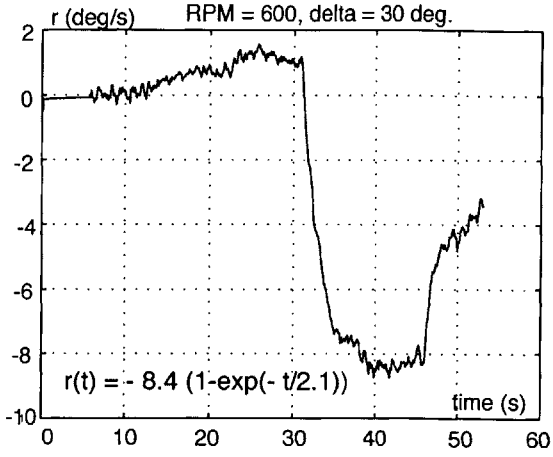

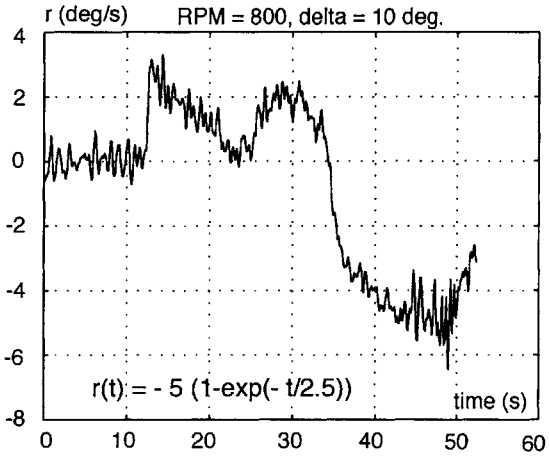

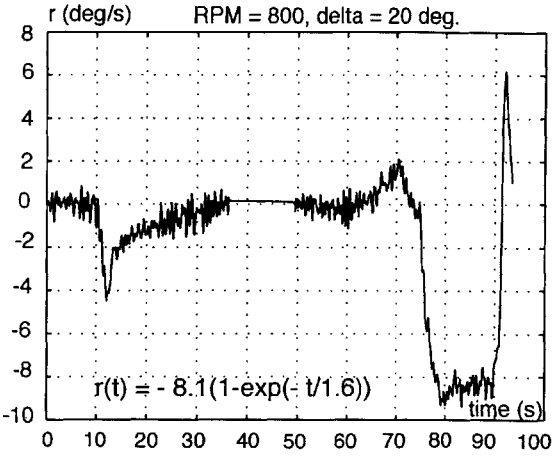

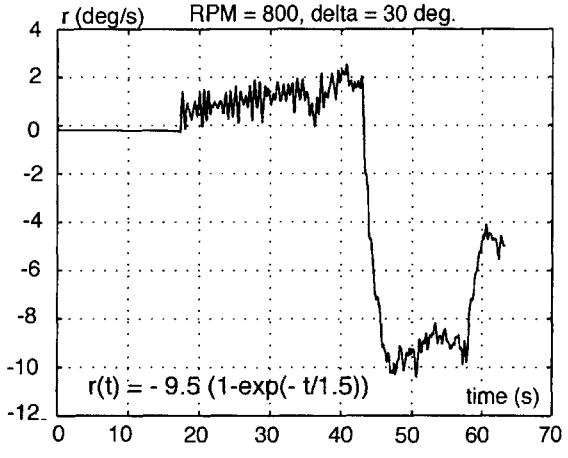

Figure G-2: Experiments in Hanscom Pool - 2/2

Appendix H

FIFO'S AND THREADS

H.1 FIFO'S

This section summarizes the structure of the data transmitted by all Fifo's used in the ship model software (in the Laptop software as well as in the PC104 software).

FIFO list and data structures			
Name	**PC104**	Link[1]	**Laptop**
rtf1	das_data_stuct		mei_cmd_struct
rtf2	- - -		wdr_msg_struct
rtf3	- - -		wdr_msg_struct
rtf4	- - -		head_msg_struct
rtf5	msg_struct		wdr_msg_struct
rtf10	mei_data_struct		- - -
rtf11	msg_struct		- - -
rtf12	msg_struct		- - -
rtf13	mei_cmd_struct		- - -
rtf14	mei_cmd_struct		- - -
rtf15	char	⟵	char
rtf16	mei_cmd_struct	⟵	mei_cmd_struct
rtf17	das_data_struct	⟶	das_data_struct
rtf18	mei_data_struct	⟶	mei_data_struct
rtf30	- - -		head_msg_struct
rtf31	head_msg_struct	⟵	head_msg_struct
rtf33	head_msg_struct		- - -
rtf36	head_msg_struct	⟵	head_msg_struct

FIFO data structures	

struct msg_command{
int command;
int period;
};
	struct wdr_msg_struct{
	int command;
	int period
	};

struct mei_cmd_struct{
int cmd;
int16 axis
double pos;
double vel;
double acc;
double jer;
hrtime_t time;
};
	struct mei_datat_struct{
	int velAxis0;
	int velAxis1;
	int velAxis2;
	int volt0;
	int volt1;
	int volt2;
	hrtime_t time;
	};

struct das_data_struct{
int data[16];
hrtime_t time;
};
	struct mei_data_struct{
	int command;
	int period;
	double value;
	};

Table H.1: FIFO list and data structure

[1]An arrow means the fifo is transmitted from one computer to the computer at which the arrow points

H.2 Threads

This section summarizes all the threads used in the ship model software. All the threads are **periodic threads** and each thread is responsible for a real-tome task to be performed periodically.

H.2.1 Laptop Threads

Three threads are implemented in the wdrmod module on the Laptop:

1. **wdrtask** thread: this thread is periodic of period T_1=msg.period×1000 (nanoseconds), where msg.period is defined in the Laptop GUI such that $\mathbf{T = 0.01s}$.
   This thread checks every T_1 seconds if a motor command (main motor or rudder motor) has been entered in the GUI in the **rtf1 Fifo**. If yes, the thread copies the command into an outgoing (**rtf16**) which is transmitted to the PC104.
   The thread is initialized when the GUI is launched, started when the remote control is activated from the GUI, and stopped when the remote control is stopped by the GUi or by the watchdog.

2. **mytask** thread: this thread is also periodic of period T_2=msg.period×5000 (nanoseconds), which means $\mathbf{T_2 = 0.05s}$.
   The thread checks every T_2 seconds if MEI and DAC data are sent by the PC104 via the incoming Fifo's **rtf17** and **rtf18**. If yes, the data are copied to the outgoing Fifo's **rtf19** and **rtf20**, which are transmitted to the GUI for display. It is initialized, started and stopped the same way as the wdrtask thread,

3. **headtask** thread: this periodic thread has a period T_3=hmsg.period×1000(ns) where hmsg.period is defined in the Laptop GUI (hmsg.period=100,000) so that $\mathbf{T_3 = 0.1s}$.
   The thread checks every T_3 seconds if a heading command is entered in the GUI (in **rtf35**), if yes the heading command is copied in the outgoing Fifo **rtf36** to be sent to the PC104.

H.2.2 PC104 Threads

The PC104 remote control module all_in_one_module, there are also three threads, each thread being the equivalent of a wdrmod thread.

- **alltask** thread: periodic thread of period T_1=msg.period×1000(ns)=**0.01s** where msg.period is defined in the allcontrol program.

  The thread checks every T_1 minutes if a motor command is sent to the PC104 via **rtf16**, if yes those commands are put in another Fifo sent to the data logging program (**rtf14**). The thread also sample the DAC and MEi cards and put the data in Fifo's to be sent to the data logging program (**rtf1** and **rtf10**).

  The thread is initialized and started when the data logging program (allcontrol.cpp) is launched and stopped when data logging is stopped,

- **mytask** thread: periodic thread of period T_2=msg×5000(ns)=**0.05s**.

  The thread samples every T_2 seconds the DAC and MEI cards and put the data into outgoing Fifo's (**rtf17** and **rtf18**) to be sent to the wdrmod module.

  It is initialized, started and stopped the same way as the alltask thread,

- **headingtask** thread: periodic of period T_3=hmsg.period×1000(ns)=**0.1s**.

  The thread checks every T_3 seconds if a heading command is sent via **rtf36** Fifo and implements the discrete heading controller with a sampling time of $T_s = T_3$.

Appendix I

YAW RATE GRAPHS

MIT Alumni Swimming Pool, Dec. 2001

The yaw rate results of the tests performed in the MIT Alumni swimming pool are presented here.

The curve fitting along with the equations used to model the yaw rate variation with time are displayed on each graph.

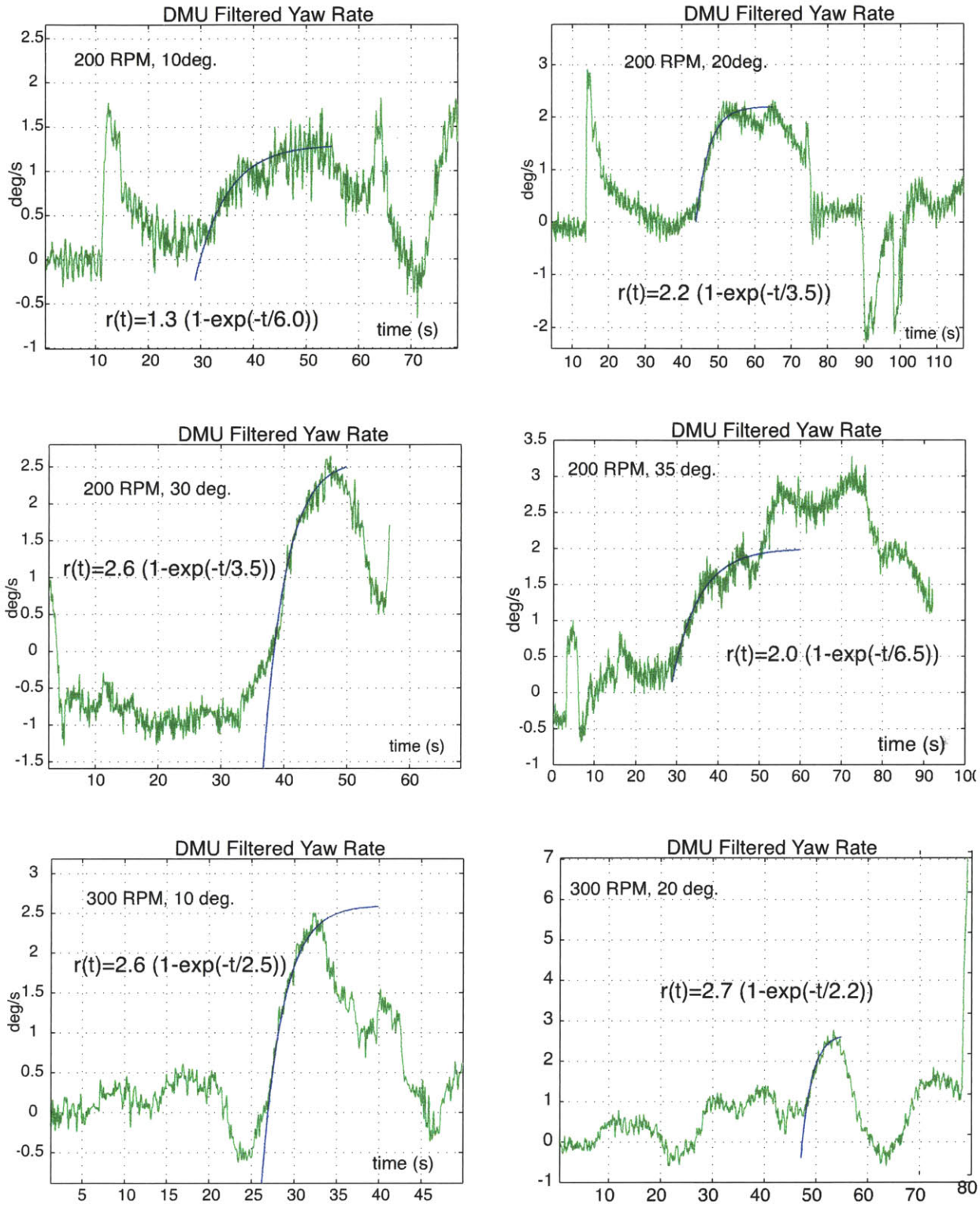

Figure I-1: Yaw rotation rates curve fitting for different experiments (1/6)

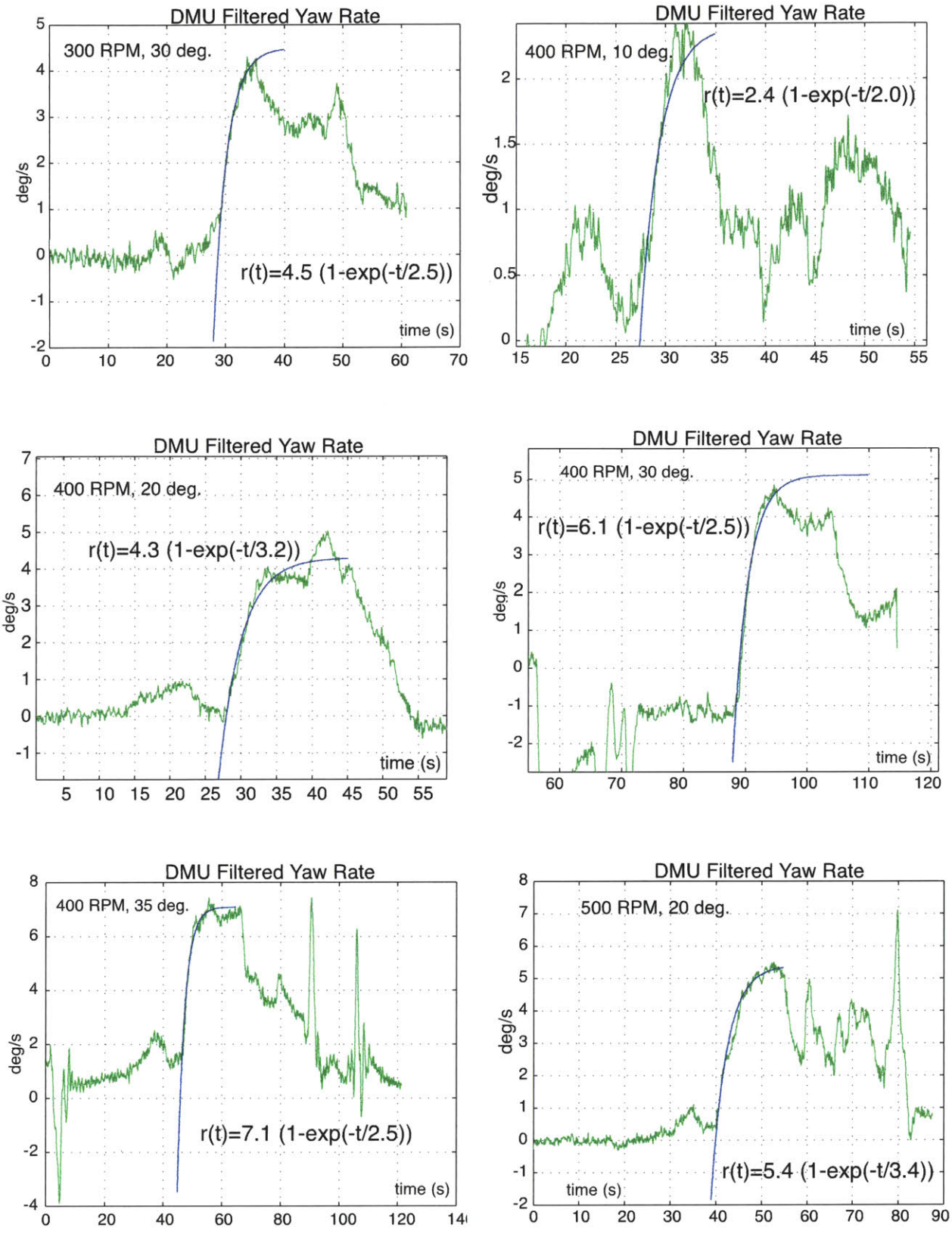

Figure I-2: Yaw rotation rates curve fitting for different experiments(2/6)

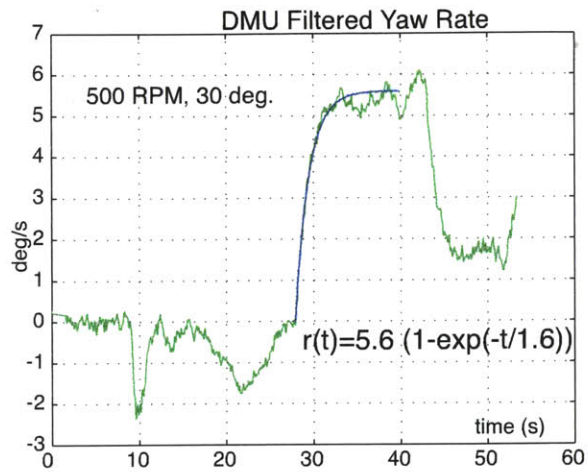

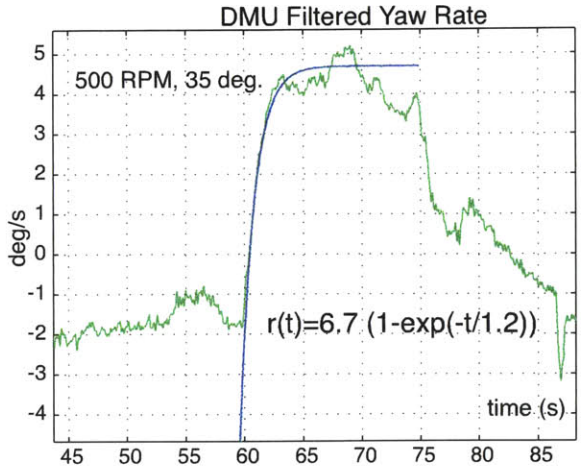

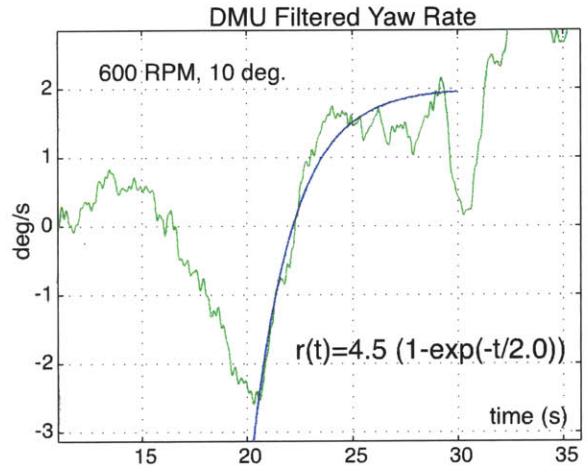

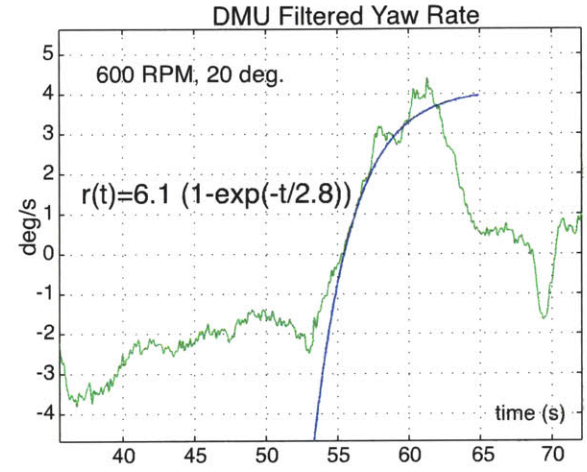

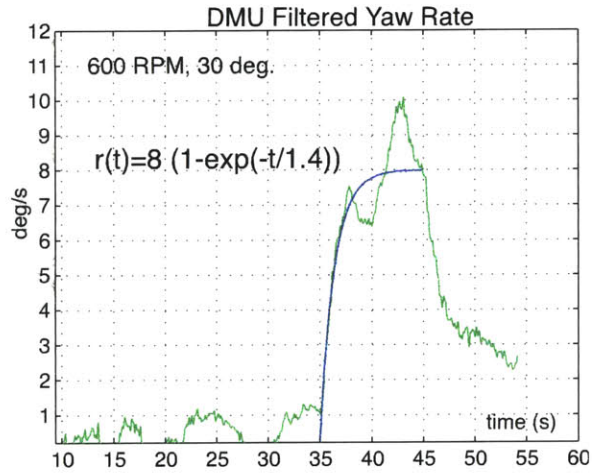

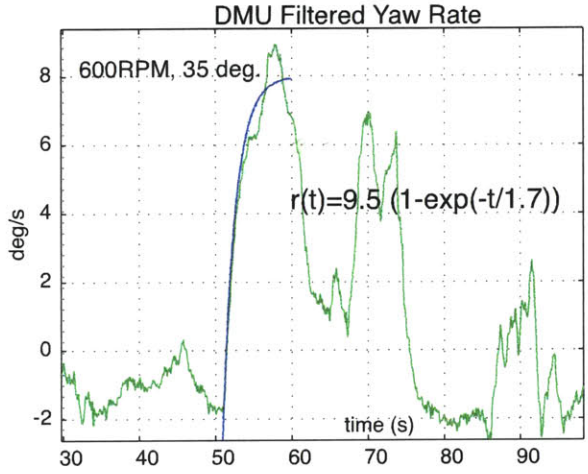

Figure I-3: Yaw rotation rates curve fitting for different experiments(3/6)

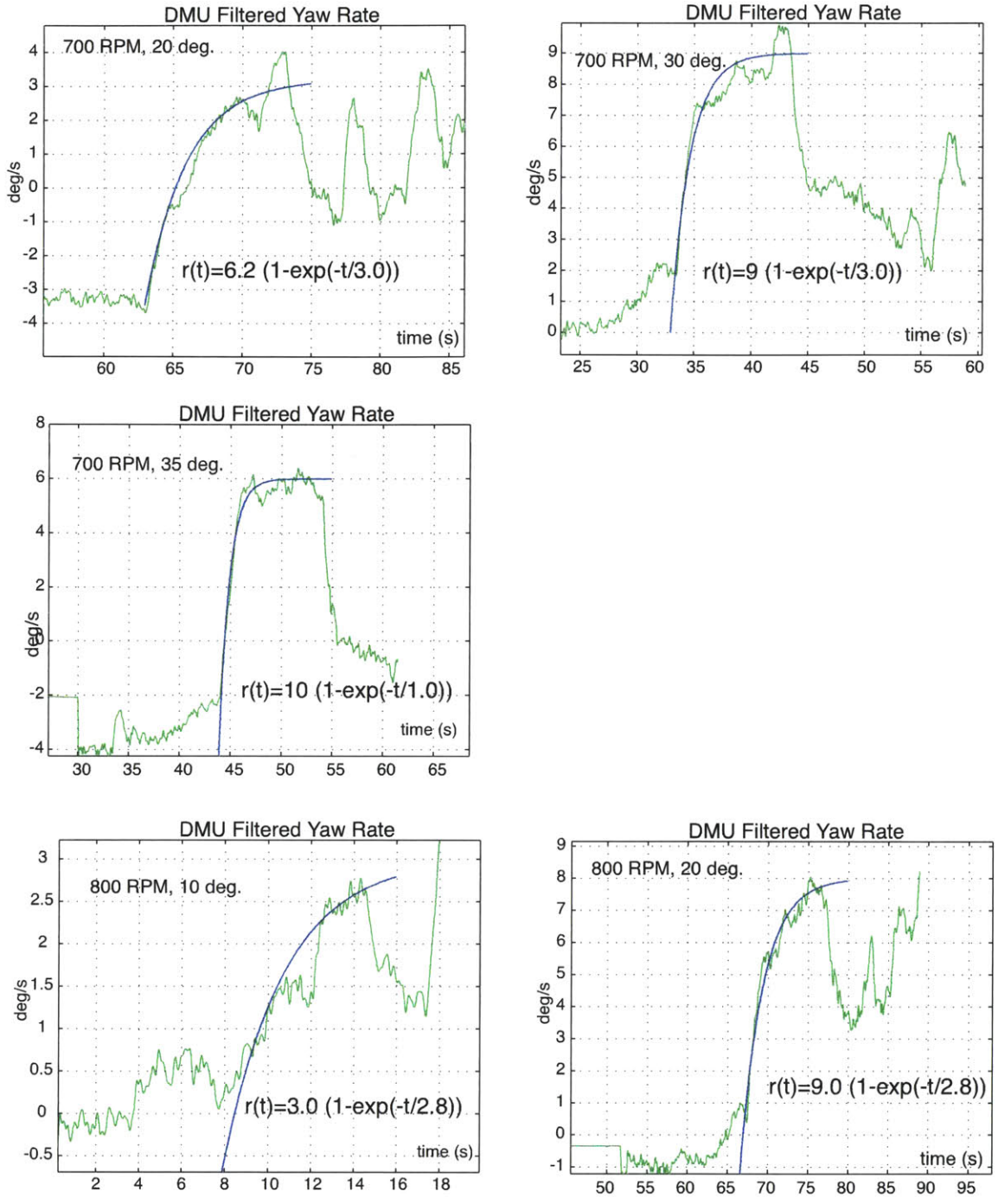

Figure I-4: Yaw rotation rates curve fitting for different experiments(4/6)

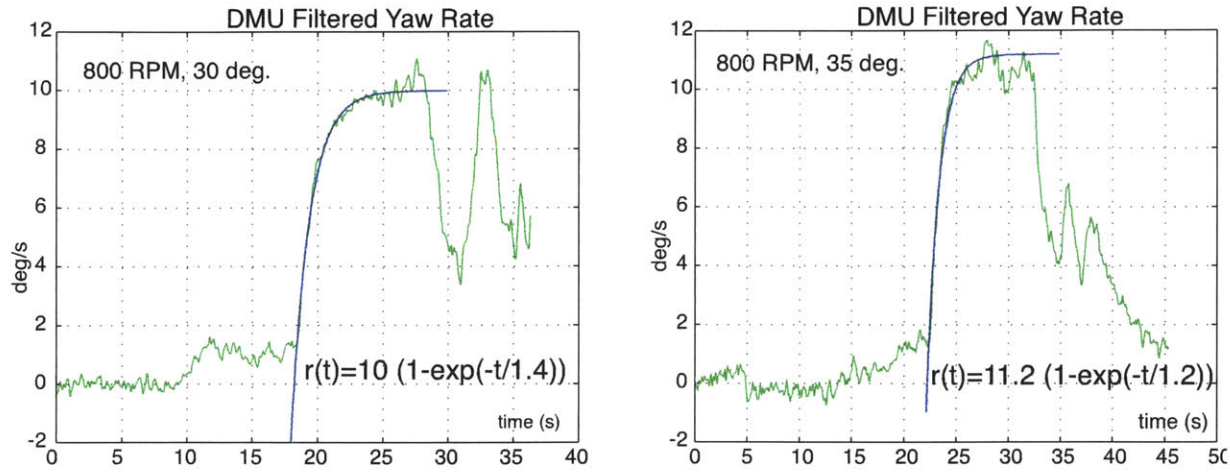

Figure I-5: Yaw rotation rates curve fitting for different experiments(5/6)

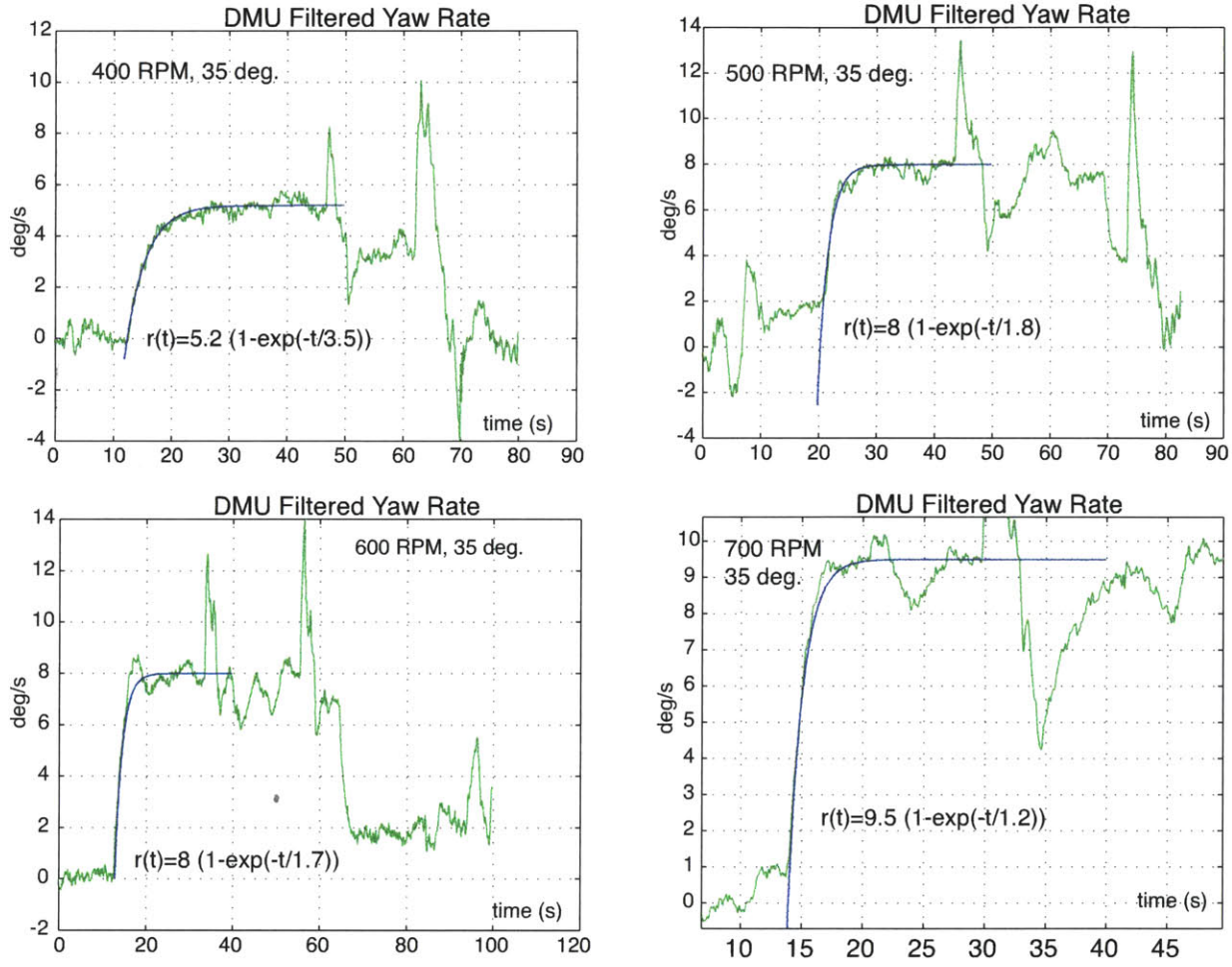

Figure I-6: Yaw rotation rates curve fitting for full turn experiments(6/6)

Appendix J

GLOBAL RESULTS

MIT Alumni Pool - Dec. 2001 Tests

In this appendix are presented all the results of the turning tests carried out at the MIT Pool December 31^{st} 2001.

Only the results of the test at 600 RPM and 30 degrees rudder angle are not listed here because it is studied in detail in Section 7.2.3. In this section, the [600,30] run is taken as an example to describe the different phenomena which appear during a turn maneuver.

The results shown here are for the following runs:

200 RPM: 30 deg. (Figure (J-1)) and 35 deg. (Figure (J-2)),

300 RPM: 10 deg. (Figure (J-3)), 20 deg. (Figure (J-4)), 30 deg. (Figure (J-5)),

400 RPM: 10 deg. (Figure (J-6)), 20 deg. (Figure (J-7)), 30 deg. (Figure (J-8)) and 35 deg. (Figure (J-9)),

500 RPM: 10 deg. (Figure (J-10)), 20 deg. (Figure (J-23)), 30 deg. (Figure (J-24)) and 35 deg. (Figure (J-25)),

600 RPM: 10 deg. (Figure (J-26)), 20 deg. (Figure (J-27)) and 35 deg. (Figure (J-28)),

700 RPM: 10 deg. (Figure (J-29)), 20 deg. (Figure (J-30)), 30 deg. (Figure (J-31)) and 35 deg. (Figure (J-32)),

800 RPM: 10 deg. (Figure (J-33)), 20 deg. (Figure (J-34)), 30 deg. (Figure (J-35)) and 35 deg. (Figure (J-36)).

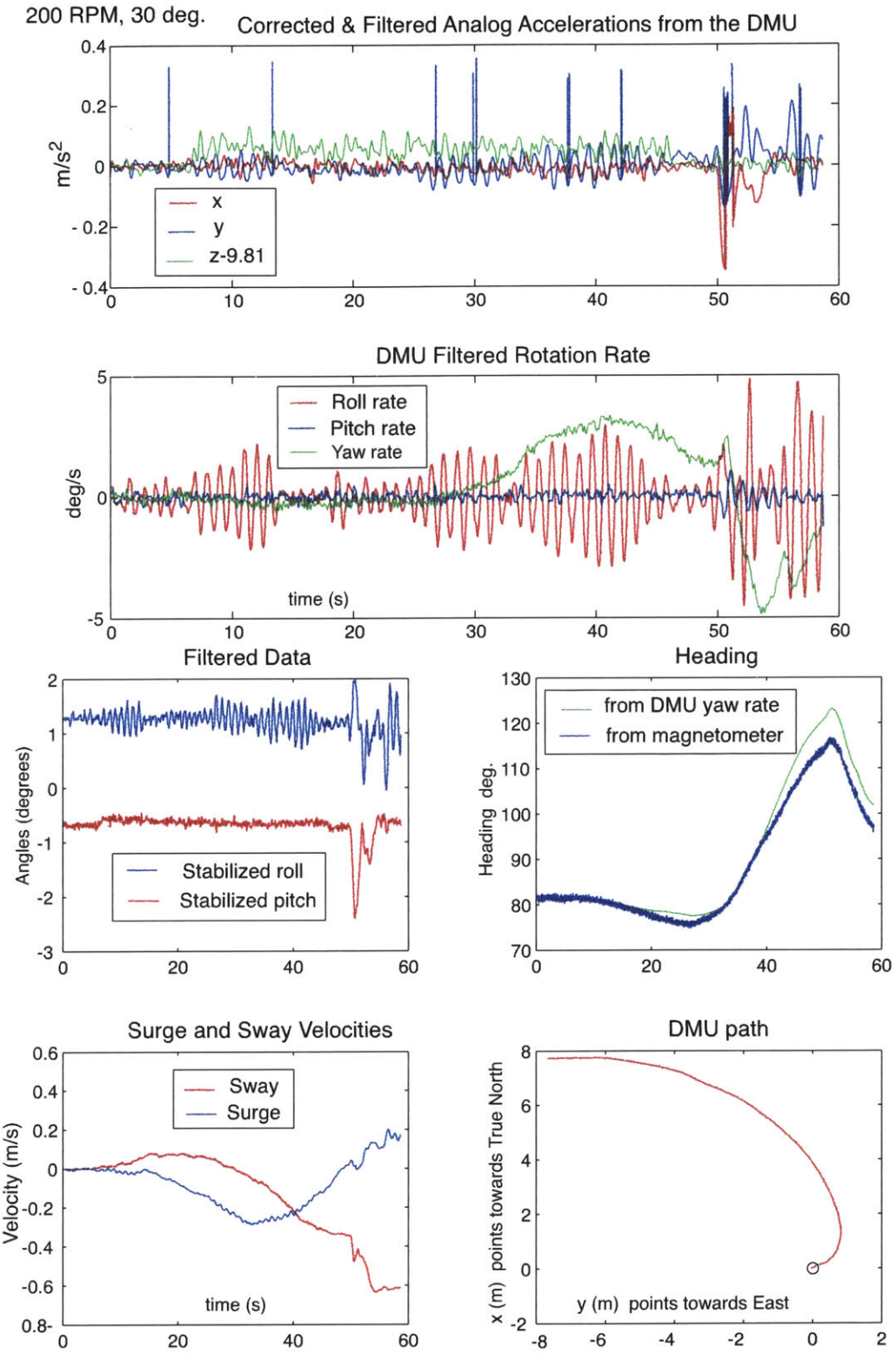

Figure J-1: Turning Tests at 200 RPM and 30 deg. - Alumni Pool

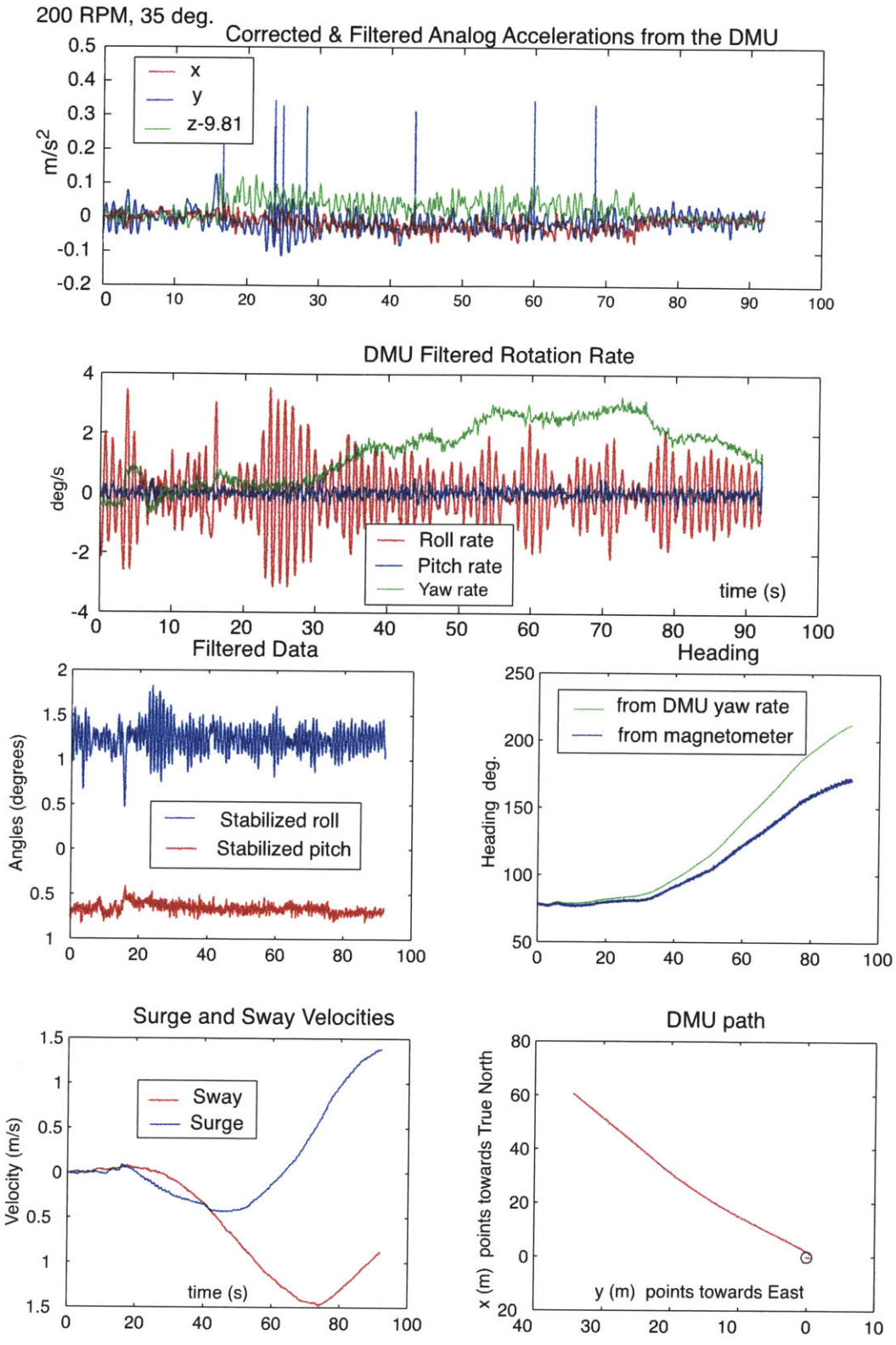

Figure J-2: Turning Tests at 200 RPM and 35 deg. - Alumni Pool

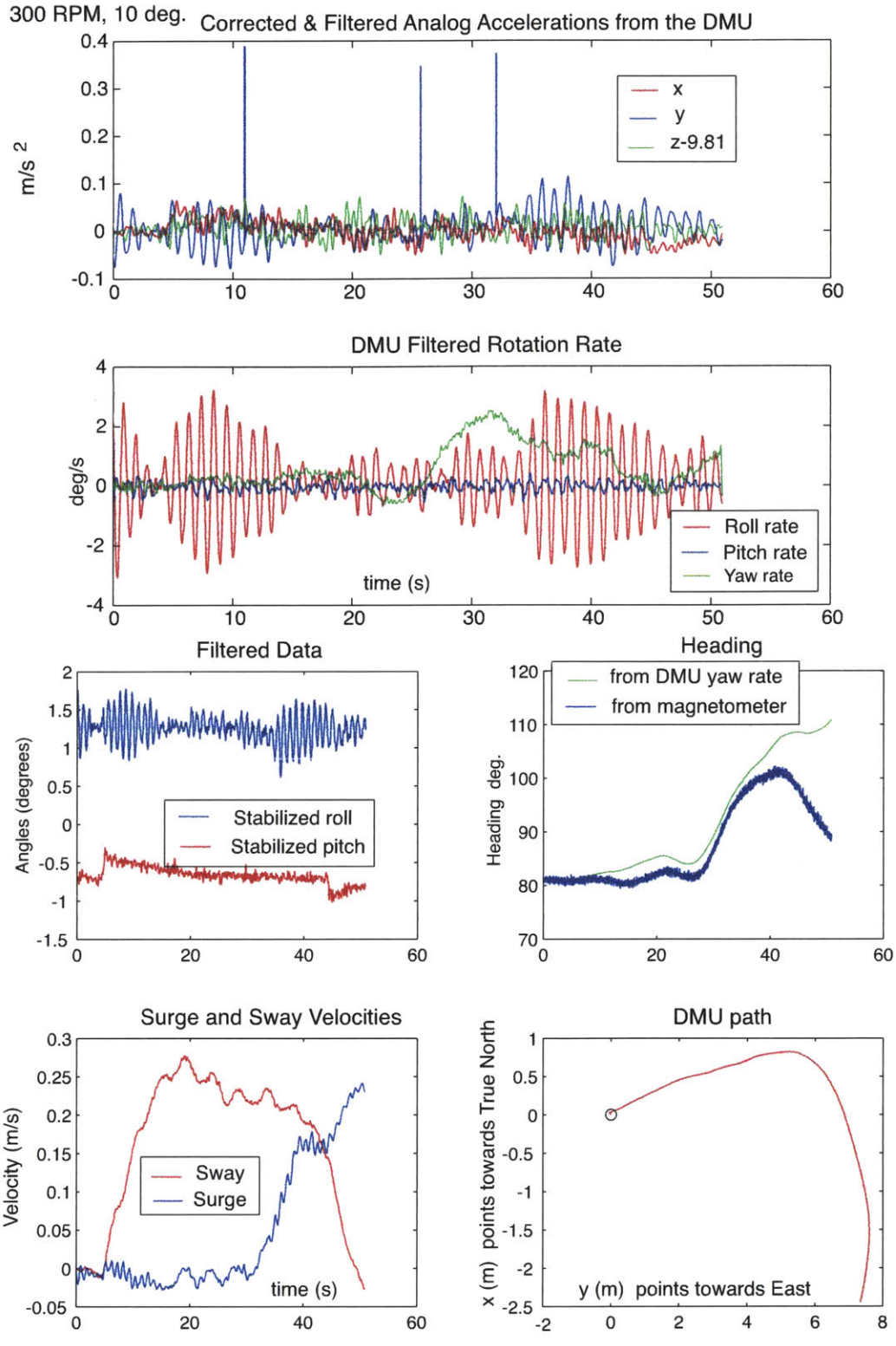

Figure J-3: Turning Tests at 300 RPM and 10 deg. - Alumni Pool

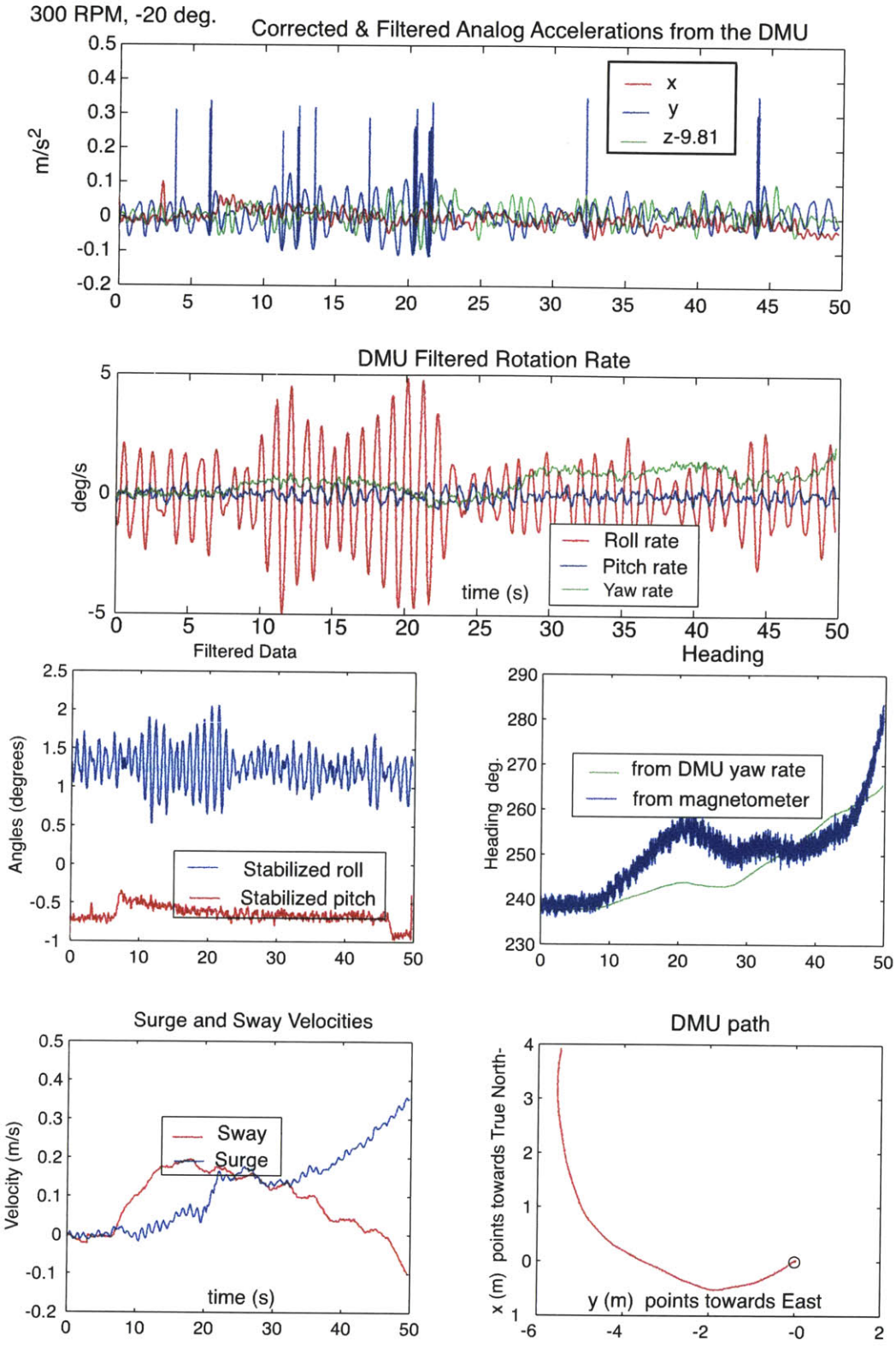

Figure J-4: Turning Tests at 300 RPM and 20 deg. - Alumni Pool

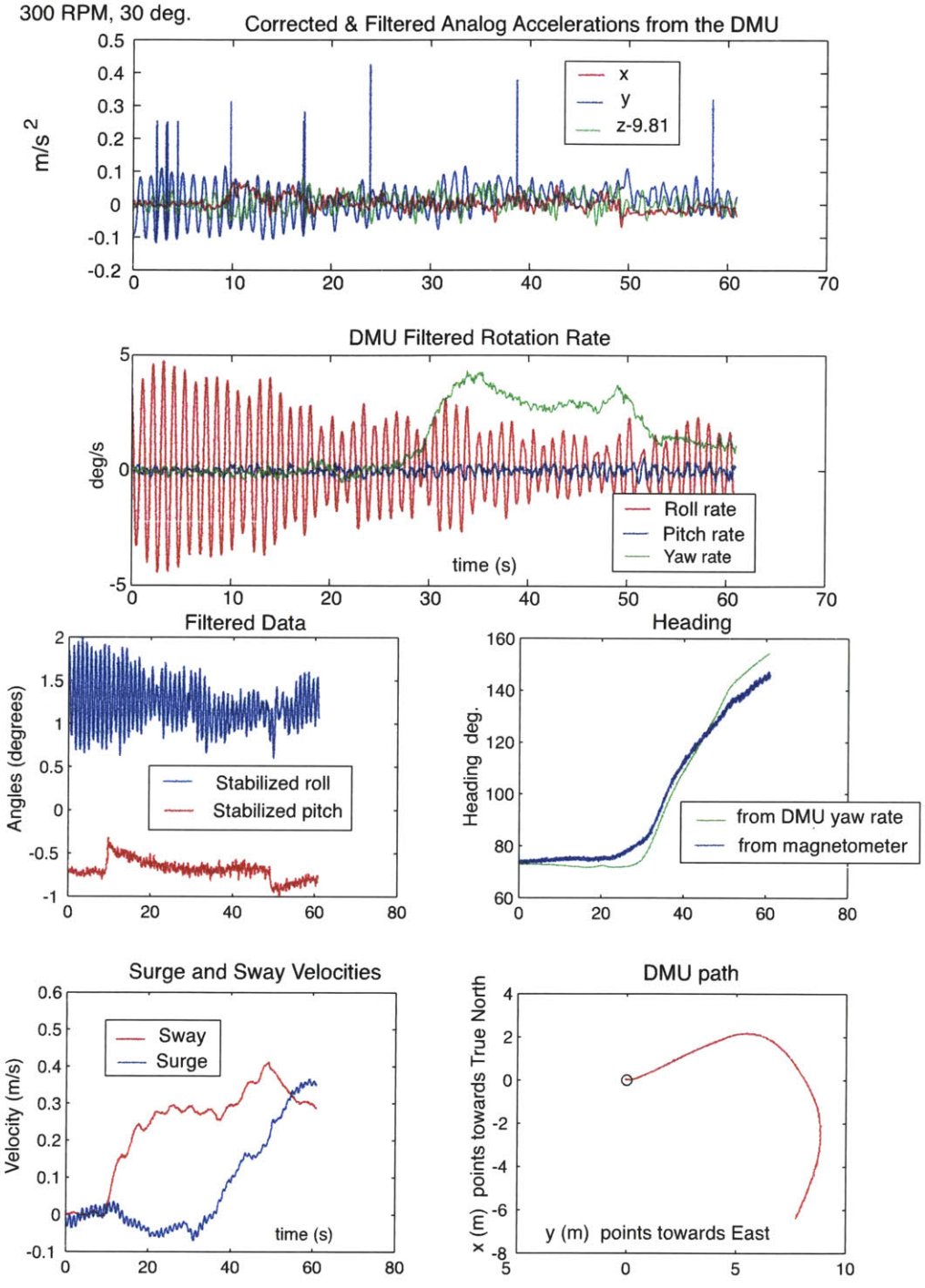

Figure J-5: Turning Tests at 300 RPM and 30 deg. - Alumni Pool

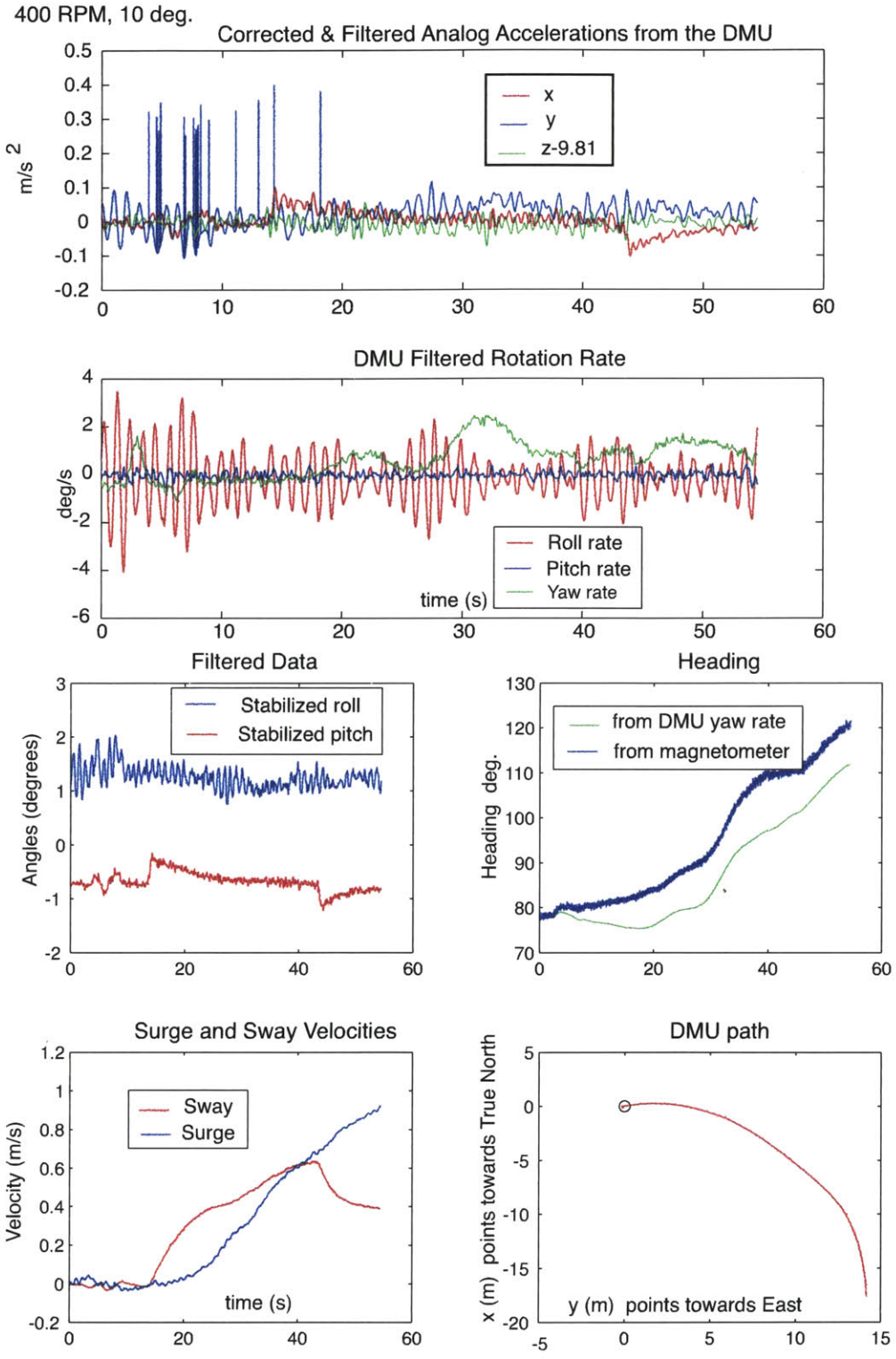

Figure J-6: Turning Tests at 400 RPM and 10 deg. - Alumni Pool

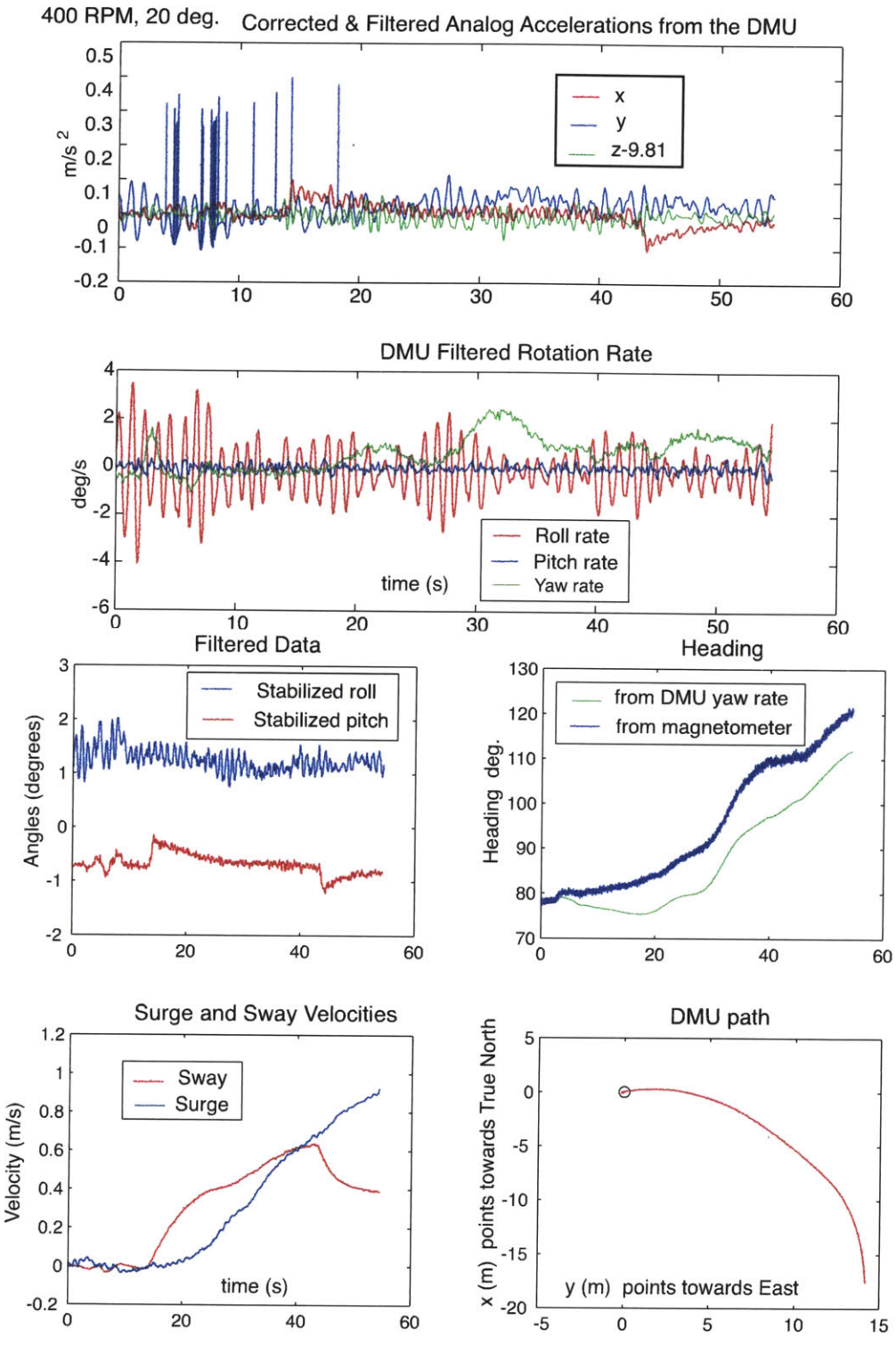

Figure J-7: Turning Tests at 400 RPM and 20 deg. - Alumni Pool

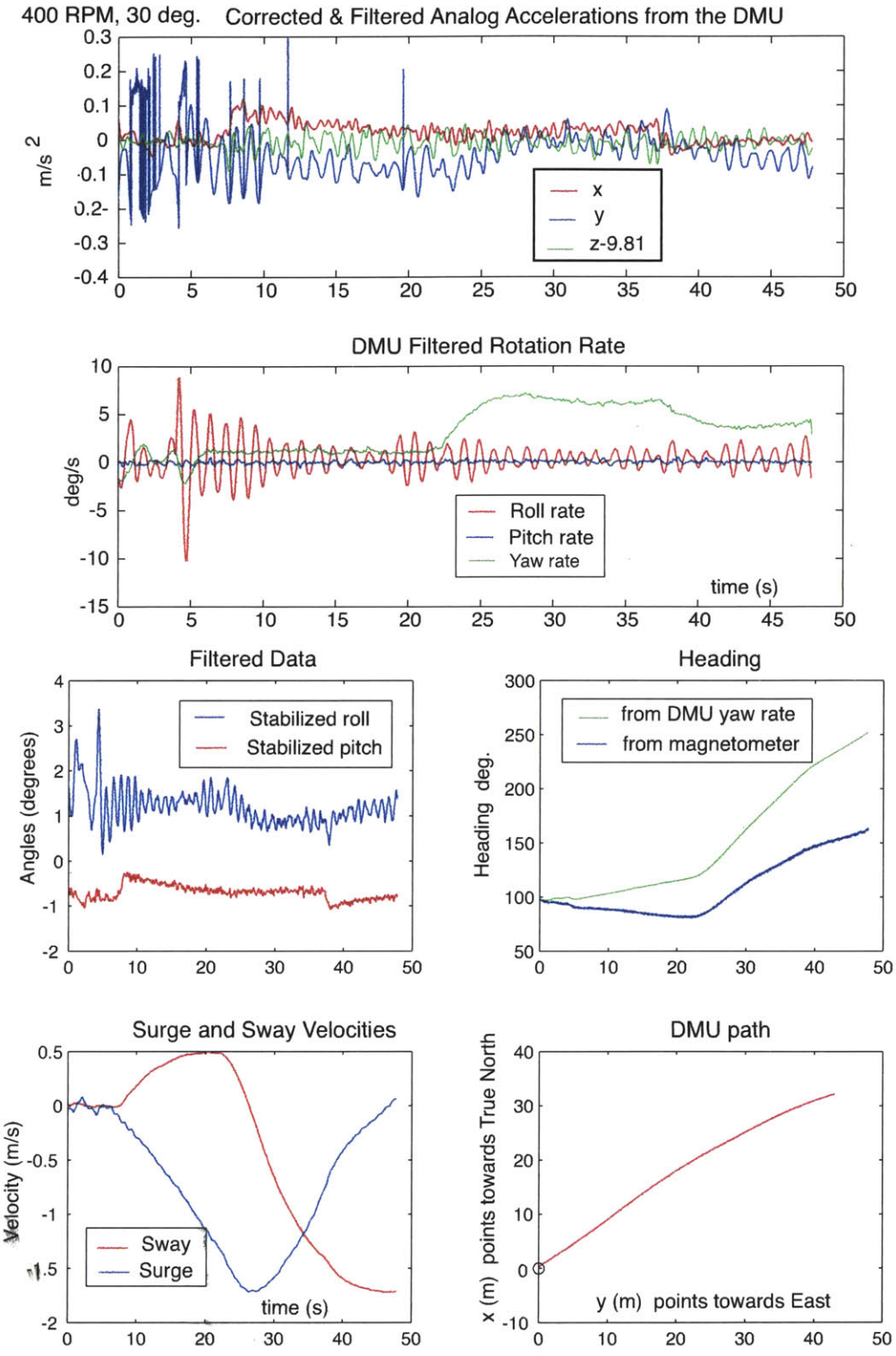

Figure J-8: Turning Tests at 400 RPM and 30 deg. - Alumni Pool

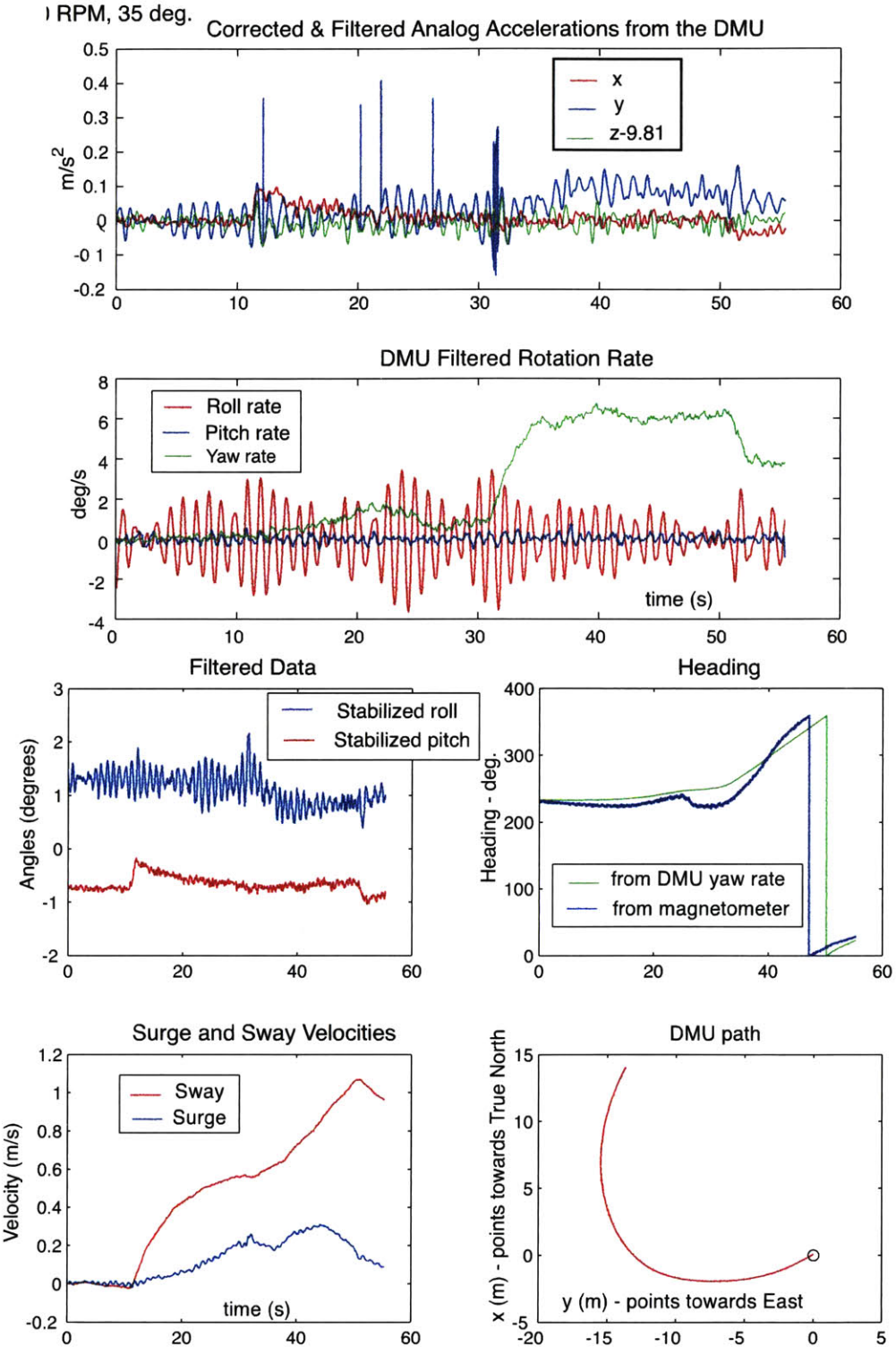

Figure J-9: Turning Tests at 400 RPM and 35 deg. - Alumni Pool

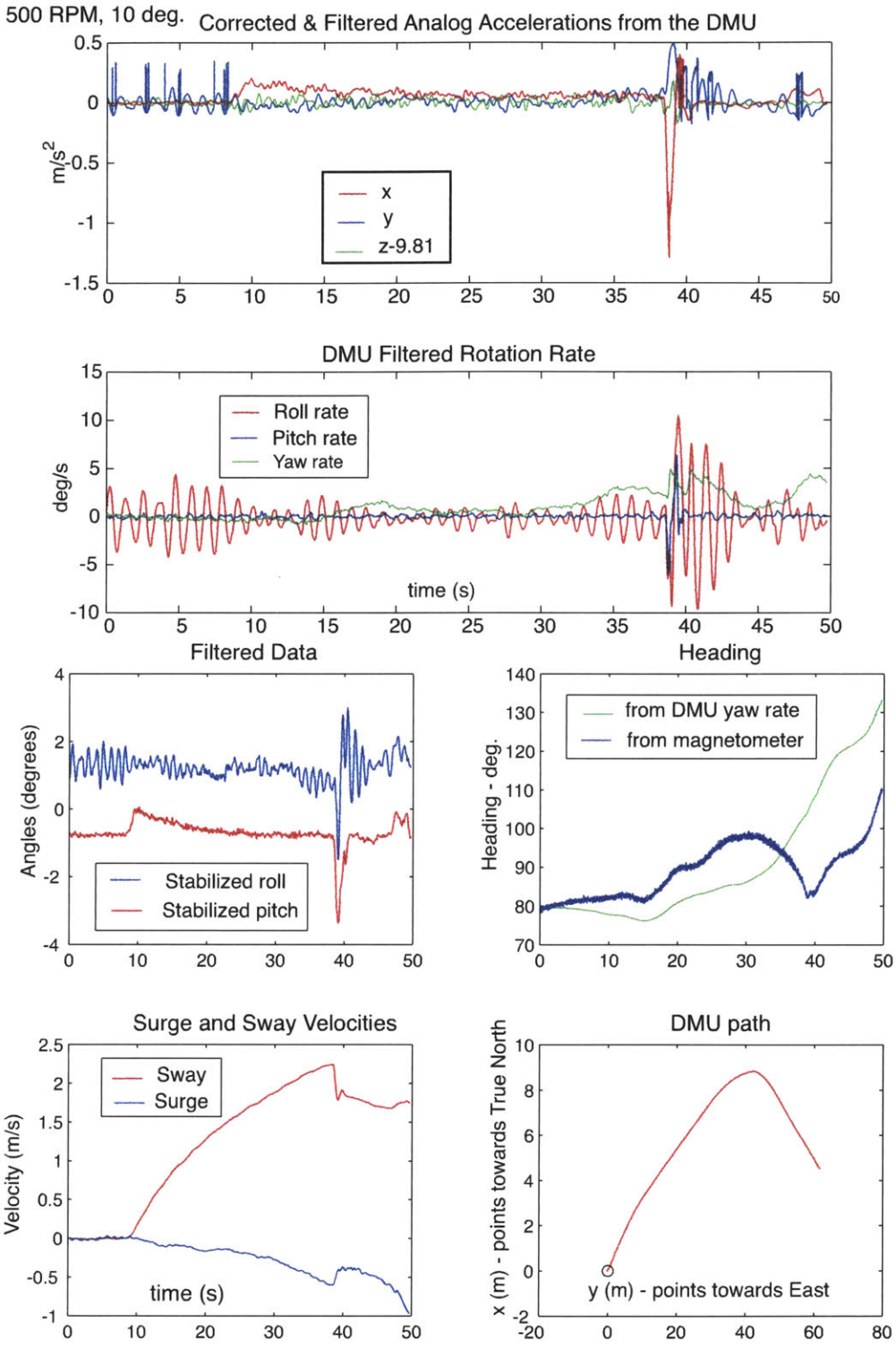

Figure J-10: Turning Tests at 500 RPM and 10 deg. - Alumni Pool

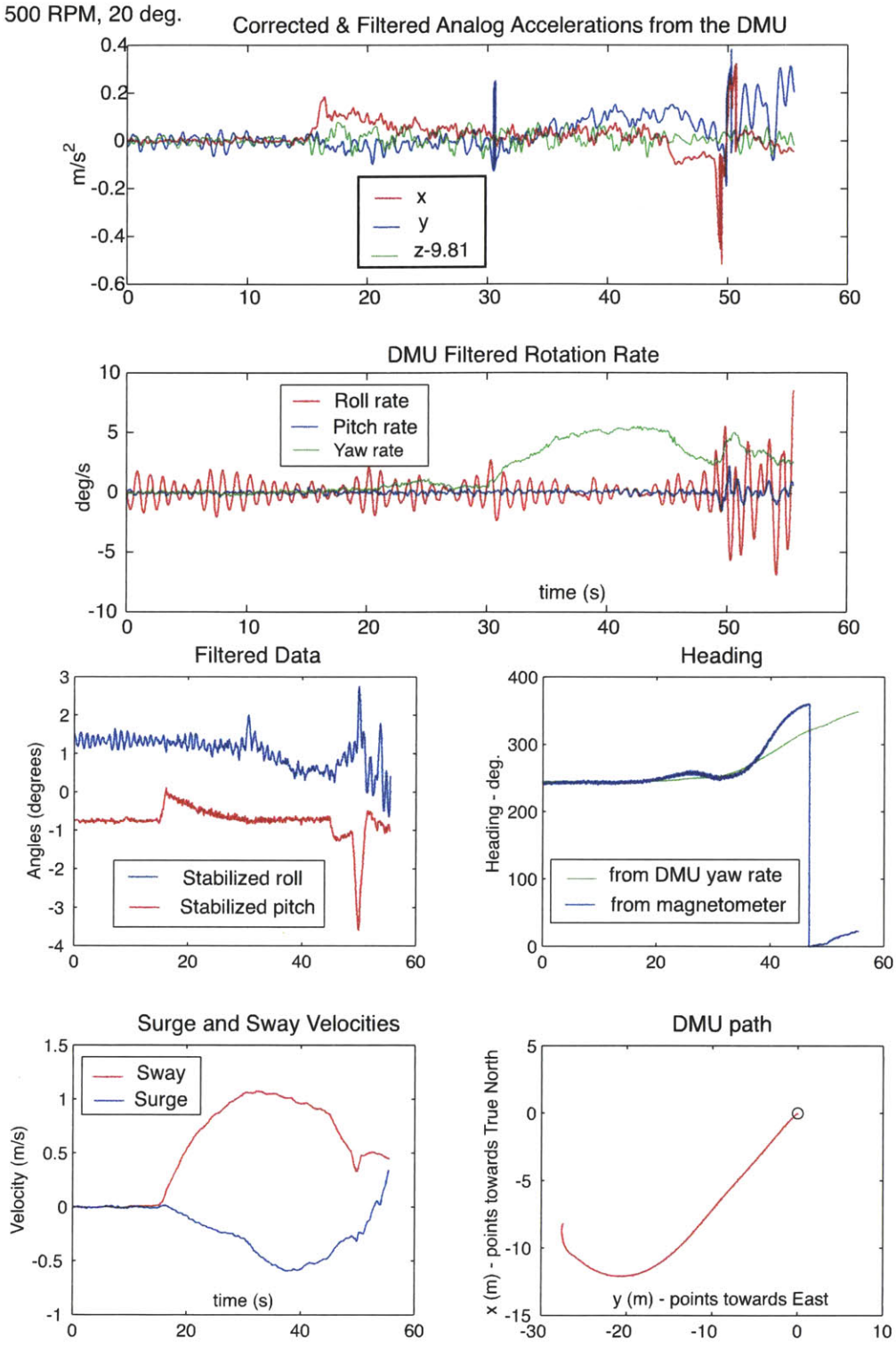

Figure J-11: Turning Tests at 500 RPM and 20 deg. - Alumni Pool

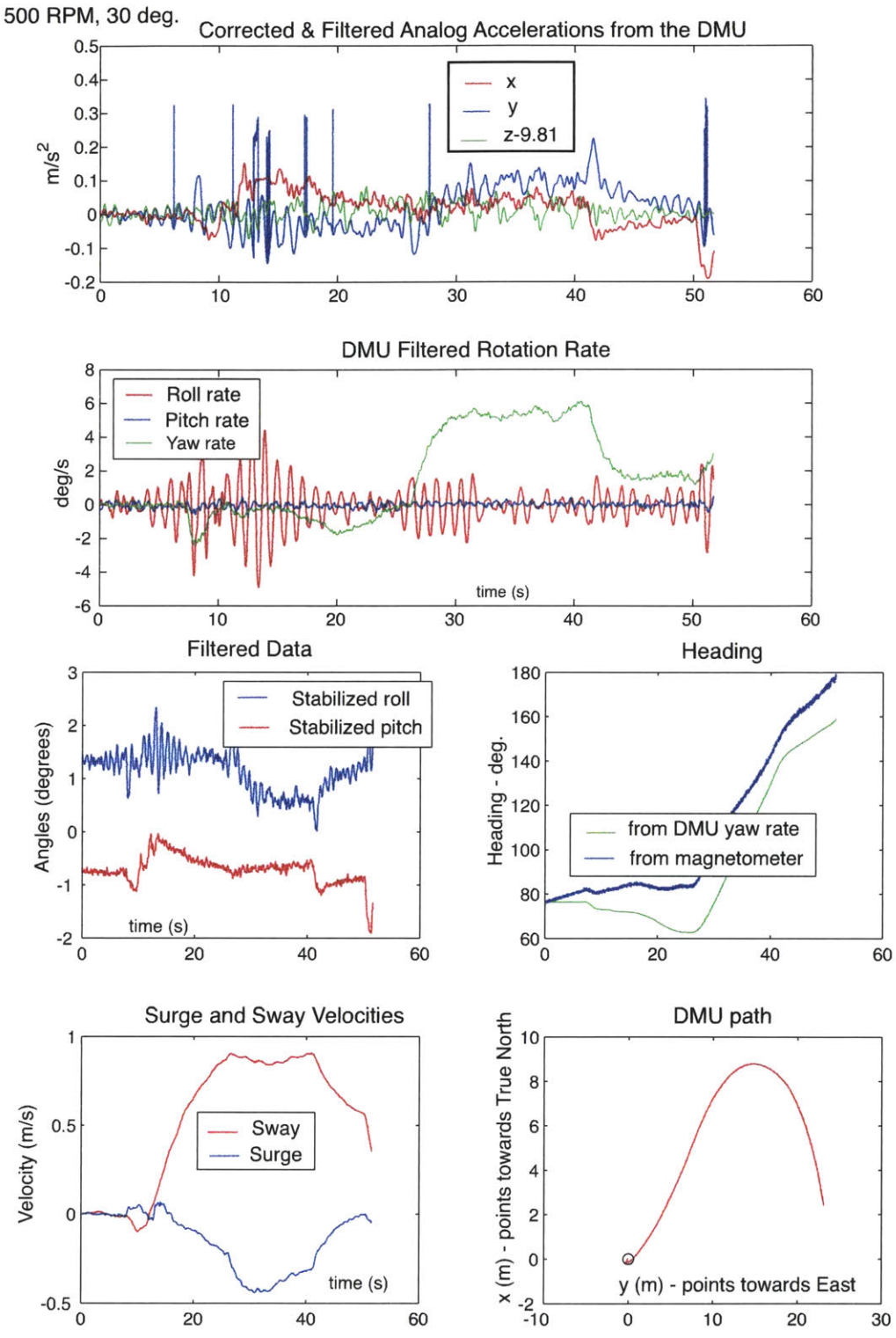

Figure J-12: Turning Tests at 500 RPM and 30 deg. - Alumni Pool

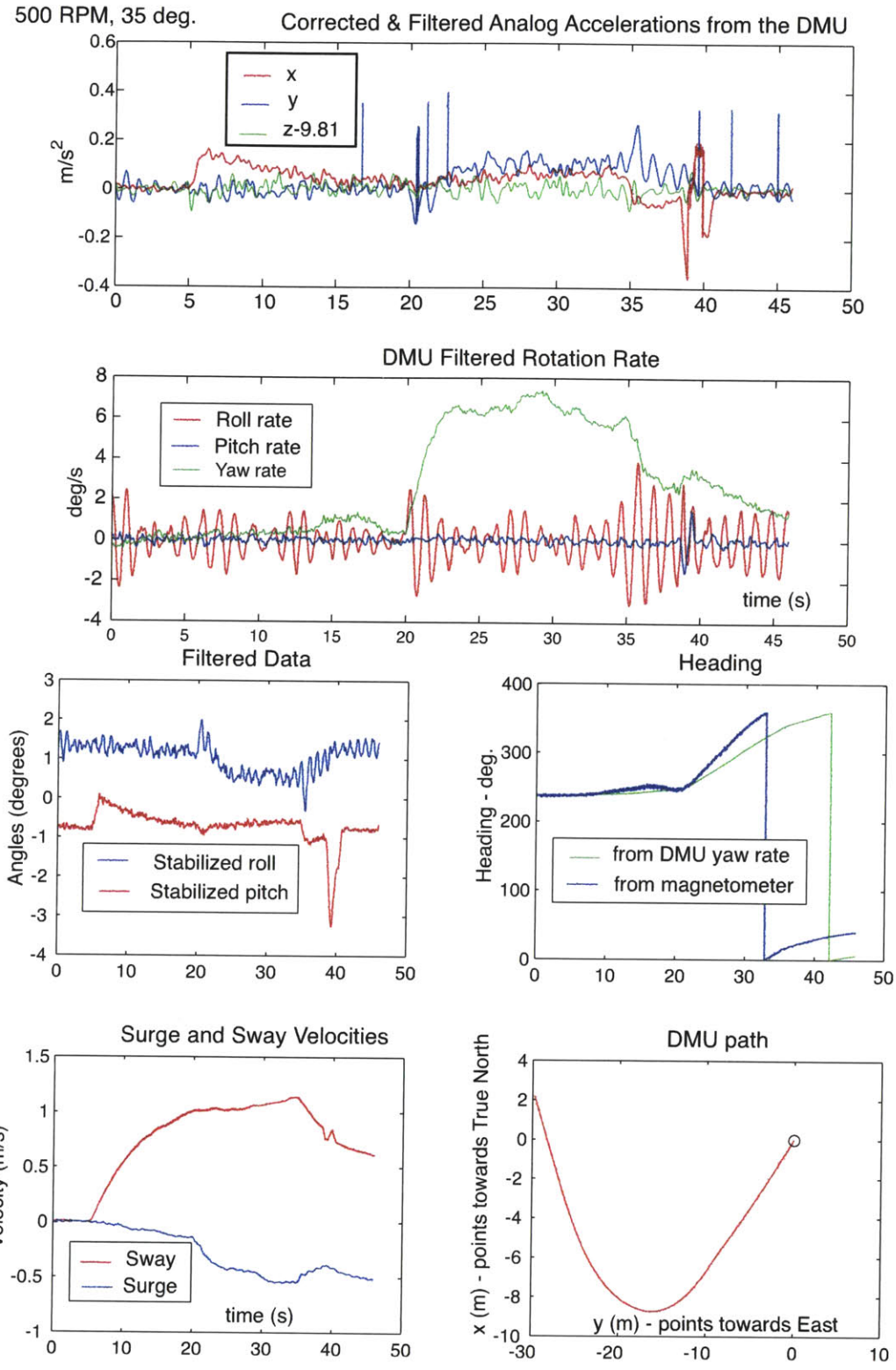

Figure J-13: Turning Tests at 500 RPM and 35 deg. - Alumni Pool

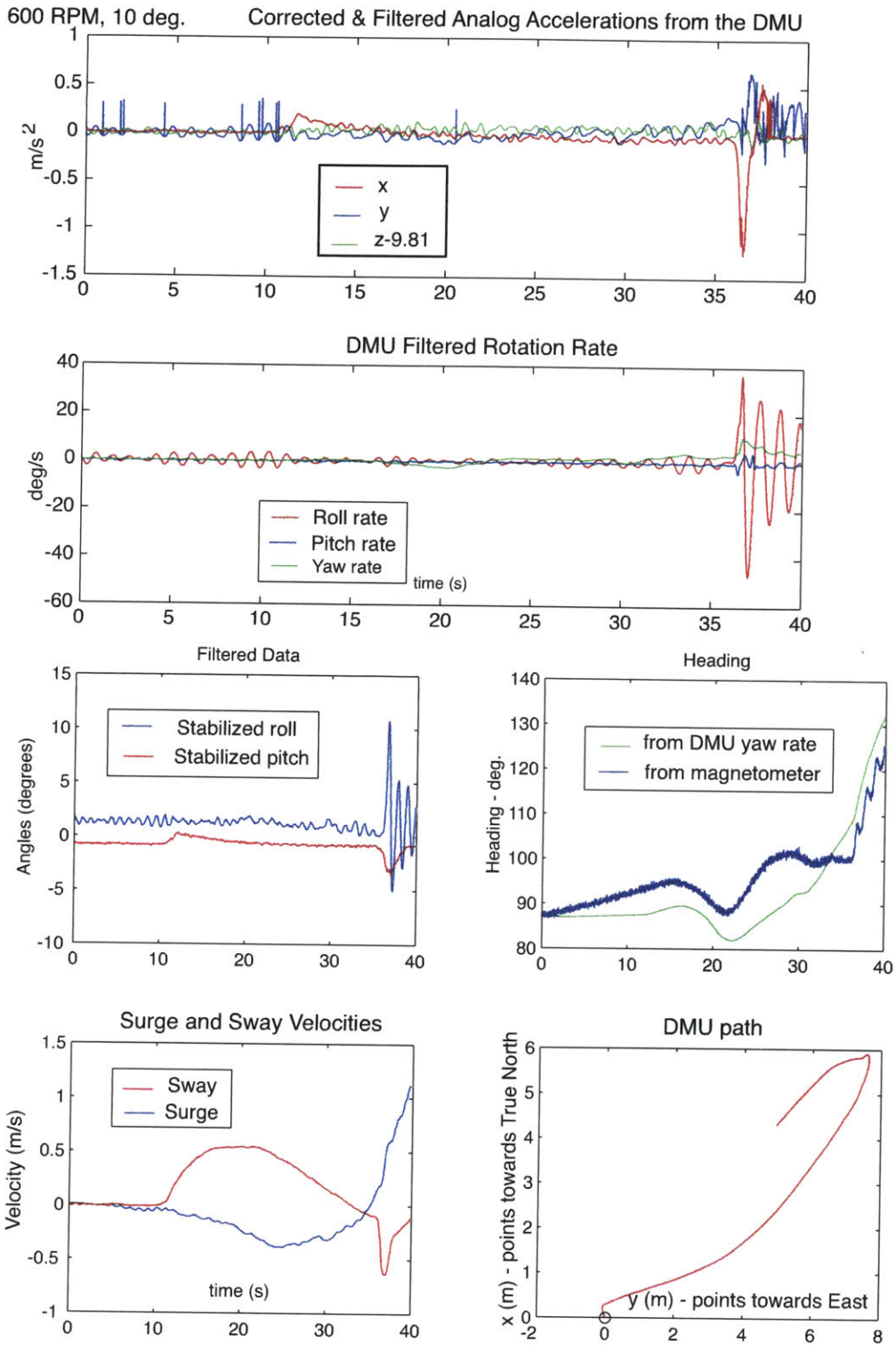

Figure J-14: Turning Tests at 600 RPM and 10 deg. - Alumni Pool

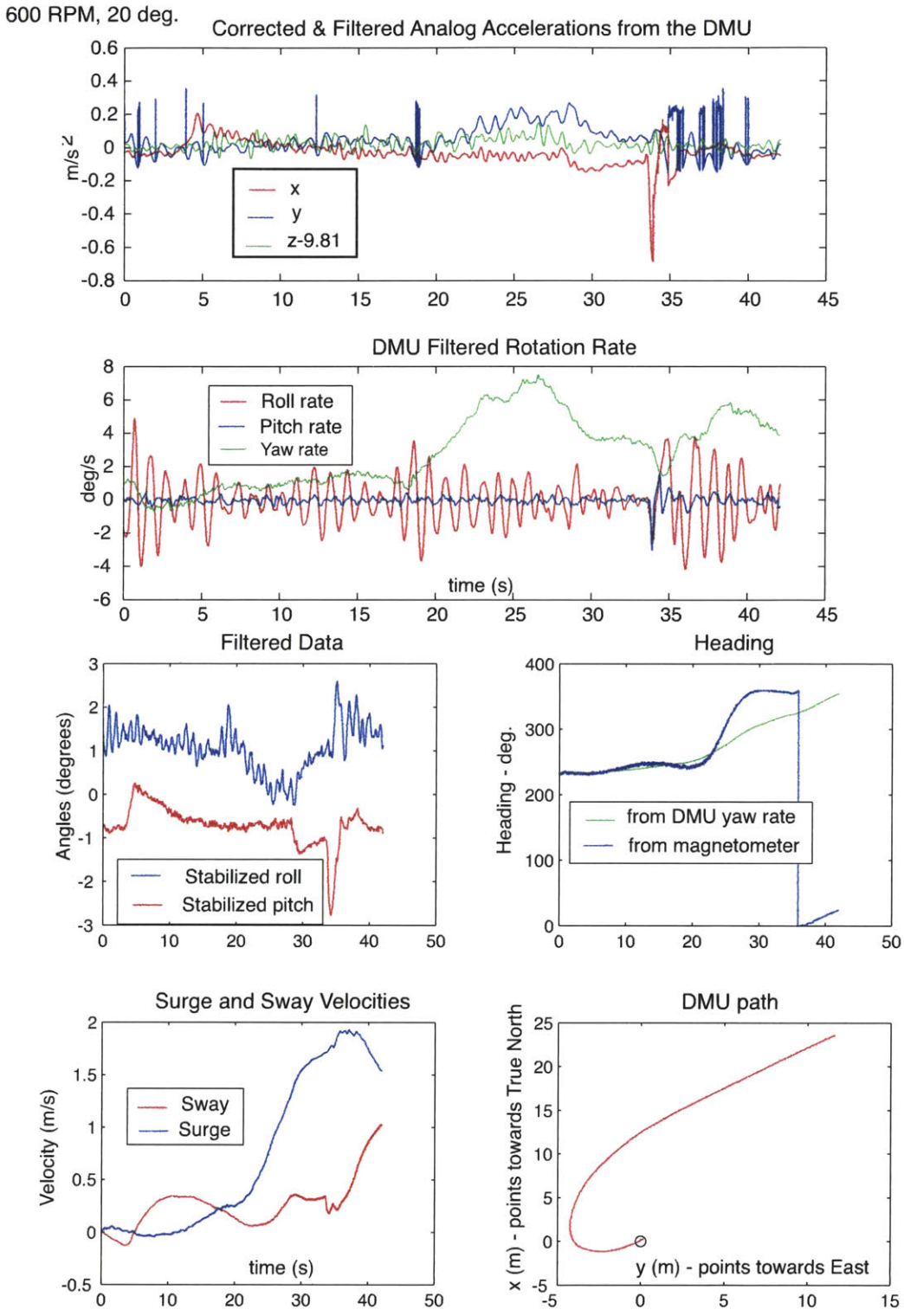

Figure J-15: Turning Tests at 600 RPM and 20 deg. - Alumni Pool

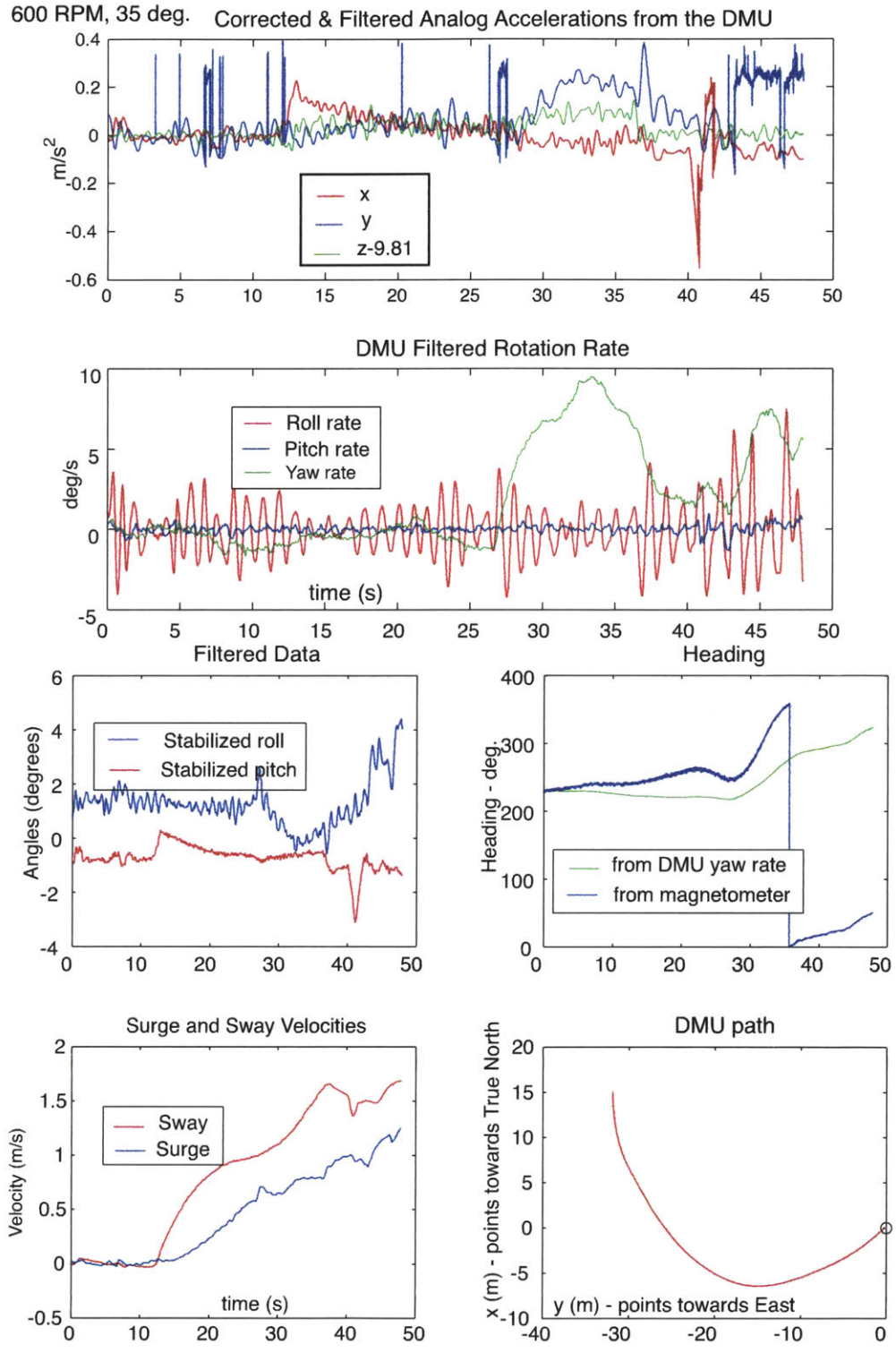

Figure J-16: Turning Tests at 600 RPM and 35 deg. - Alumni Pool

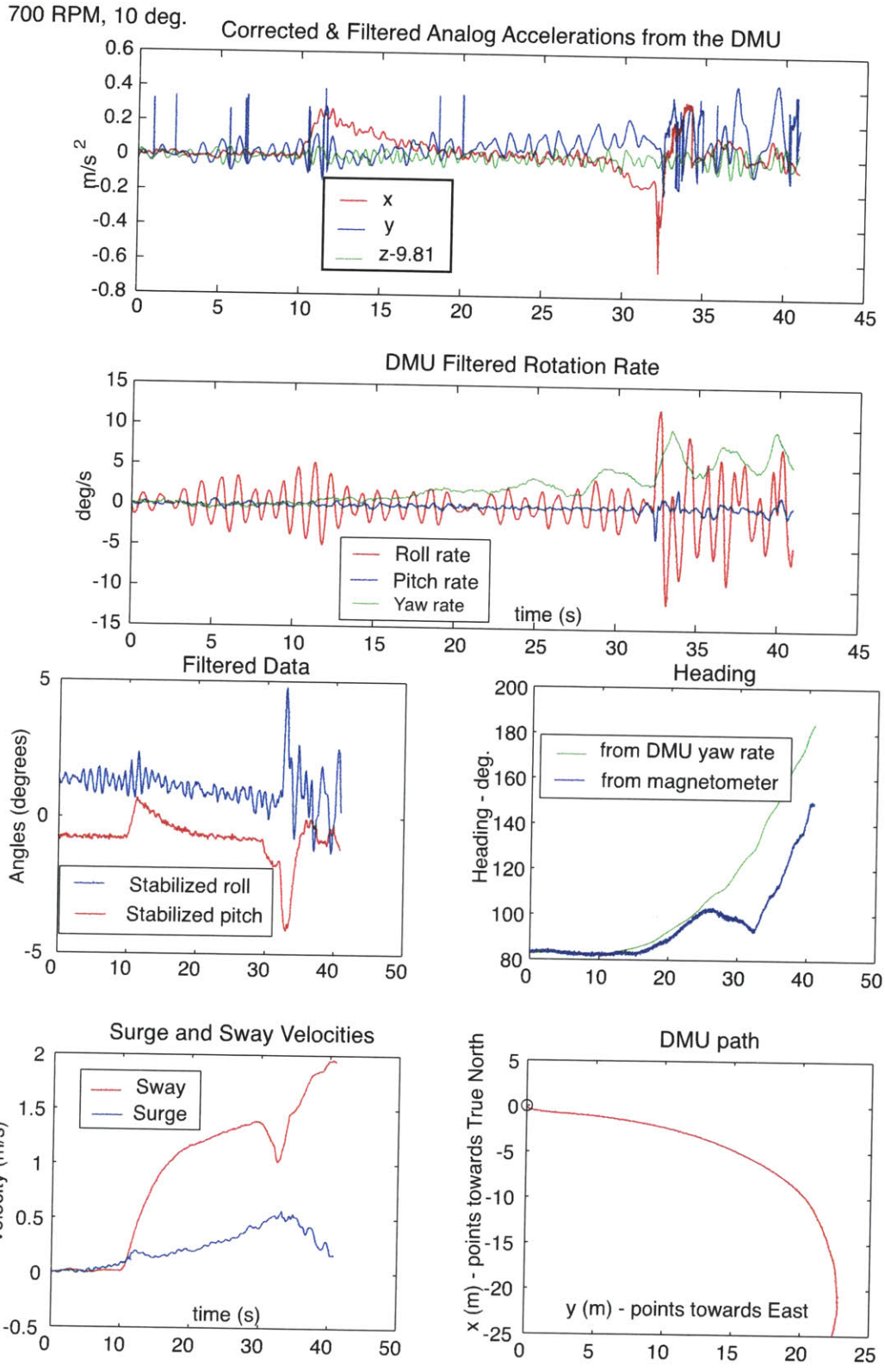

Figure J-17: Turning Tests at 700 RPM and 10 deg. - Alumni Pool

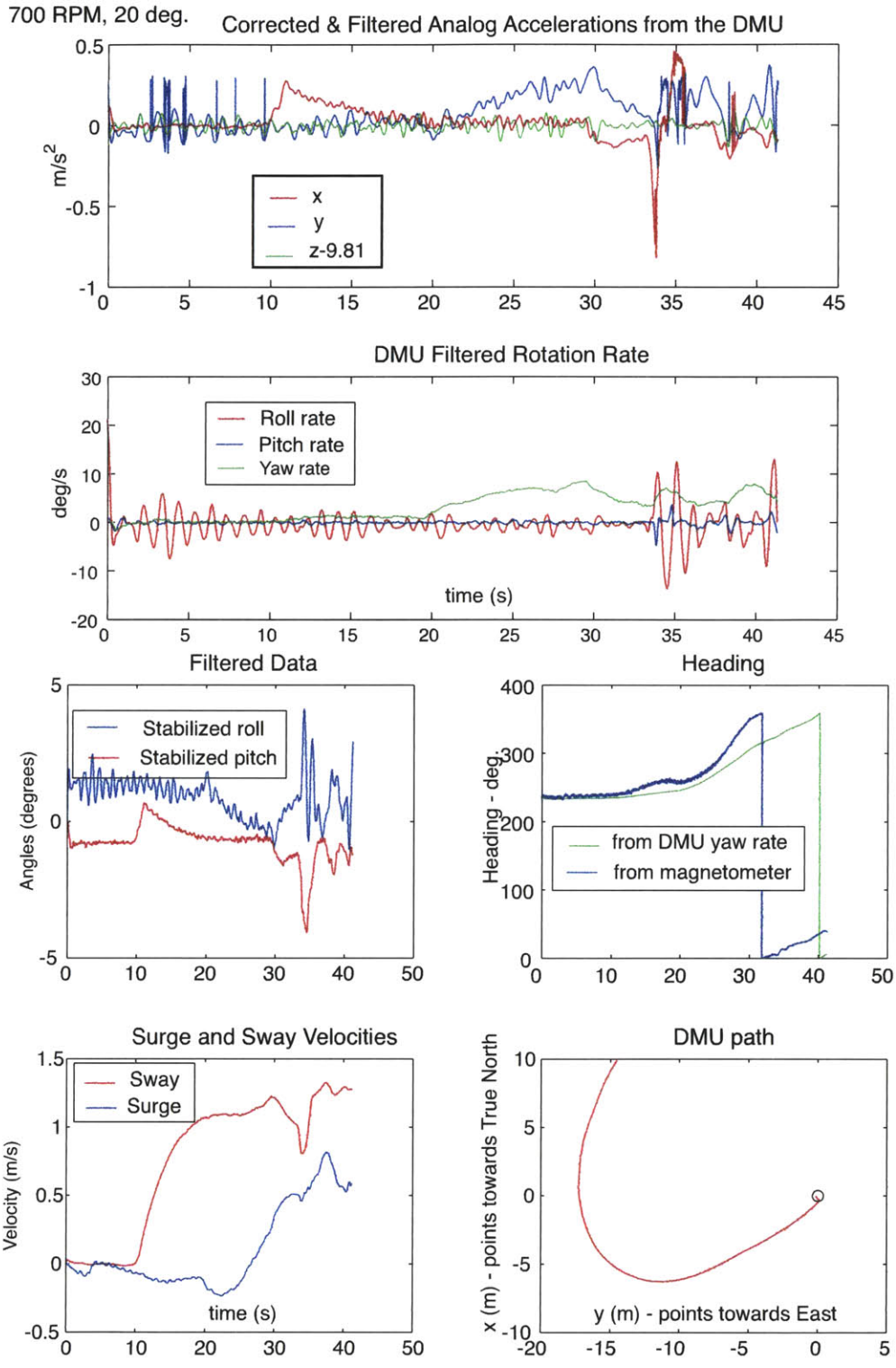

Figure J-18: Turning Tests at 700 RPM and 20 deg. - Alumni Pool

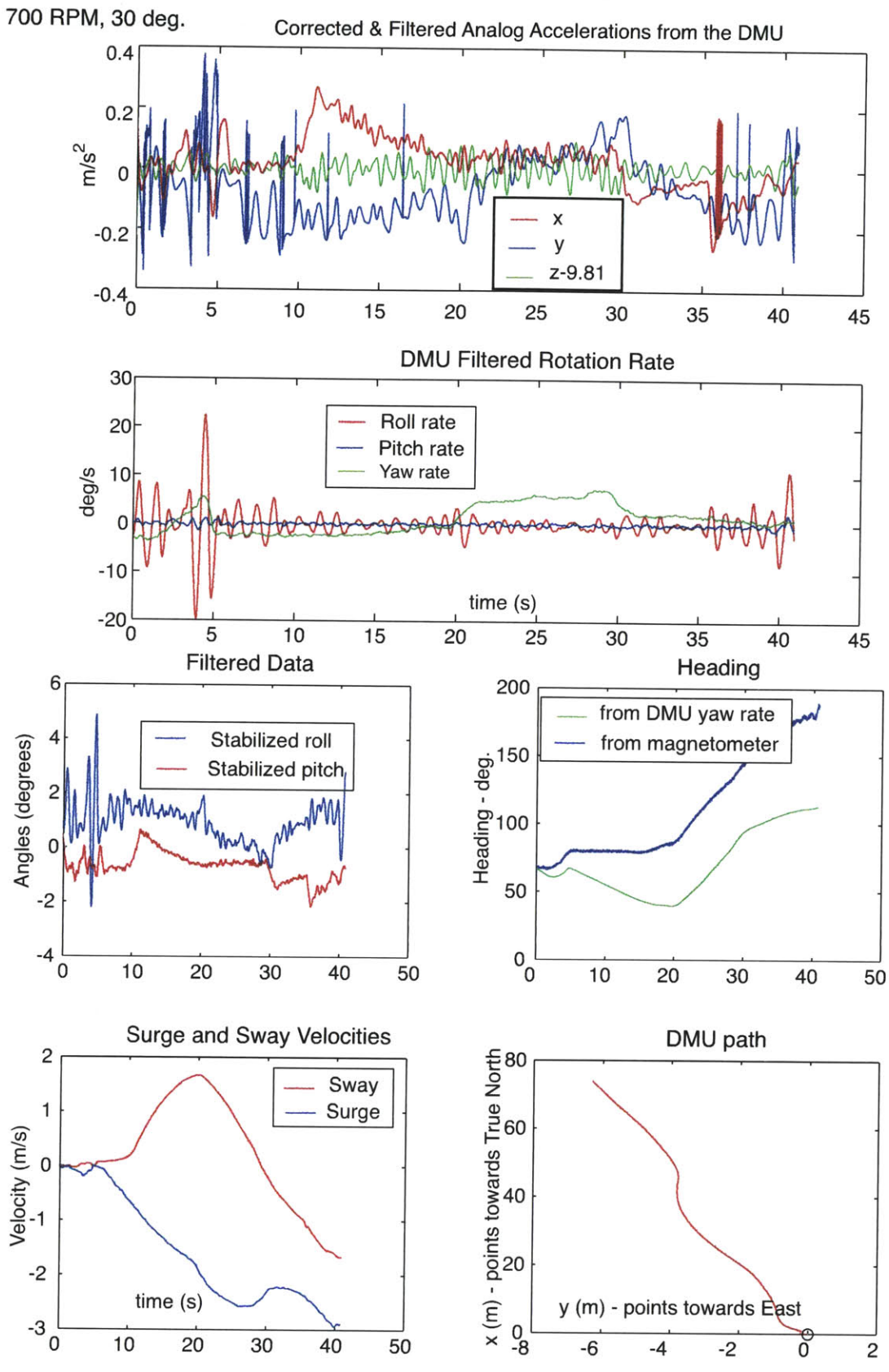

Figure J-19: Turning Tests at 700 RPM and 30 deg. - Alumni Pool

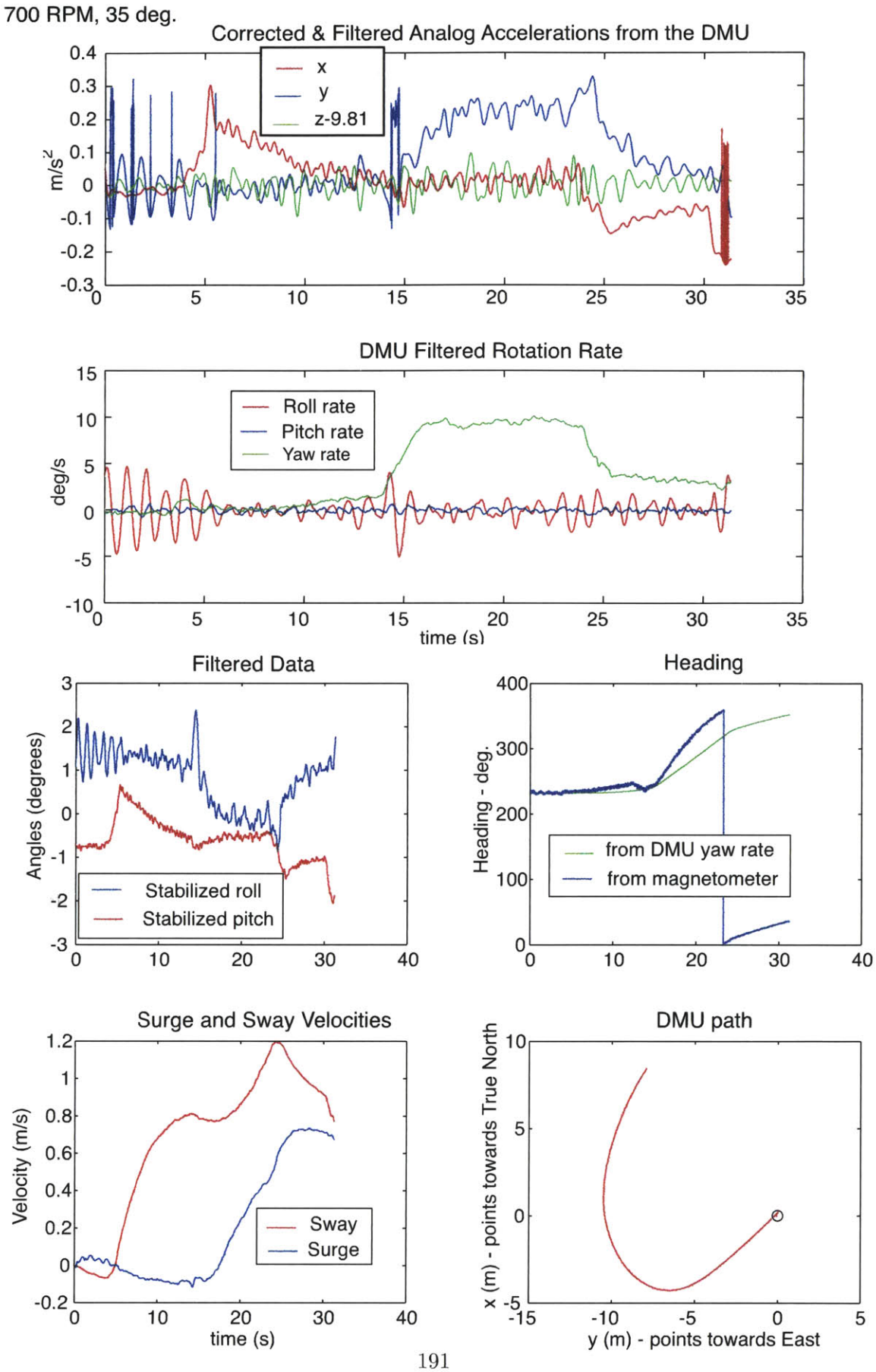

Figure J-20: Turning Tests at 700 RPM and 35 deg. - Alumni Pool

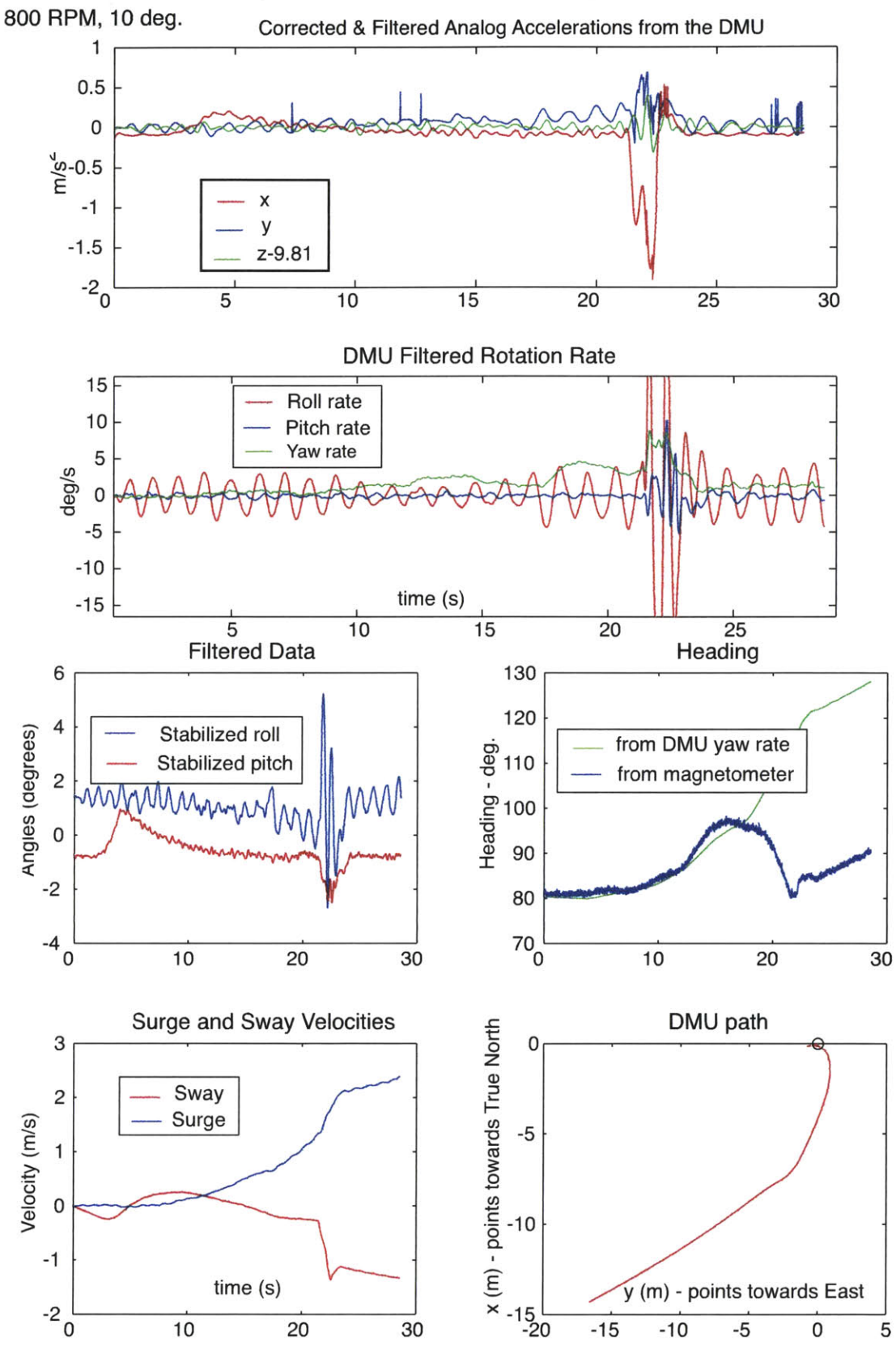

Figure J-21: Turning Tests at 800 RPM and 10 deg. - Alumni Pool

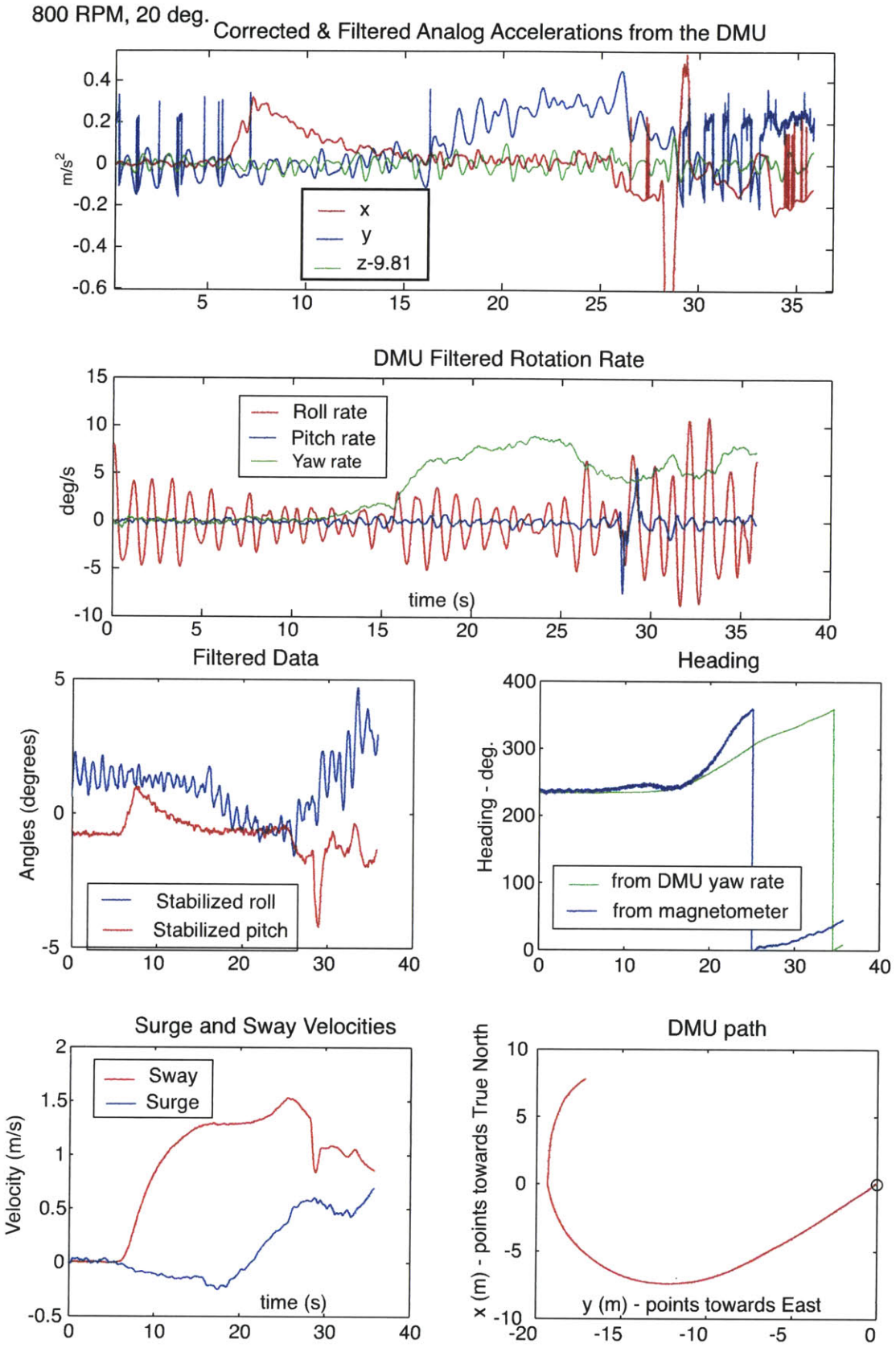

Figure J-22: Turning Tests at 800 RPM and 20 deg. - Alumni Pool

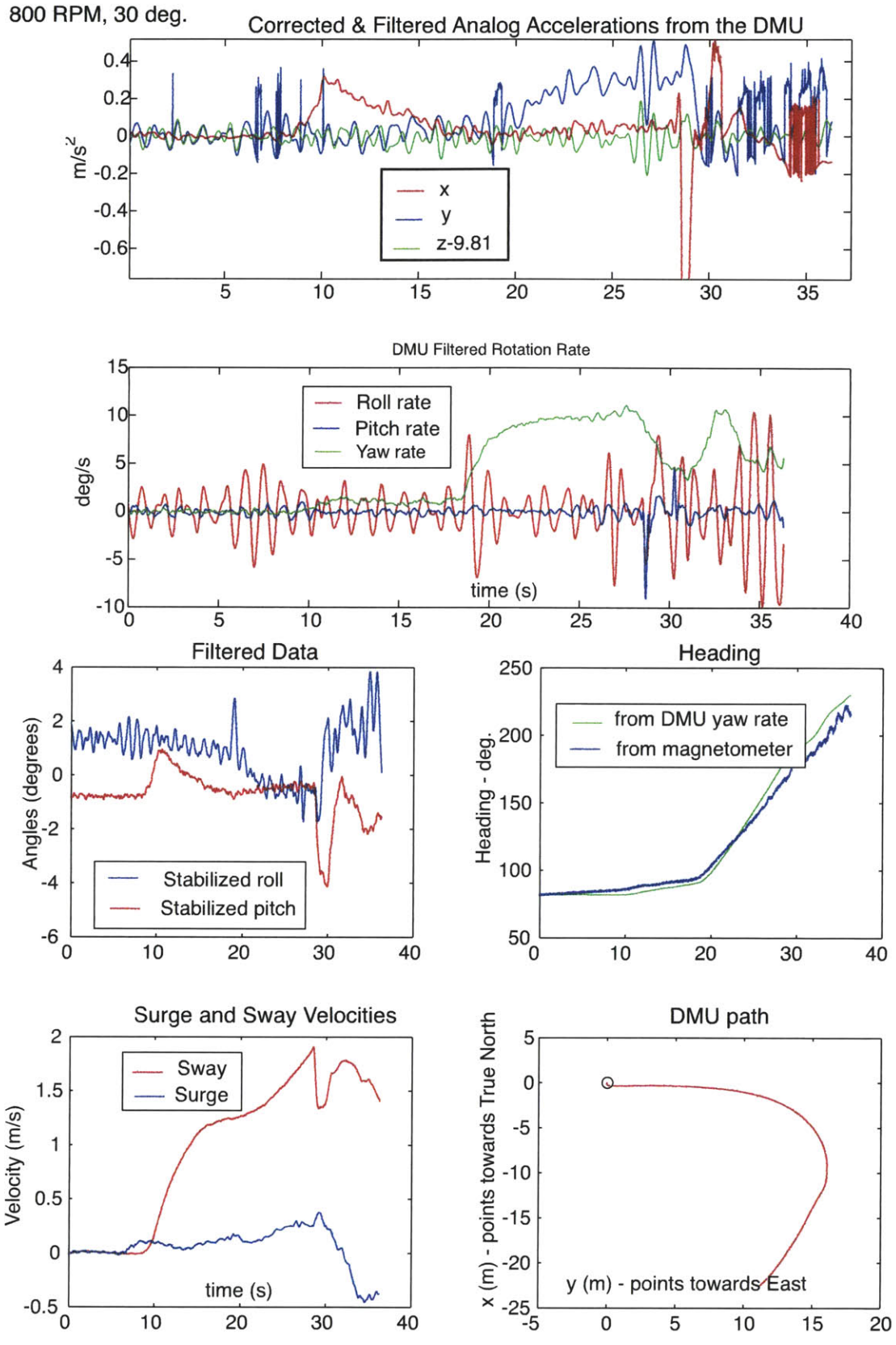

Figure J-23: Turning Tests at 800 RPM and 30 deg. - Alumni Pool

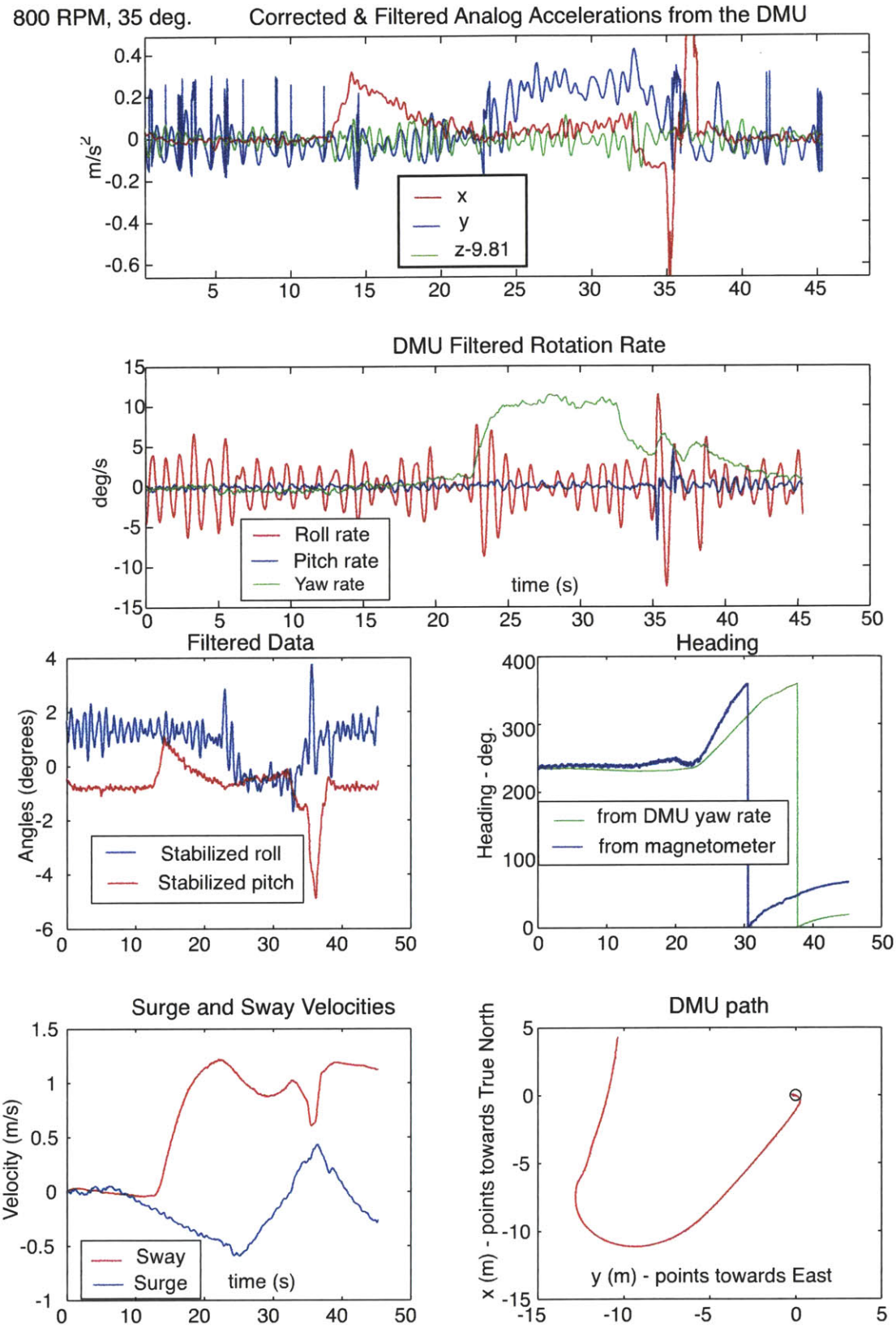

Figure J-24: Turning Tests at 800 RPM and 35 deg. - Alumni Pool

Appendix K

TESTS IN BAE TESTING FACILITY

First, the GPS positions are presented for all tests, then the results are presented test by test. For each test, 5 figures are displayed:

- Figure 1: the three linear accelerations,
- Figure 2: the 3 rotation rates,
- Figure 3: the 3 different ways to obtain the heading (magnetometer, integrated yaw rate and GPS heading),
- Figure 3: the stabilized angles (pitch and roll);
- Figure 4: the GPS velocity (directly given by the GPS or computed with GPS position data)

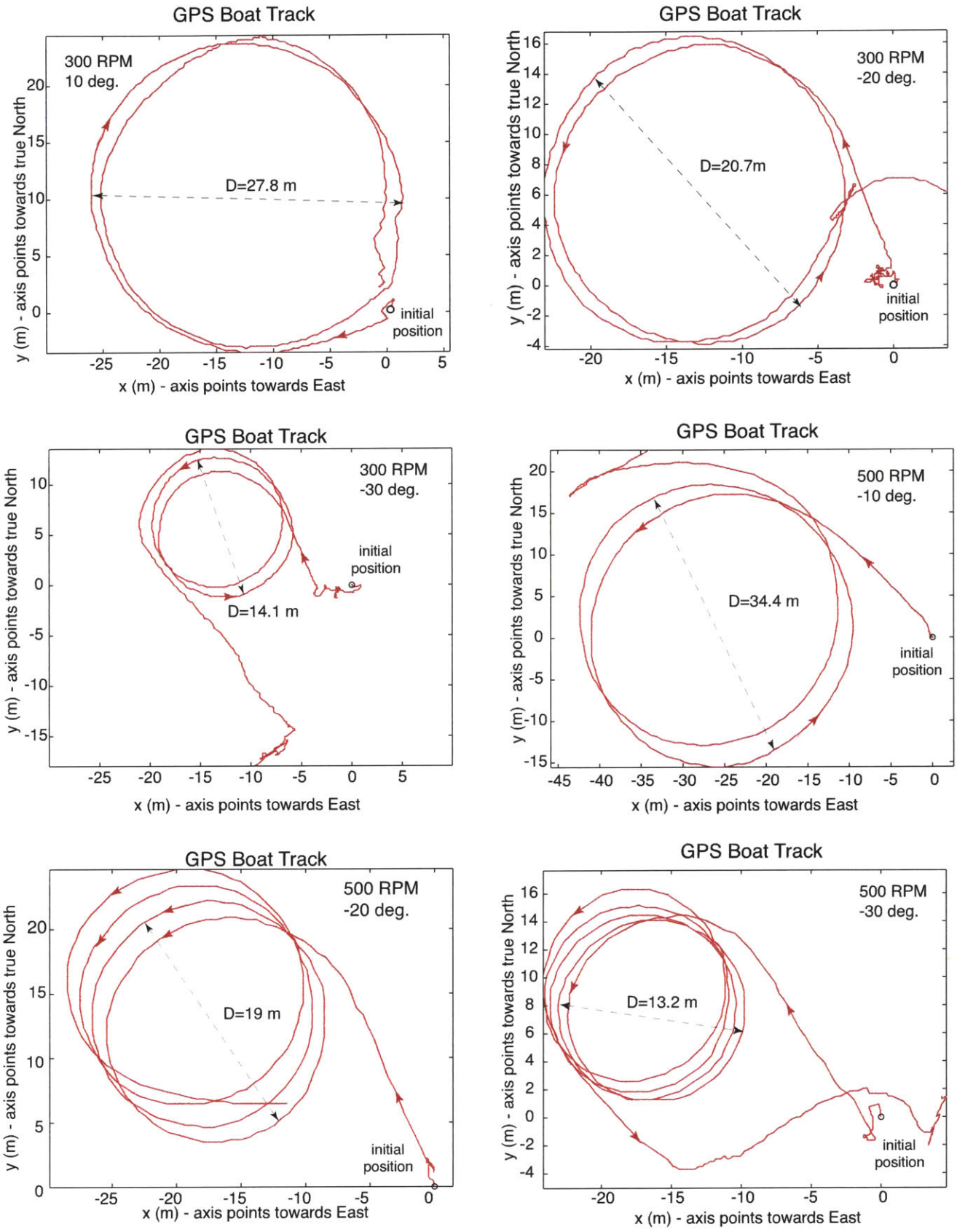

Figure K-1: GPS position data - BAE Quarry (1/2)

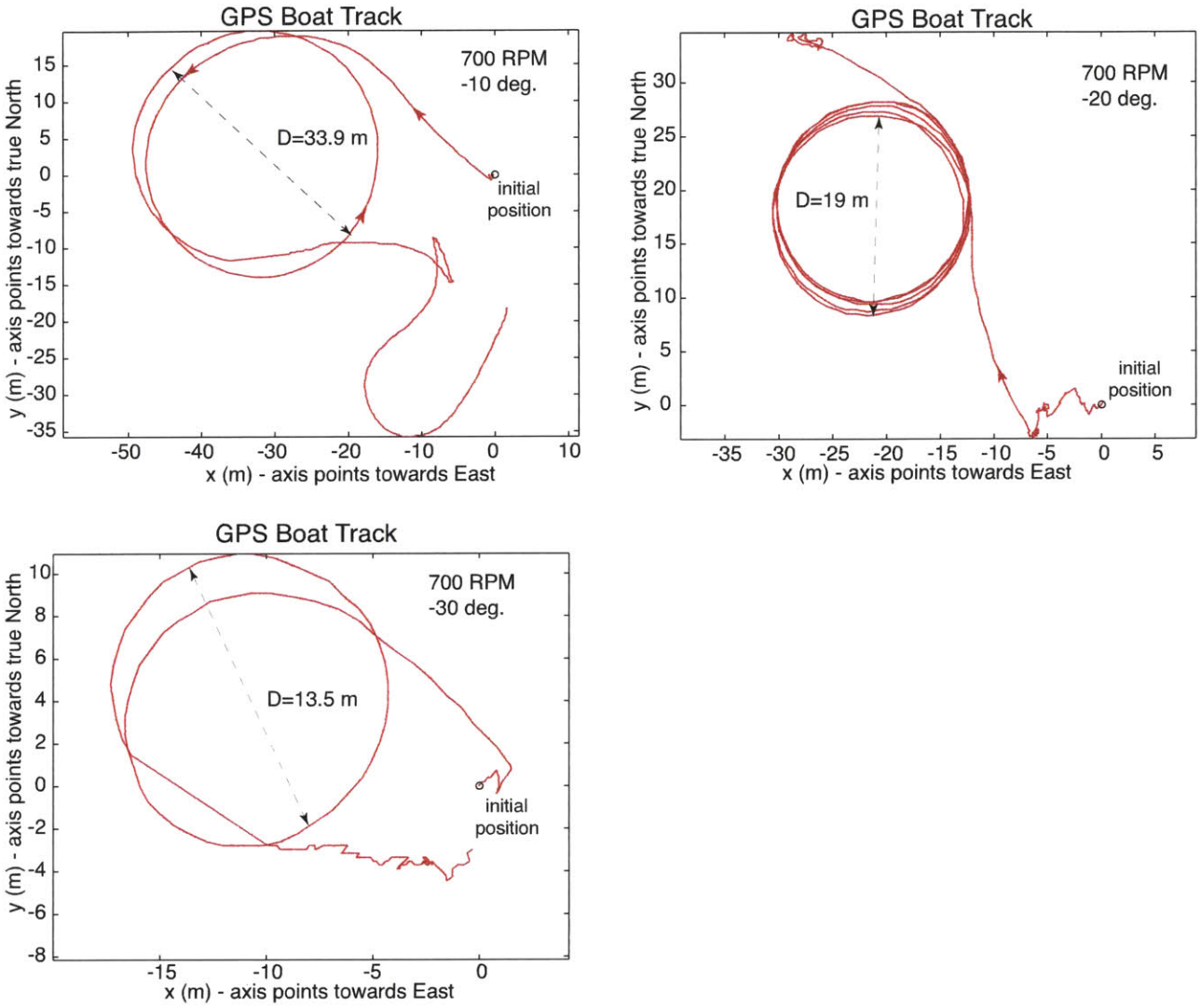

Figure K-2: GPS position data - BAE Quarry (2/2)

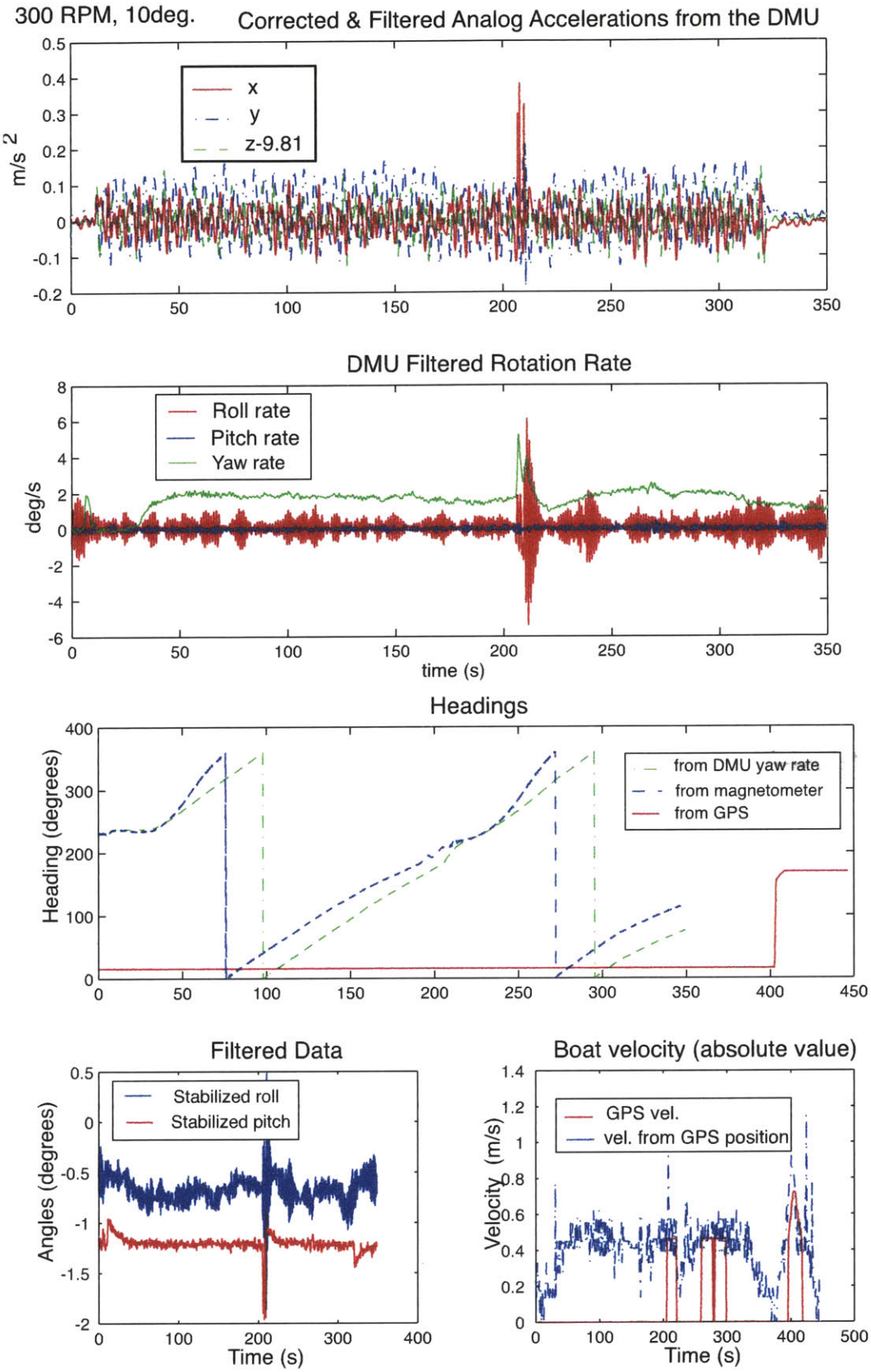

Figure K-3: Circle Maneuver tests at 300 RPM and 10 deg. - BAE Quarry

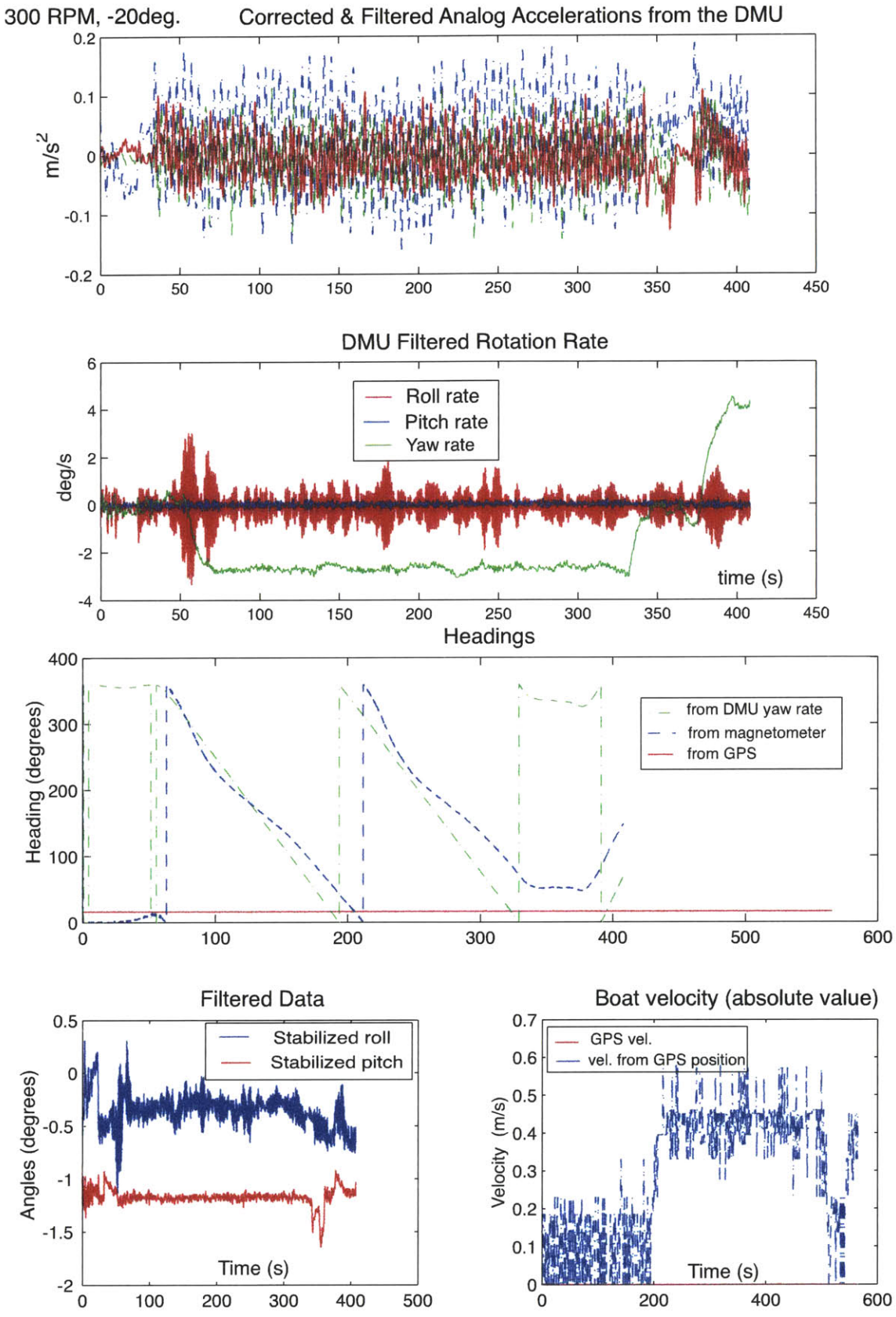

Figure K-4: Circle Maneuver tests at 300 RPM and -20 deg. - BAE Quarry

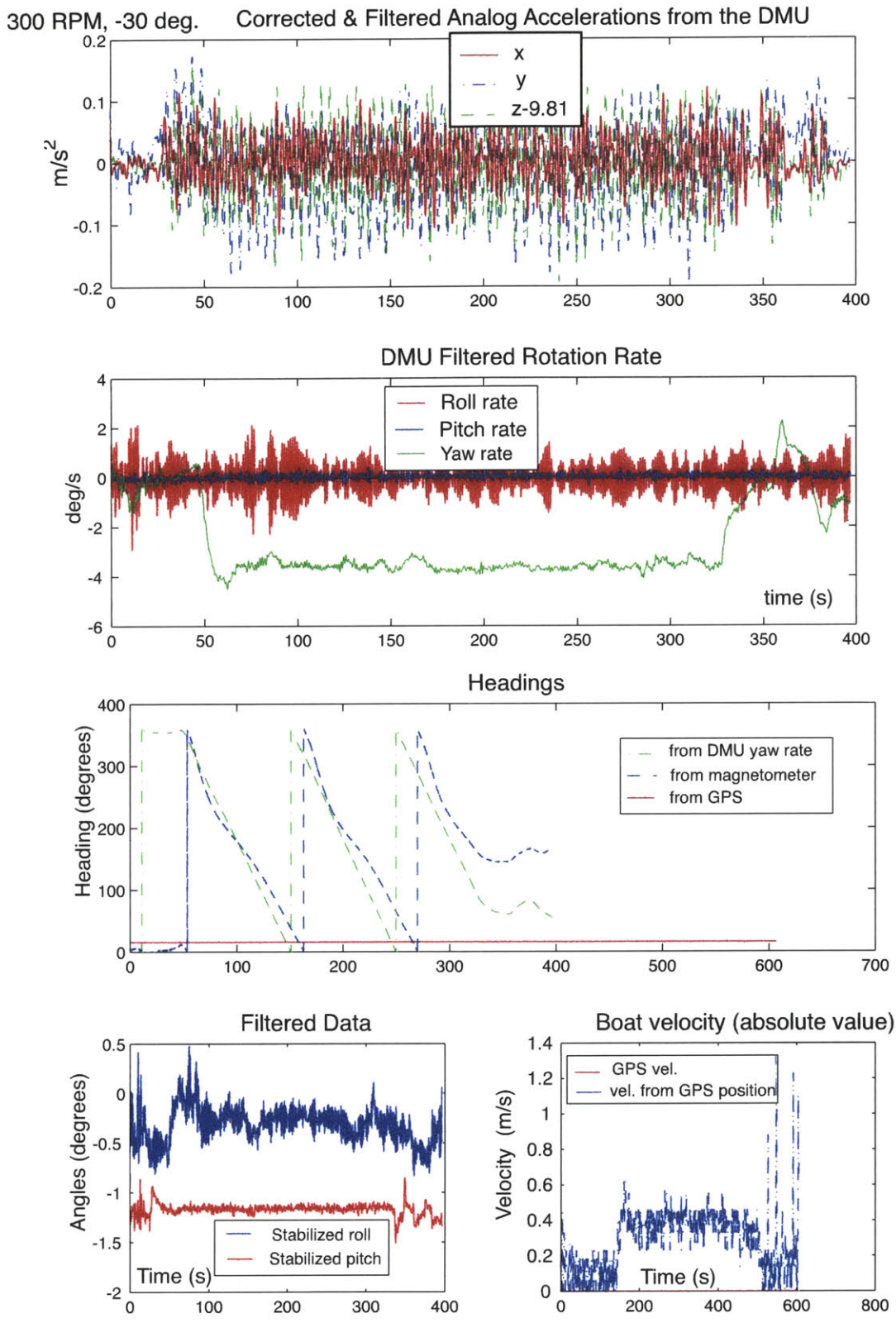

Figure K-5: Circle Maneuver tests at 300 RPM and -30 deg. - BAE Quarry

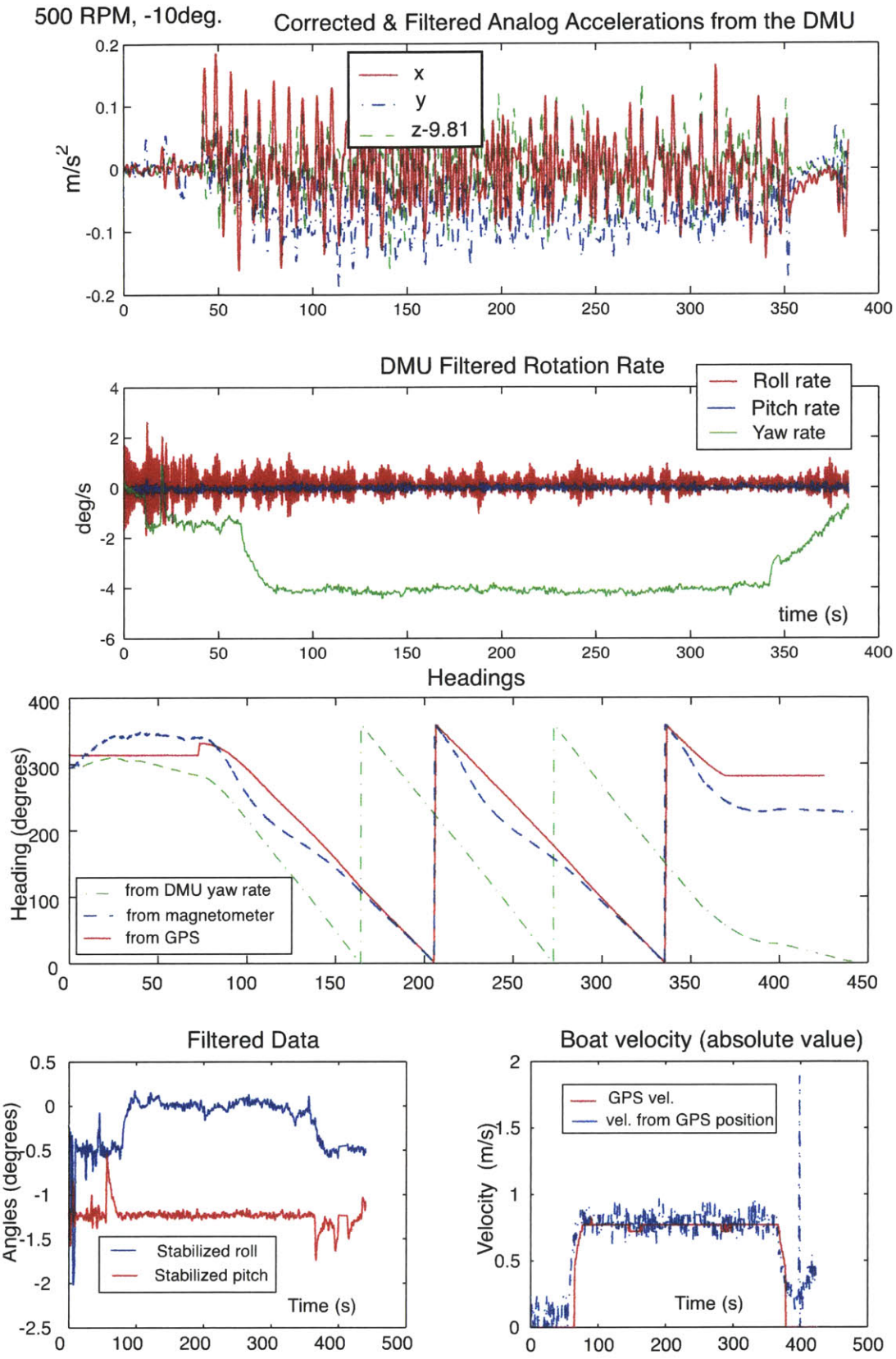

Figure K-6: Circle Maneuver tests at 500 RPM and -10 deg. - BAE Quarry

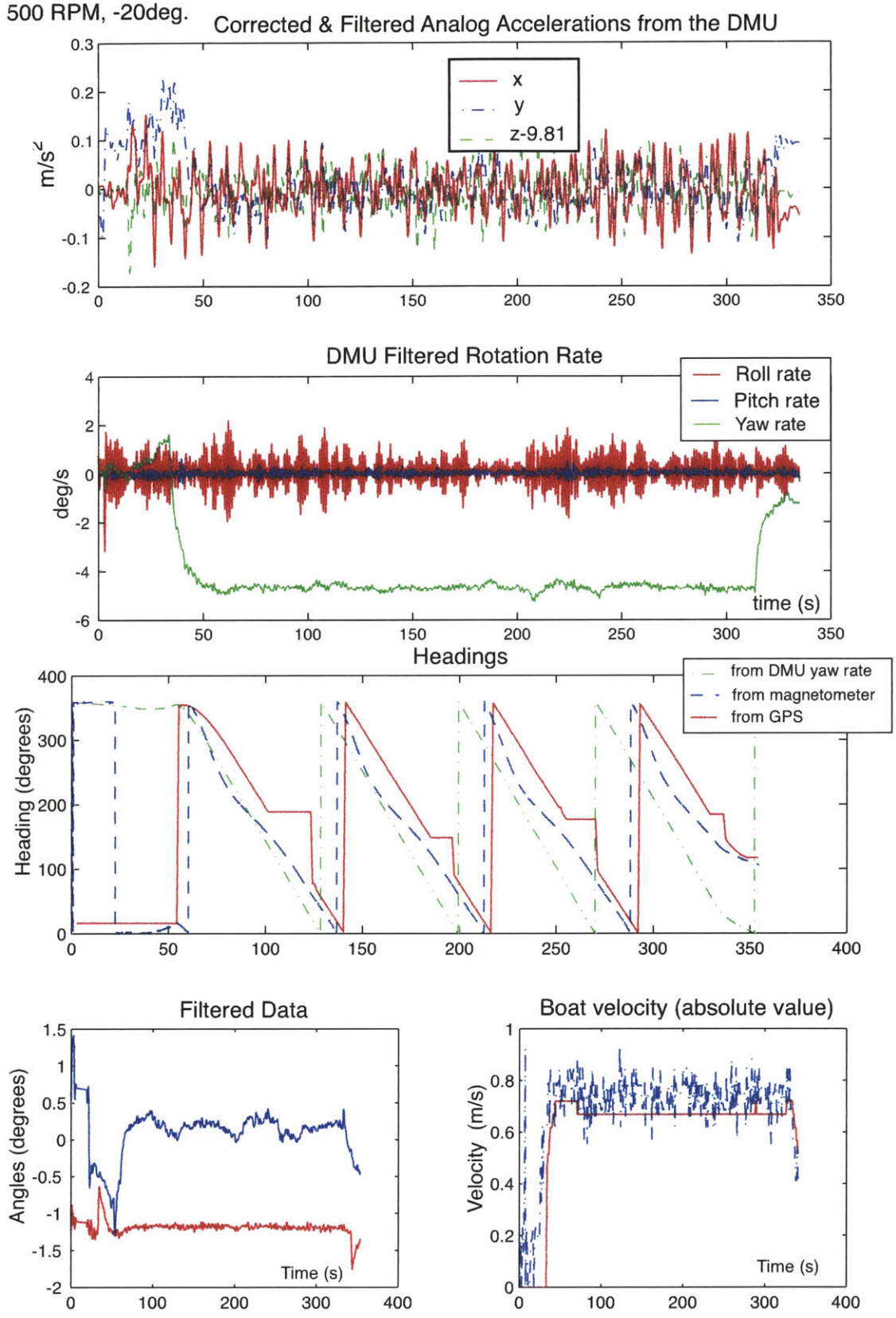

Figure K-7: Circle Maneuver tests at 500 RPM and -20 deg. - BAE Quarry

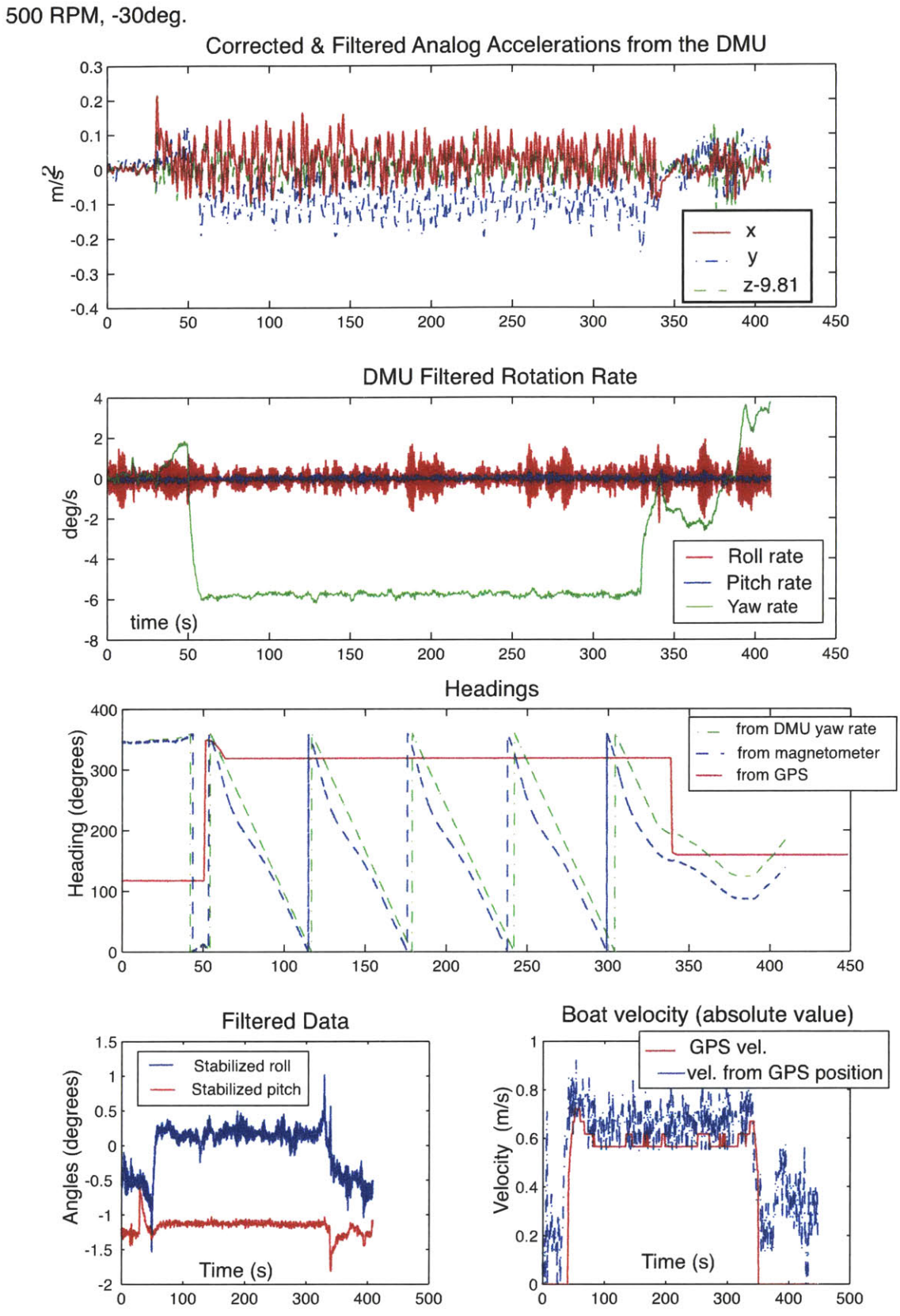

Figure K-8: Circle Maneuver tests at 500 RPM and -30 deg. - BAE Quarry

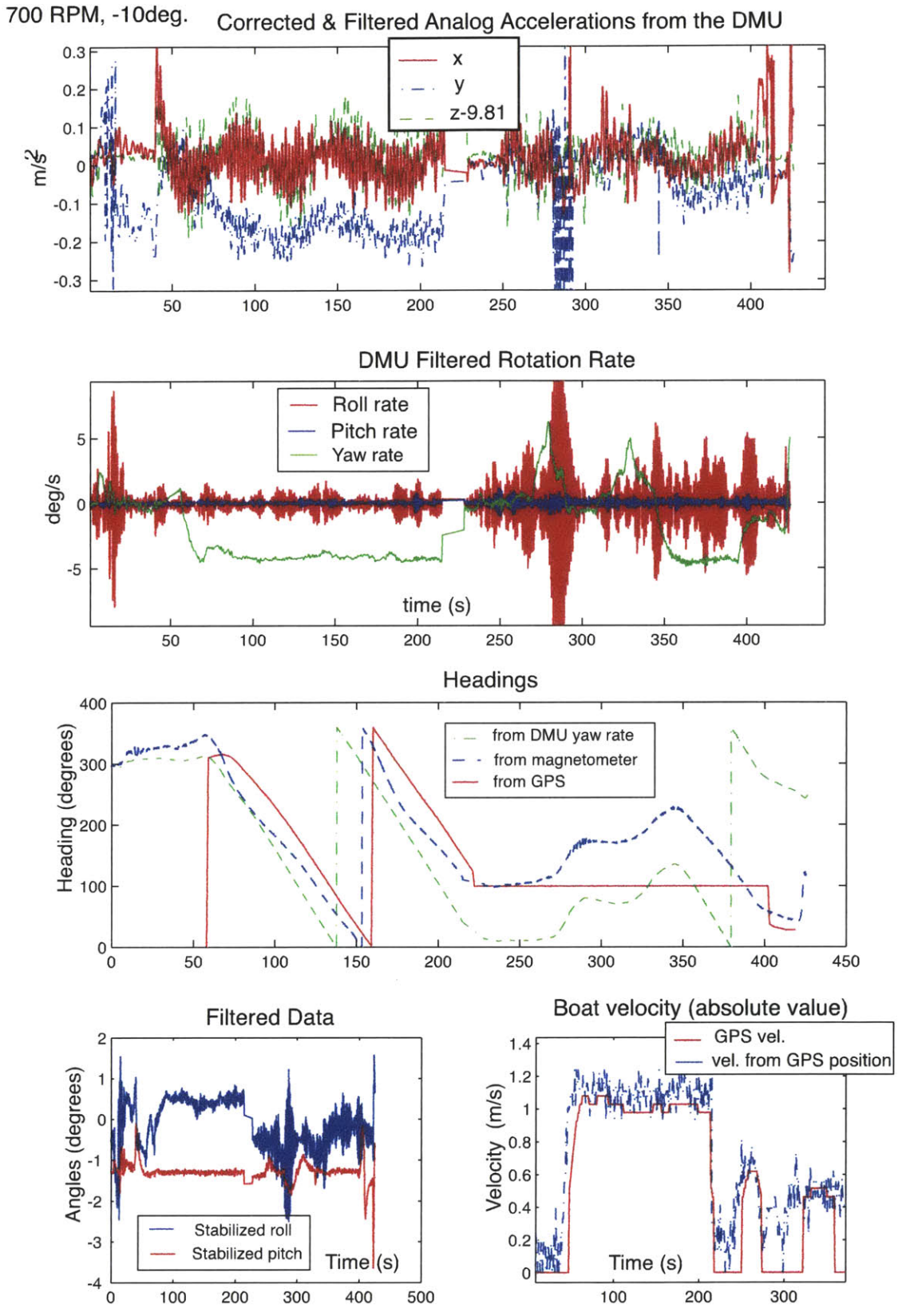

Figure K-9: Circle Maneuver tests at 700 RPM and -10 deg. - BAE Quarry

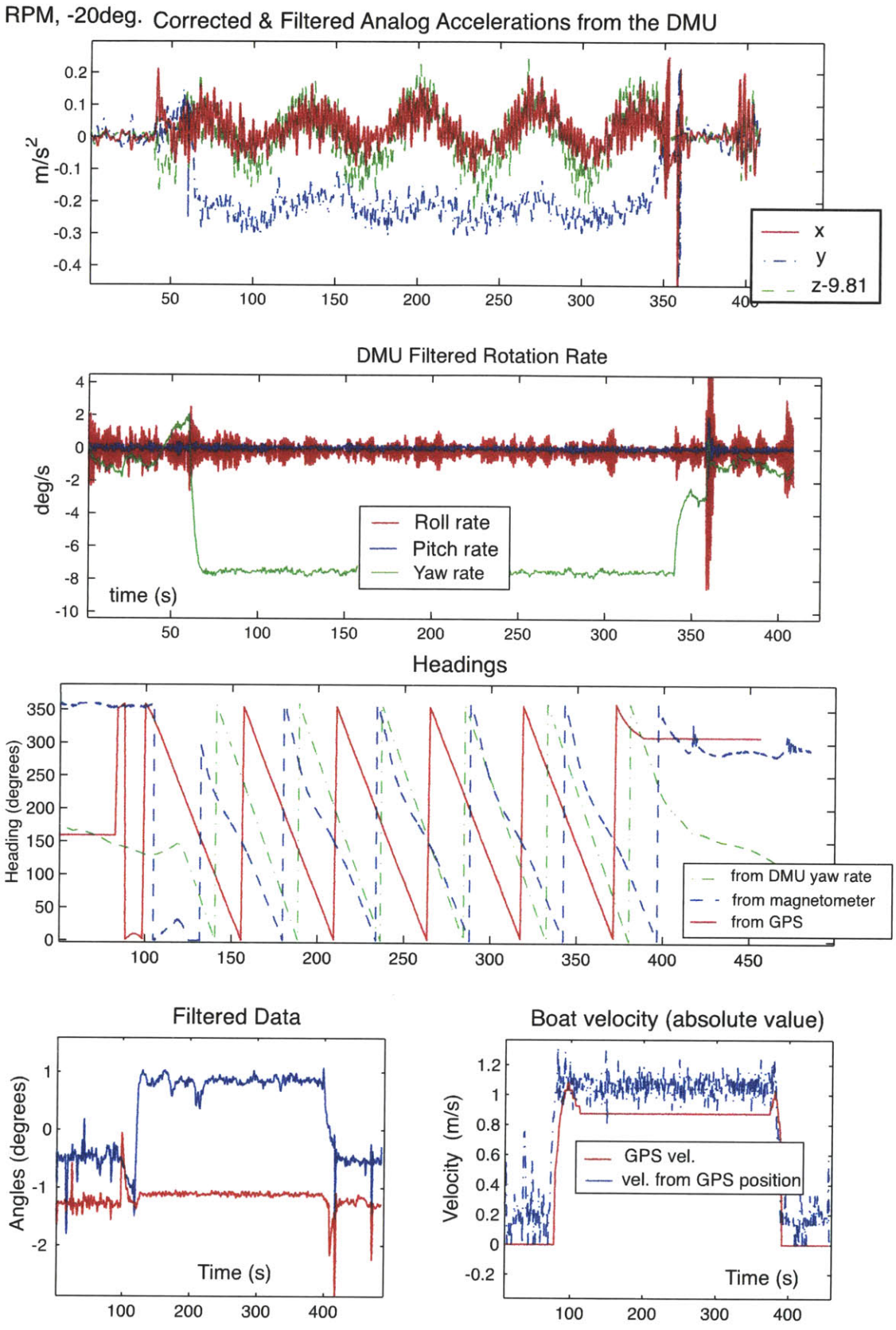

Figure K-10: Circle Maneuver tests at 700 RPM and -20 deg. - BAE Quarry

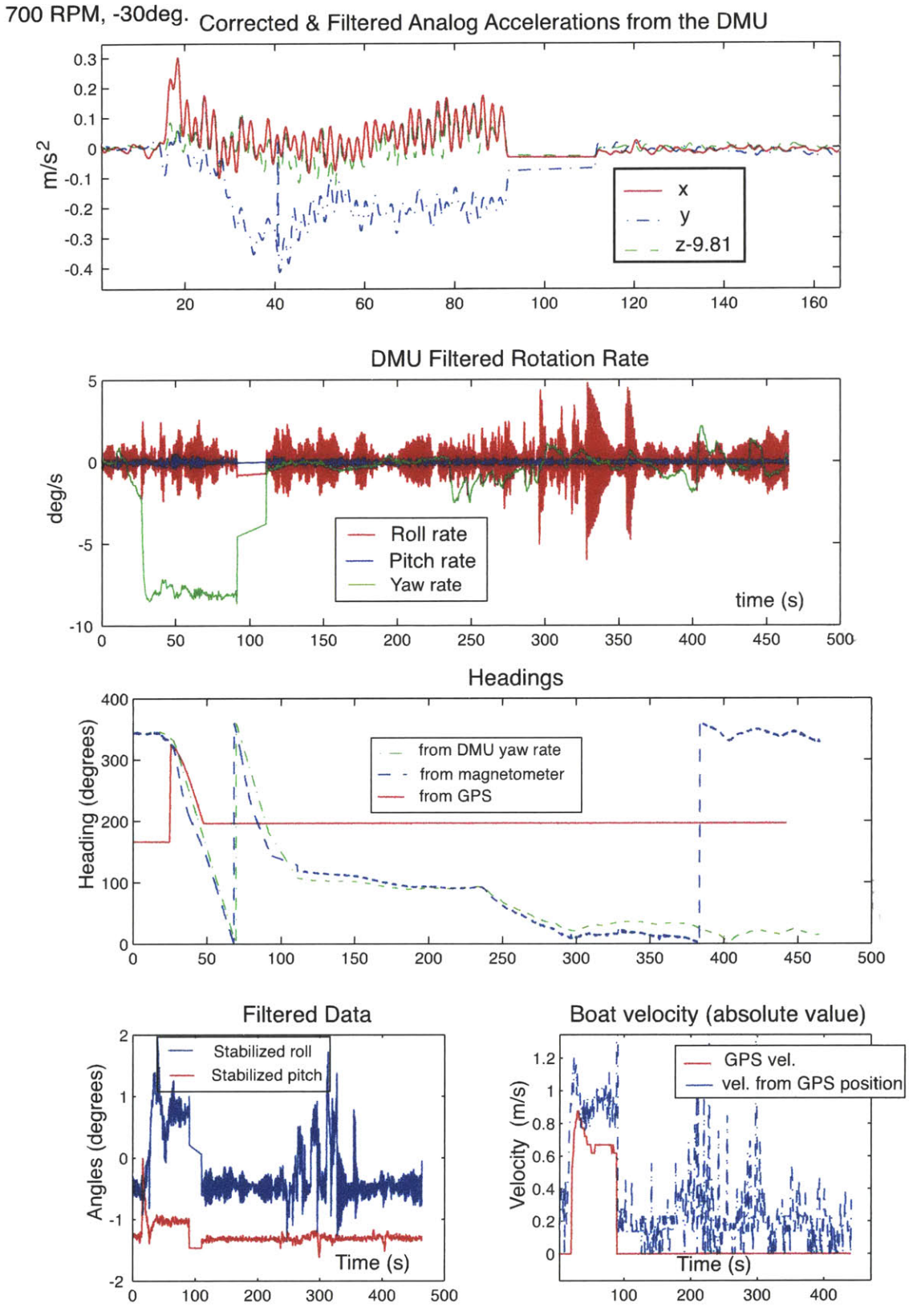

Figure K-11: Circle Maneuver tests at 700 RPM and -30 deg. - BAE Quarry

Bibliography

[1] D. Clarke, P. Gedling, and G. Hine. *The Application of Maneuvering Criteria in Hull Design. RINA Transactions*, 1982.

[2] Jim Czarnowski. *Exploring the Possibilities of Placing Traditional Marine Vessels Under Oscillating Foil Propulsion* . Master's thesis, Massachusetts Institute of Technology, Department of Ocean Engineering and Department of Mechanical Engineering, Cambridge, MA, 1997.

[3] Thor I. Fossen. *Guidance and Control of Ocean Vehicle.* John Wiley & Sons, 1994.

[4] Eric Foxlin. *Head Tracking Realtive to a MOving Vehicle or Simulator Platform Using Differential Inertail Sensors. Proceedings of Helmet and Head-Mounted Displays V, AeroSense 2000*, SPIE vol. 4021, April 24-25, 2000.

[5] Eric Foxlin, Michael Harrington, and Yury Altshuler. *Miniature 6-DOF Inertial System for Tracking HMDs. Proceedings of Helmet and Head-Mounted Displays III, AeroSense 98*, SPIE vol. 3362, April 13-14, 1998.

[6] Justin A. Harper and Robert M. Scher. John J. McMullen Assoc., Inc., *Improvements in the Prediction of Maneuvering Characteristics of Ships Using Regression Analysis. 26^{th} American Towing Tank Conference*, July 23-24, 2001.

[7] S. Inoue, M. Hirano, and K. Kijima. *International Shipbuilding Progress, Rotterdam, Netherlands. SNAME Transactions*, Vol. 28, No 325, September 1981.

[8] Edward V. Lewis. *Principles of Naval Architecture*, volume Volume III - Motion in Waves and Controllability. The Society of Naval Architects and Marine Engineers, Jersey City, NJ, second revision edition, 1989.

[9] J.N. Newman. *Marine Hydrodynamics.* MIT Press, Cambridge, MA, 1977.

[10] K. Nomoto, T. Taguchi, K. Honda, and S. Hirano. *On The Steering Qualities of Ships.* Technical report, International Shipbuilding Progress, Vol. 4, 1957.

[11] N. H. Norrbin. *Theory and Observation of the Use of a mathematical model for Ship maneuvering in Deep and Confined Waters. Swedish Experimental Tpwing Tank, Publication 68*, 1971.

[12] Department of Defense. *Department of Defense World Geodetic System 1984 - Its Definition and Relationships with Local geodetic Cooridnate Systems.* Technical report 8250.2, Defense Mapping Agency, 1987.

[13] PDI. *Design and Analysis of an Alternate Programmed Control Module (PCM) for DDG51 Class Ships*, volume 1 (unclassified). Technical Report 336091-01, February 1994.

[14] Rene E. Quezada Ojeda. *Robust Control Design and Simulation of the Maneuvering Dynamics of an Arleigh Burke Class Destroyer.* Master's thesis, Massachusetts Institute of Technology, Department of Ocean Engineering, Cambridge, MA, 2000.

[15] Wilson J. Rugh. *Analytical Framework for Gain Scheduling. I.E.E.E. Control System Magazine*, 1(1), 1991.

[16] L. W. Smitt. *Steering & Maneuvering of Ships - Full Scale and Model Tests. European Shipbuilding, Parts I and II, No 6,1970 and No 1, 1971.*

[17] Martin Stoffel. *Design of a Real-Time Sensory and Control System for a Destroyer Model.* Diploma thesis, Institute of Fluid Dynamics, Zürich, Dept. of Mathematics and Physics, 2000-2001. Written at MIT, Department of Ocean Engineering, Cambridge, MA, USA.

[18] Mike E. Taylor. *System identification and Control of an Arleigh Burke Class Destroyer Using an Extended Kalman Filter.* Master's thesis, Massachusetts Institute of Technology, Department of Ocean Engineering and Mechanical Engineering, 2000.

[19] Crossbow Technology Inc. *DMU User's Manual.* Version 1.8, February 2000.

[20] Karl J. Åström and Wittenmark Björn. *Adaptative Control.* Addison Wesley Publishing Company, Inc., second edition edition, 1995.

[21] Mike Triantafyllou and Franz S. Hover. *Class Notes for Menuvering and Control of Surface and Underwater Vehicles.* Technical report, Massachusetts Institute of Techmology, Department of Ocean Engineeing, Cambridge, MA, 2000.

[22] Albert Wu. *Design and Control of an Autonomous Destroyer Model.* Master's thesis, Massachusetts Institute of Technology, Department of Ocean Engineering, Cambridge, MA, 2000.

5916-S